Benchmarking for Validation and Verification of THM Simulators with special Regard to Fluid Dynamic Processes in Repository Systems

Project BenVaSim

GRS - 588

**Gesellschaft für Anlagen-
und Reaktorsicherheit
(GRS) gGmbH**

Benchmarking for Validation and Verification of THM Simulators with special Regard to Fluid Dynamic Processes in Repository Systems

Project BenVaSim

Oliver Czaikowski
Larissa Friedenberg

April 2020

Abstract

For the geological disposal of heat-emitting radioactive waste in Germany, the safe containment has to be demonstrated for a time period of one million years. For predicting the long-term behaviour of a repository and for making realistic statements about the long-term safety, various numerical simulations are needed. Independent of the host rock and repository concept, there are thermal-hydraulic-mechanical (THM) coupled basic processes forming the background of all numerical simulations. The aim of this THM-coupled simulator benchmarking project was to apply well specified and simplified modelling tasks to investigate basic processes, especially flow phenomena, which are included in mostly all THM-coupled simulations in porous media. Therefore, different modelling phases were planned, starting with single phase flow coupled with mechanics extending to two-phase flow and finally reaching a full THM-coupled model. To have a clear focus on the model evolution and the influences of the various processes, it was started with a very simple one-dimensional model. With time the geometry complexity was increased by simulating a backfilled drift seal and finally assuming a generic repository drift, still in one-dimension. During the modelling work it was shown that differences exist for the treatment of basic processes in the various simulators which are of importance for more complex numerical models. In frame of this project, a deepened understanding of the simulator itself and the numerical treatment of coupled processes was gained, and improvements of the simulators were achieved.

Zusammenfassung

Für die langzeitlich sichere Einlagerung von wärmeentwickelnden, radioaktiven Abfällen in tiefen geologischen Formationen muss in Deutschland der sichere Einschluss über einen Zeitraum von einer Millionen Jahre demonstriert werden. Um das Langzeitverhalten eines Endlagers prognostizieren und realistische Aussagen treffen zu können, werden verschiedene numerische Simulationen benötigt. Den Hintergrund der numerischen Simulationen bilden thermisch-hydraulisch-mechanische (THM) gekoppelte Prozesse, welche grundlegend unabhängig von dem Wirtsgestein und dem Endlagerkonzept auftreten. Das Ziel des Projekts BenVaSim (Internationales **Ben**chmarking zur Verifizierung und **Va**lidierung von TH^{2}M-**Sim**ulatoren insbesondere im Hinblick auf fluiddynamische Prozesse in Endlagersystemen) war die Untersuchung derjenigen Prozesse, welche in den meisten THM-gekoppelten Simulationen in porösen Medien als grundlegende Basisprozesse betrachtet werden mittels eines THM-gekoppelten Simulator-Vergleichs. Ein besonderes Augenmerk sollte hierbei auf fluiddynamische Prozesse gelegt werden. Um den Fokus auf die ablaufenden Prozesse zu richten, sollten vereinfachte und gut definierte Modelle angewendet werden, wofür eindimensionale Modelle gewählt wurden. In diesem Zuge wurden verschiedene Modellierungsschritte geplant. Begonnen wurde mit der Untersuchung von Einphasenfluss gekoppelt mit mechanischen Aspekten, was im weiteren Verlauf auf Zwei-Phasenfluss erweitert wurde und final in einem voll THM-gekoppelten Model endete. Auch die Geometrie des Models wurde mit steigendem Fortschritt komplexer. So wurde zunächst ein Model bestehend aus einem Material betrachtet, welches schrittweise erweitert und zu einer generischen Einlagerungsstrecke finalisiert wurde. Während der Modellierungsarbeiten wurden Unterschiede in der Handhabung der Basisprozesse der einzelnen Simulatoren aufgezeigt, die grundlegende Auswirkungen auf komplexere Modelle haben. Im Zuge dieses Projekts wurde ein vertieftes Verständnis des jeweils angewendeten Simulators mit Blick auf die gekoppelten Basisprozesse entwickelt und bei Bedarf einzelne Simulatoren um relevant Aspekte erweitert.

Acknowledgement

Table of Content

1   Introduction

For the geological disposal of heat-emitting radioactive waste, researches on different types of host rock are done, e. g. in Germany rock salt, clay and crystalline rock are considered. The concept for a safe disposal of heat-emitting radioactive waste in Germany is based on a disposal in deep geological formations with a high containment capacity. Favourable aspects are the geological long-term stability and the long-term inclusion of radionuclides. The safety concept is based on a multiple barrier system including the geological barrier, the sealings in shafts and drifts, the backfilling of open cavities and the waste containers. According to this, the safe containment of the radioactive waste has to be assured for a time period of one million years. For predicting the long-term behaviour of a repository and for making realistic statements about the long-term safety, numerical simulations are needed.

Within a repository system, relevant thermal-hydraulic-mechanical (THM) coupled processes occur influencing the behaviour of the whole system and their individual components. Independent of the host rock, various basic processes arise which can be described by generally accepted constitutive laws. Hence the comprehensive process understanding is a fundamental property for the application of numerical simulations and the correct evaluation of the results, the basic processes must be understood first. Afterwards, the complex material models can be applied in a more reliable manner.

However, there can be differences in the application and implementation of the basic processes in the different simulation codes. Basically, a numerical simulator needs to be validated and verified which is realized in most cases due to a simulator benchmarking. A frequent approach is the simulation of existing laboratory or in-situ experiments to have a comparability between the results of the simulation codes and an additional comparability with reliable data. However, the modelling of laboratory or in-situ experiments is quite complex due to the multiplicity of involved processes and the focus is mostly set on the extended material behaviour.

In the project BenVaSim a THM-coupled simulator benchmarking should be conducted with the focus on the basic processes, especially on flow phenomena. Therefore, different modelling phases were planned, starting with one-phase flow coupled with mechanics extending to two-phase flow and finally reaching a full THM-coupled model. It was started with a very simple one-dimensional model, to have a clear focus on the model evolution and the influences of the various processes.

In chapter two the background of the project is described including the objectives and the participating organizations.

The modelling work is carried out in different phases with stepwise increasing complexity. In Chapter 3 the structure and the intention behind is explained together with mechanical, hydraulic and thermal constitutive laws, which are used in the modelling phases including the process coupling. To focus on the investigation and understanding of numerical processes, the model was simplified to a one-dimensional problem and fundamental laws were applied.

For a basically understanding of the coupling between hydraulic and mechanical processes in the first modelling phase a single-phase flow problem is simulated in a unified material (Chapter 0). Therefore, a basic scenario was determined, and the influences of different material properties, initial conditions and mesh discretization were evaluated.

Becoming more complex, in the next modelling step, two-phase flow was considered in Chapter 5 assuming water as liquid phase and air as gas phase. Since the boundary conditions might not remain stable over the whole operation time of a repository, a change of conditions was simulated.

Using a model consisting of only one material is sufficient for the first investigation of HM-coupled processes, however, the interactions of different materials and especially the processes in the transition zones are important. Thus, the model geometry was enhanced in the third modelling phase to a simplified one-dimensional backfilled and sealed drift (Chapter 6). A basic scenario was determined and different changes of mechanical and hydraulic conditions, material parameters and process coupling equations are elaborated.

Finally, the thermal aspect is added, extending the investigation to THM-coupled problem (Chapter 7). In the same course, the geometry is getting more complex by assuming a generic repository drift including two canister sections with heat emitting waste, several backfilled openings, a drift seal and host rock.

In the final discussion in Chapter 8 difficulties during the modelling process are concluded and explained. Furthermore, differences in the numerical results compared to project partners are elaborated and discussed.

2 Background

The project BenVaSim was started in 2017 for the verification and validation of several numerical simulators which are in use for dealing with issues related to the final repository research. The main objective of the project is to gain independent numerical simulation tools which are verified and meaningful related to geotechnical aspects, especially for thermal-hydraulic-mechanical (THM) coupled processes of the host rock and engineered barrier systems (EBS) in a repository. This represents quality assurance which should result in improved forecast reliability leading to a strengthening confidence in prognostic statements. In Germany, for example, the knowledge resulting from this project could support the new side selection procedure for a repository for high-level waste. Another objective is the project partners personal advancement of new skills and deepened expertise with their applied simulators and possible further development of the simulators, as well as with the basic THM processes. The participation of international partners is leading to an exchange of expertise which will benefit all contributors /Lux 18/.

Within the BenVaSim project there were six international partners participating which are listed in Tab. 2.1. The initiator of the project was the Chair of Waste Disposal Technologies and Geomechanics of Clausthal University of Technology (TUC) which was the project coordinator, too. In a former project they developed a coupling called FTK simulator ($\underline{F}$LAC^{3D}-$\underline{T}$OUGH2-$\underline{K}$opplungssimulator) between the simulators FLAC^{3D} for geomechanically problems and TOUGH2 for geothermal-hydraulic problems /LUX 15/. So, their aim in the BenVaSim project was to improve and develop their FTK-simulator. There are some other project partner using different couplings between the programs TOUGH2 and FLAC^{3D}. Since the last decades, the Lawrence Berkeley National Laboratory (LBNL) developed and implemented a THM simulator called TOUGH-FLAC. Related to this simulator the Gesellschaft für Anlagen- und Reaktorsicherheit in Cologne (GRS K) enhanced a coupled simulator called TFC ($\underline{T}$OUGH2-$\underline{F}$LAC^{3D}-$\underline{C}$oupling) and also the Swiss Federal Nuclear Safety Inspectorate (ENSI) is using a TOUGH-FLAC coupling. Next to the variations of coupling TOUGH2 and FLAC^{3D}, there are some other applied simulators. The Gesellschaft für Anlagen- und Reaktorsicherheit in Braunschweig (GRS BS) uses the finite-element code CODE_BRIGHT which is developed by the Polytechnical University of Barcelona (UPC). The Federal Institute for Geosciences and Natural Resources (BGR) and the ENSI are using OpenGeoSys which development started at the Helmholtz Centre for Environmental Research (UFZ) and follows the Open-Source-Concept where the code is developed in collaboration from researchers all over the world.

The last applied simulator is COMSOL Multiphysics which is used by ENSI, too. Further information about the applied simulators can be found in /LUX 18/.

Tab. 2.1   Participating organisations and the applied simulators

Organisation	Simulator	
Federal Institute for Geosciences and Natural Resources (BGR), Sub-Department Geotechnical Safety Analyses, Hannover, Germany	OpenGeoSys	/KOL 12/
Gesellschaft für Anlagen- und Reaktorsicherheit gGmbH, Repository Research Department (GRS BS), Braunschweig, Germany	CODE_BRIGHT	/UPC 19/
Gesellschaft für Anlagen- und Reaktorsicherheit gGmbH, Decomissing and Waste Management Division (GRS K), Köln, Germany	TOUGH-FLAC-Coupling	/HOT 14/
Lawrence Berkeley National Laboratory (LBNL), Department Hydrology, Berkeley, USA	TOUGH-FLAC	/RUQ 11/
Swiss Federal Nuclear Safety Inspectorate (ENSI), Department Disposal and Analyses, Brugg, Switzerland	TOUGH-FLAC COMSOL Multiphysics OpenGeoSys	/RIN 18/ /COM 12/ /KOL 12/
Clausthal University of Technology (TUC), Chair for Waste Disposal Technologies and Geomechanics, Clausthal-Zellerfeld, Germany	FLAC-TOUGH-Kopplungssimulator	/RUT 18/

3 Basics for the numerical modelling

3.1 Structure of modelling work

For a fundamental investigation and an extended process understanding, the modelling work is done stepwise with increasing complexity. First, the emphasis lies on the basic processes that occur in a repository system and their implementation in the different simulation codes. Therefore, in the early modelling work only single-phase flow coupled with mechanics was considered, extending the complexity during the project to a full coupled thermal-hydraulic-mechanical model.

Because of focussing on the elementary processes and their interactions, a one-dimensional model is chosen which allows outlining differences in the results and figuring out feasible reasons due to the elementariness. This leads to a more precise estimation of simulation and process quality. Due to this simplified approach in some cases a comparison of the numerical results with analytical ones is possible allowing a verification of the outcomes. The THM-coupled processes considered in this project may occur in a repository in every type of host rock, however, there is a dependence of this processes on the surrounding rock formation. Within the very fundamental investigation of the basic processes, it should not be focussed on one rock type, that's why a generic elastic isotropic material is chosen. Even with not concentrating on a special host rock and the related repository concept, the material parameters are chosen with tendency for a repository in claystone.

During the working progress different model variations were done, started with consideration of single-phase flow, widened out to two-phase flow further changes of geometry related to the disposal of radioactive waste through simulating a generic drift containing a thermal source and backfilling and sealing elements. In every model, there is one basic scenario and some scenario variations where parameter, initial conditions or mesh discretization are changed.

3.2 Applied constitutive equations

CODE_BRIGHT is a Finite-Element-Method (FEM) Code for solving coupled problems in geological media which is developed by the Polytechnical University Barcelona (UPC).

It is written in FORTRAN and uses for pre- and post-processing the system GID developed by the International Centre for Numerical Methods in Engineering (CIMNE) Barcelona /CIM 20/. The code formulations are based on a multi-phase, multi-species approach /UPC 20/.

3.2.1 Mechanical laws

Because of simplicity, only linear-elastic behaviour is considered. For describing the linear-elastic behaviour of a geologic medium Hook's law combined with variation of Young Modulus with porosity is used following /UPC 20/:

$$E = E_0 + (\Phi - \Phi_0)\frac{dE}{d\Phi} \geq E_{min}$$
(3.1)

E = Young's modulus [MPa]

E_0 = Initial Young's modulus [MPa]

Φ_0 = Initial porosity [-]

$dE/d\Phi$ = Variation of the Young's modulus with porosity [MPa]

E_{min} = Minimum elastic modulus [MPa]

3.2.2 Hydraulic laws

Because of the poromechanical approach of CODE_BRIGHT the relationship between saturation and pore pressure must always be defined by a retention curve. There are different options of retention curves which can be used, however, the most frequently used approach follows the van Genuchten model which is described by /UPC 20/:

$$S_e = \frac{S_l - S_{rl}}{S_{ls} - S_{rl}} = \left(1 + \left(\frac{P_g - P_l}{P}\right)^{\frac{1}{1-\lambda}}\right)^{\lambda}$$
(3.2)

With $P = P_0 \frac{\sigma}{\sigma_0}$
(3.3)

S_e = effective saturation [-]

S_l = liquid saturation [-]

S_{rl} = residual liquid saturation [-]

S_{ls} = maximum liquid saturation [-]

P_g = gas pressure [MPa]

P_l = liquid pressure [MPa]

λ = shape function for retention curve [-]

P_0 = pressure of air entrance [MPa]

Due to the assumption of neglecting coupled phase processes in the first modelling stage a second description of retention curve is required. For minimizing the effects of retention curve on the results and for minimizing errors, the linear model was chosen which follows /UPC 20/:

$$S_e = \frac{S_l - S_{rl}}{S_{ls} - S_{rl}} = 1 - \frac{P_g - P_l}{P_0} \tag{3.4}$$

For the specification of the relative permeabilities the van Genuchten model was used, so that relative permeability depends on effective saturation by /UPC 20/:

$$k_{rl} = \sqrt{S_e}\left(1 - \left(1 - S_e^{\frac{1}{\lambda}}\right)^{\lambda}\right)^2 \tag{3.5}$$

$$k_{rg} = (1 - S_e)^{\gamma}\left(1 - S_e^{\frac{1}{\lambda}}\right)^{2\lambda} \tag{3.6}$$

k_{rl} = liquid phase relative permeability [-]

k_{rg} = gas phase relative permeability [-]

S_e = effective saturation [-]

λ = van Genuchten parameter [-]

γ = pore connectivity parameter [-]

Additionally, in CODE_BRIGHT a default law for the gas phase relative permeability is specified following /UPC 20/:

$$k_{rg} = 1 - k_{rl} \tag{3.7}$$

3.2.3   Thermal laws

For keeping the modelling work simple, in the thermal processes only heat convection and heat conduction are considered, therefore Fourier's law is used /UPC 20/:

$$\boldsymbol{i}_c = -\lambda \nabla T \tag{3.8}$$

i_c = conductive heat flux [W/m]

λ = thermal conductivity of the medium [W/(m*K)]

∇T = temperature gradient [K/m]

3.2.4   Process couplings

Following Terzaghi's theory of effective stresses /TER 43/ and the subsequent modification by Biot and Willis /BIO 1957/, the equation for effective stresses is expressed as:

$$\sigma_{eff} = \sigma_{tot} - \alpha p_f = \sigma_{tot} - \alpha(S_g p_g + S_l p_l) \tag{3.9}$$

With: $\alpha = 1 - \dfrac{C_s}{C} \tag{3.10}$

σ_{eff} = effective stress [MPa]

σ_{tot} = total stress [MPa]

α = Biot's coefficient [-]

p_f = fluid pressure [MPa]

p_l = liquid pressure [MPa]

p_g = gas pressure [MPa]

S_l = liquid saturation [-]

S_g = gas saturation [-]

C_s = solid phase compressibility [1/MPa]

C = porous materials undrained compressibility [1/MPa]

For a complete consideration of Biot's theory, the Biot modulus should be incorporated following:

$$\breve{M}_l = \frac{\breve{K}_l}{\Phi + (\alpha - \Phi) * (1 - \alpha) * \breve{K}_l / \breve{K}} \tag{3.11}$$

$\breve{M}_l$ = Biot modulus [MPa]

$\breve{K}_l$ = liquid bulk modulus [MPa]

Φ = porosity [-]

α = Biot coefficient [-]

$\breve{K}$ = solid bulk modulus [MPa]

There are different approaches for the calculation of effective stresses. When using linear elasticity in CODE_BRIGHT the default option for the effective stress calculation follows the approach from Bishop where the maximal fluid pressure is subtracted from the total stresses /BIS 61/. It is implemented following /UPC 20/:

$$\sigma_{eff} = \sigma_{tot} - \alpha * \max(p_g, p_l) \tag{3.12}$$

For the consideration of thermal problems, various dependencies of thermal conductivity can be included. In this frame, the dependence on the degree of fluid saturation is examined in the following way /UPC 20/:

$$\lambda = \lambda_{dry}(1 - S_l) + \lambda_{sat}S_l \tag{3.13}$$

λ = Thermal conductivity [W/(m*K)]

λ_{dry} = Thermal conductivity of the totally dry porous medium [W/(m*K)]

λ_{wet} = Thermal conductivity of the porous medium in full saturated state [W/(m*K)]

S_l = Liquid saturation degree [-]

4   1st modelling phase – single phase flow

For the beginning of the modelling work, the first approach was to consider single-phase flow coupled with mechanical aspects. There is a strong interactive influence between hydraulics and mechanics in a repository system, especial in the host rock and the EBS. If compaction or relaxation occur due to a changed stress state, the porosity in the material will decrease or increase, respectively, leading to a change in permeability and flow properties. Hence, the pore pressures are changing affecting the effective stresses and resulting in a modification of strains. The hydraulic component includes two phases, gas and liquid, which complicate the coupled processes. For a first approximation only a HM-coupling with one liquid phase is considered.

Fig. 4.1 shows the simplified one-dimensional model geometry which has a length of 10 m and a height of 1 m. Only processes in horizontal direction are considered. The boundary conditions are symbolized by the arrows where the blue one present hydraulics and the black one presents mechanical aspects.
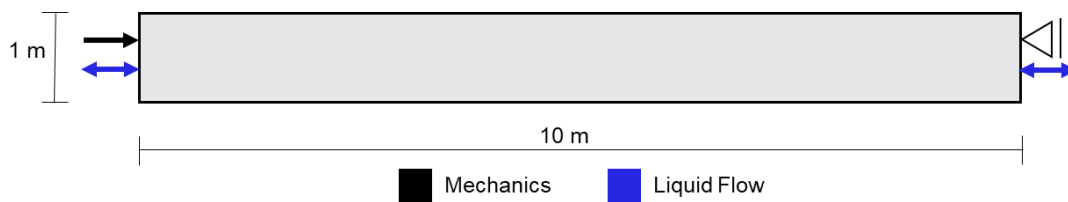
Fig. 4.1   Model geometry and considered processes in the 1st modelling phase

For simplification and the possibility of comparing the numerical results with analytical ones, the gas phase is kept at a fixed reference pressure and phase interactions are neglected. This assumption leads to problems in the application of CODE_BRIGHT which basis is a poromechanical approach for coupled analysis in geological media requiring phase interactions. To keep the divergence to the analytical solution as small as possible a very flat linear retention curve following Equation (3.4) is chosen for representing the phase interactions and presented in Fig. 4.2. Further, the specification of a saturation in CODE_BRIGHT always occurs due to the upset of a negative liquid pressure, also called suction pressure, determined by the retention curve.
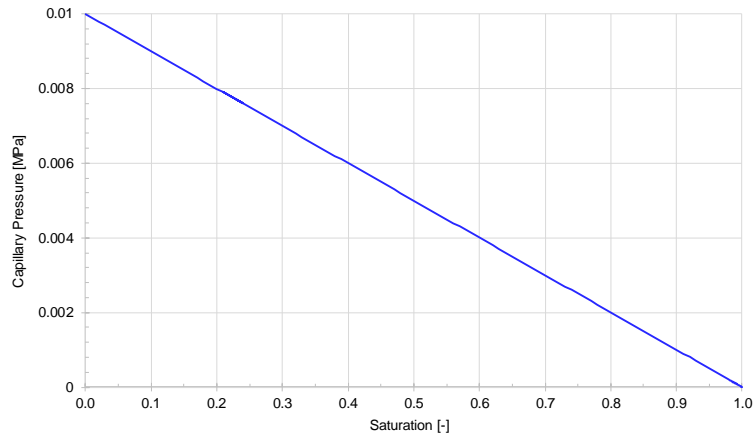
Fig. 4.2   Linear retention curve for the simulations of the first modelling stage with CODE_BRIGHT

For the evaluation of the modelling results there are in general two methods. First, the time evolution of the analysed quantity is considered in different points of the model which are shown in Fig. 4.3. Second, profiles of quantities are considered for different time steps and specified for every scenario individually.
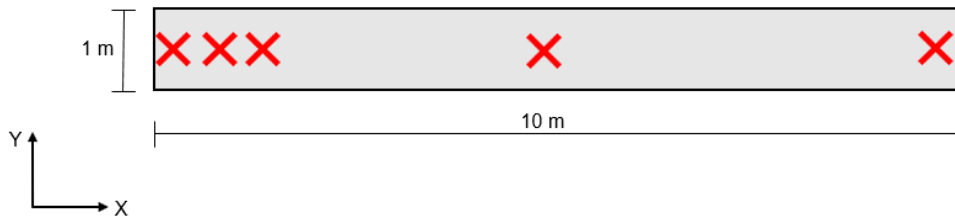

Fig. 4.3.   Points for time evaluation of analysed quantities in the first modelling phase. X-coordinates for the points with increasing distance to the left boundary of the model: 0.25 m, 0.75 m, 1.25 m, 5 m, 9.75 m. Y-coordinate for all points: 0.5 m

4.1   Basic scenario

In the basic scenario, single-phase flow is realized in a simple way due to assuming a full saturated model and permeable borders which are marked by the blue arrows in Fig. 4.4. Further, a mechanical stress is applied. The material parameters, initial and boundary conditions are presented in Tab. 4.1.
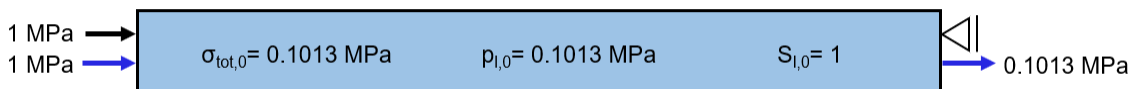
Fig. 4.4   Basic scenario for the 1st modelling phase

The assumptions for the initial state of the model are a saturation degree of 100 % and an initial stress and liquid pressure of 0.1013 MPa, which correlates to atmospheric pressure. On the left-hand side (lhs) of the model flooding is assumed and a mechanical stress of 1 MPa is acting, however, on the right-hand side (rhs) the boundary is permeable and displacements are not allowed. There are no changes in boundary conditions over the modelling time of 30 years.

Tab. 4.1   Material parameters for the basic scenario of the 1st modelling stage

Parameters			
Young's modulus	E	8,000	[MPa]
Poisson's ratio	v	0	[-]
Porosity	Φ	0.15	[-]
Intrinsic permeability	K	10^{-20}	[m²]
Biot coefficient	α	1	[-]
Liquid viscosity	η	10^{-9}	[MPa*s]
Liquid bulk modulus	$\breve{K}_l$	2,100	[MPa]

To evaluate the hydraulic processes the liquid pressure evolution is consulted (Fig. 4.5). In the beginning, the liquid pressure in the whole model increase rapidly from the initial pressure of 0.1013 MPa to 0.67 MPa due to the instantaneous mechanical stress resulting in a compaction of the model. In the following course, the inflow of liquid on the left boundary leads to a rise in pressure in the left part of the model. Close to the right border, the pressure decreases over time due to the possibility of outflow of liquid and approximates to the atmospheric pressure. The liquid pressure in the middle of the model remains constant over one year and then start to decrease, because of the equilibration process. Fig. 4.6 presents the equilibration of the liquid pressure in the model, starting from the boundaries. The gradient close to the model borders is very high in the beginning but reduces with time till 30 years when the equilibration process achieved a linear steady-state.

Regarding the mechanical reaction of the model, Fig. 4.7 shows the strain evolution with time. There is also a rapid increase in strains due to the elastic response of the material referring to the instantaneous mechanical stress. Because strains are calculated from the effective stresses, with ongoing time, the strain reduces in the left part of the model due to the increasing liquid pressure resulting in decreasing effective stresses. The other way around happens in the right part of the model (x = 9.75 m), the liquid pressure decreases with time leading to an increase in effective stresses and strains. Further, the strain in the right part increases due to the restriction in displacements. The development

of displacements shows a strong reaction on the mechanical load in the beginning of the modelling process and a further increase over time till a maximum displacement of 0.56 mm correlating to 0.056 ‰ is reached after 30 years (Fig. 4.8).

Considering the agreement of numerical results with analytical ones, it could be stated that they are in good accordance. Only small discrepancies are to be found which may results from numerical inaccuracies.
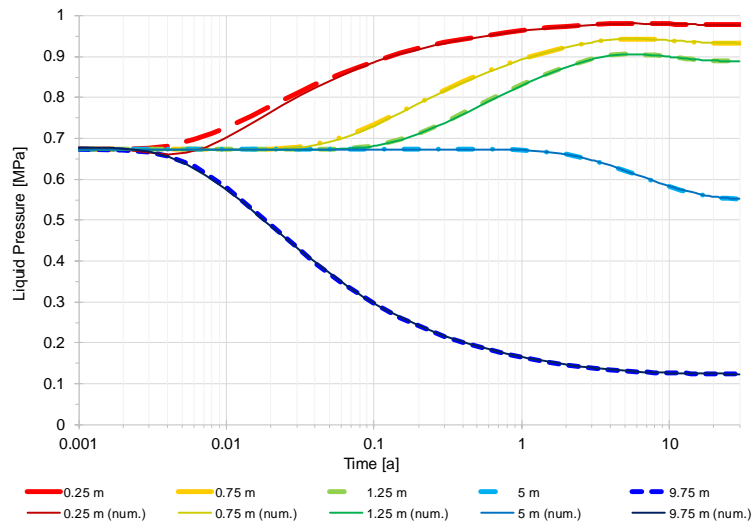

Fig. 4.5   Liquid pressure evolution for the basic scenario in the 1st modelling stage
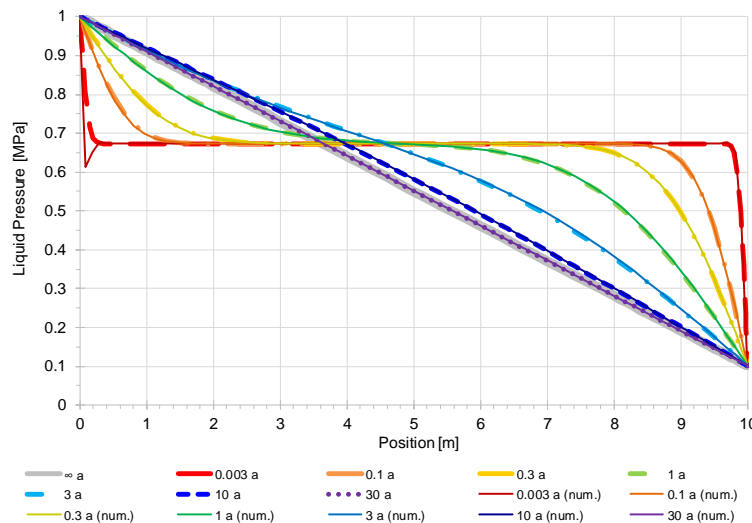
Fig. 4.6   Profiles of liquid pressure for the basic scenario in the 1st modelling stage
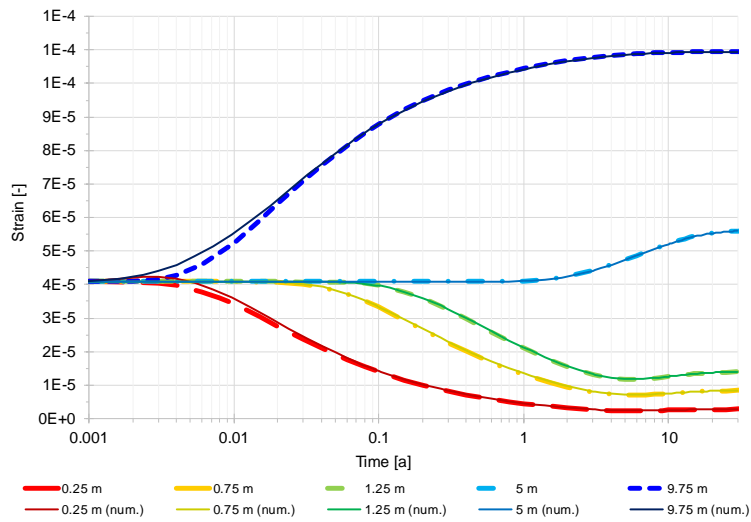
Fig. 4.7 Strain evolution for the basic scenario in the 1st modelling stage
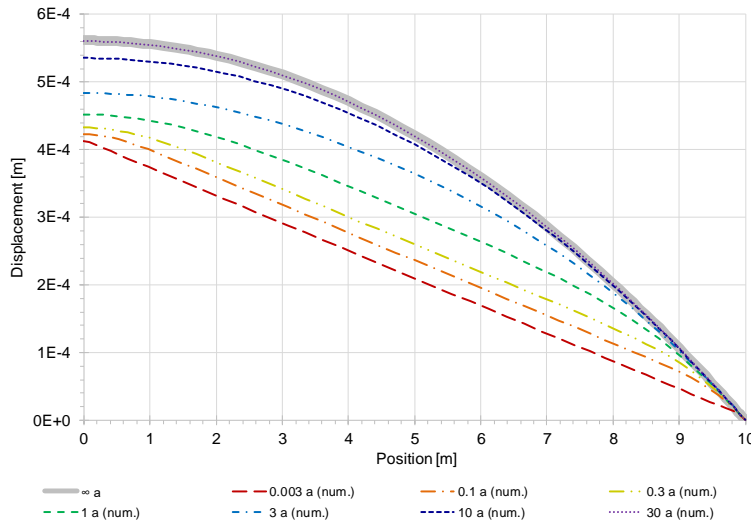
Fig. 4.8 Profiles of displacement for the basic scenario in the 1st modelling stage

4.2 Scenario variations

Seven scenario variations are elaborated. For simplifying the designation, the basic scenario is called scenario a and the variations are named with following letters. Further, for simplifying the handling of figures, the simulation runs are named with 1 for the first modelling phase plus the letter for the scenario.

4.2.1   Scenario b – softer material

In this framework, the mechanical behaviour is simulated by using linear elasticity following Hook's law which describes a proportional stress-strain-relationship. In this law the Young's modulus describes the stiffness as an elastic property depending on the material. For example, the Young's modulus of rock salt is about 25,000 MPa, for clay rock it is approximately 2,000 – 3,000 MPa and for crystalline rock much higher (> 40,000 MPa). However, there are cases in a repository where the Young's modulus is considerably lowered, e. g. in the excavation damaged zone or in the backfill material, having an important influence on the mechanical behaviour and the stability of the underground facility. This scenario should illustrate the influence of Young's modulus on material behaviour due to its decreasing to 150 MPa. For comparability, the initial and boundary conditions are equal to the basic scenario (Fig. 4.4).

The numerical results are in good accordance with the analytical calculations. The liquid pressure evolution (Fig. 4.9) shows some oscillations in the first 0.1 years of simulation time due to numerical issues. With reducing the stiffness, the material gets more compacted inducing an instantaneous rise in pore pressure to 1 MPa in the whole model. Up to 0.1 years the liquid pressure starts to reduce in the right part of the model (x = 9.75 m) due to the outflow of liquid. On the right border of the model, the gradient in liquid pressure is very high, however, it equilibrates with time (Fig. 4.11). The steady-state for liquid pressure is similar to the basic scenario ones.

Because of the great value range the strains in Fig. 4.10 are shown with logarithmic y-axis. Due to the instantaneous mechanical stress in the beginning, the strain rises to $5*10^{-5}$ which is slightly higher in comparison with the basic scenario ($4*10^{-5}$). The model behaviour follows the elastic law, means that with lowering the stiffness the strains become larger. With time the strains decrease within the first three evaluation points up to 70 years due to stress rearrangement and starts to increase again when liquid pressure dissipation starts.

The displacement of the model is nearly constant in the early simulation time (Fig. 4.12). With time the model becomes more compacted and the displacements increase. The maximum displacement of the model reaches a value of 3 cm correlating to 3 ‰. There is a good correlation of the results with the linear-elastic approach considering the basic scenario and the actual one, hence, the Young's Modulus was reduced by a factor of

~53 (from 8,000 MPa to 150 MPa) resulting in an increase in displacements by a factor of ~53.
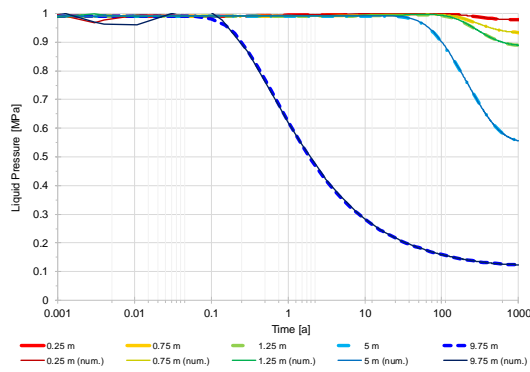
Fig. 4.9 Liquid pressure evolution for model 1b
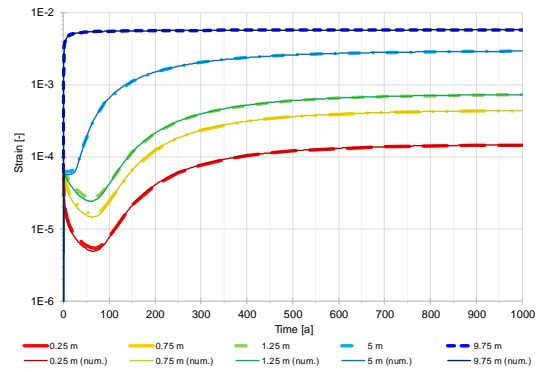
Fig. 4.10 Strain evolution for model 1b
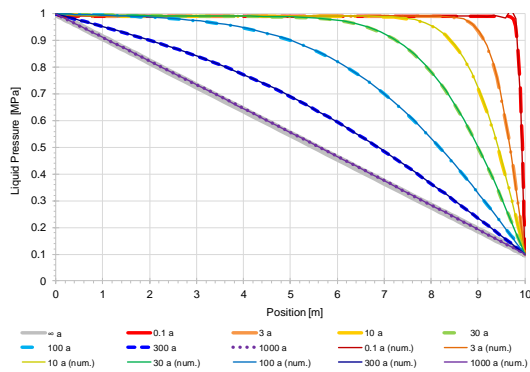
Fig. 4.11 Profiles of liquid pressure for model 1b
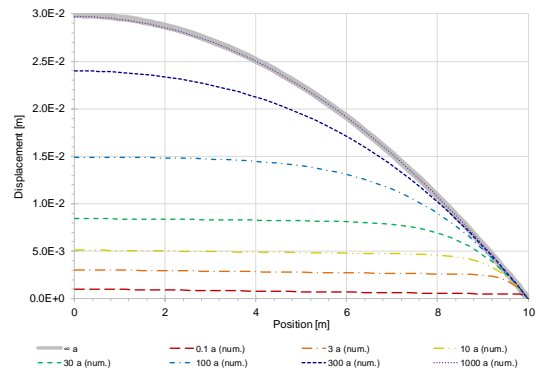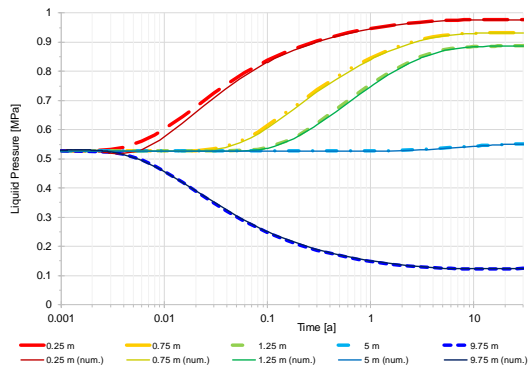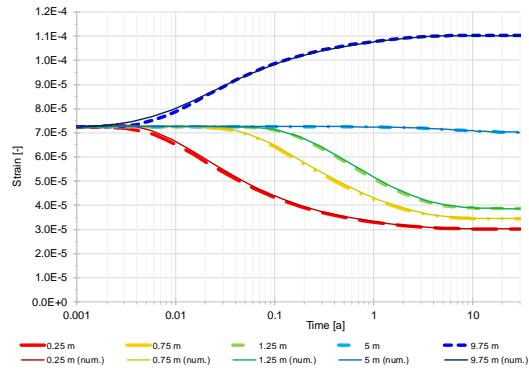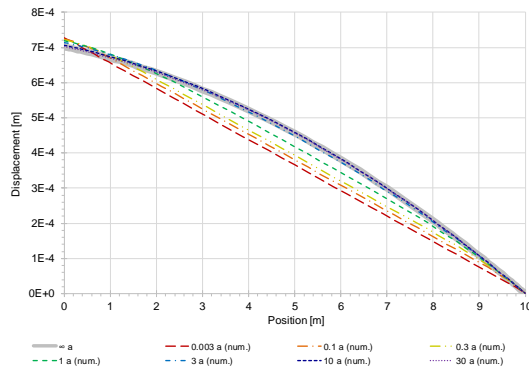

Fig. 4.12 Displacement profiles for model 1b

4.2.2 Scenario c – higher grain compressibility

In porous rocks, like clay, the mechanical and hydraulic material behaviour is closely linked to each other. The pore fluid has an important influence on the deformation behaviour of porous rocks having an apparent time-depending influence on the mechanical properties. For describing this behaviour Terzaghi developed in 1923 a one-dimensional consolidation theory which was later extended by Biot and co-authors to three dimensions. Following Terzaghi's theory of effective stresses /TER 43/ and the subsequent modification by Biot and Willis /BIO 1957/, Equation (3.9) was used in this modelling work.

In most cases, the adoption of $\alpha = 1$ is made assuming very low compressible particles and a skeleton with high compressibility. However, it is only valid for soft soils /BIO 57/.

Hence, the change in compressibility of grains should be investigated and the Biot's co-efficient is set to α = 0.75 in this scenario. For a consideration of Biot's theory in its entirety, the Biot modulus should be incorporated (3.11), however, it is not implemented in CODE_BRIGHT. To solve this issue the solid compressibility was iteratively adapted with a final value of $\kappa_s = 9.7*10^{-5}$ 1/MPa. For ensuring comparability, the initial and boundary conditions are equal to those in the basic scenario (Fig. 4.4).

The behaviour in this model is similar to the basic scenario, as there is a rapid increase in liquid pressure (Fig. 4.13) and strain (Fig. 4.14) due to the mechanical loading. However, the liquid pressure reaches a smaller value of 0.53 MPa compared to the basic scenario (0.68 MPa) and the strain becomes a value of $7.3*10^{-5}$ which is larger than the basic scenarios strain of $4.1*10^{-5}$. The minimized Biot coefficient in Equation (3.9) is resulting in a higher grain compressibility, reducing the influence of fluid pressure on mechanics and leading to an increase in effective stresses. This increase in stresses causes the higher strains in the model and resulting consequently in higher displacements (Fig. 4.16). Additional processes result from the change in Biot modulus which represents the possibility of higher pore fluid expansion due to the smaller grain compressibility resulting in a smaller liquid pressure build-up. Comparing Fig. 4.6 and Fig. 4.15 the quantitative difference in liquid pressure level and following the influence of grain compressibility becomes very clear, however, the steady state is similar in both cases.

Regarding the time evolutions for liquid pressure in this scenario (Fig. 4.13) and the basic scenario (Fig. 4.5) a different development in the model's middle can be observed. Up to one year the liquid pressure decreases in the basic scenario and slightly increases with higher grain compressibility. Since the analytical solutions are equal for the steady states in both cases, the liquid pressure in the middle of model 1c has to rise to reach the final linear distribution resulting from the lower instantaneous liquid pressure.

Altogether there is a good accordance between the numerical and the analytical results.
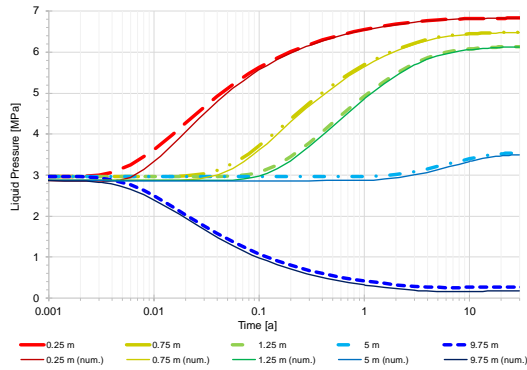
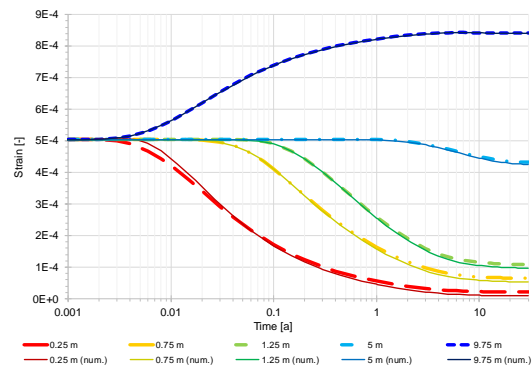**Fig. 4.13** Liquid pressure evolution for model 1c

Fig. 4.14 Strain evolution for model 1c
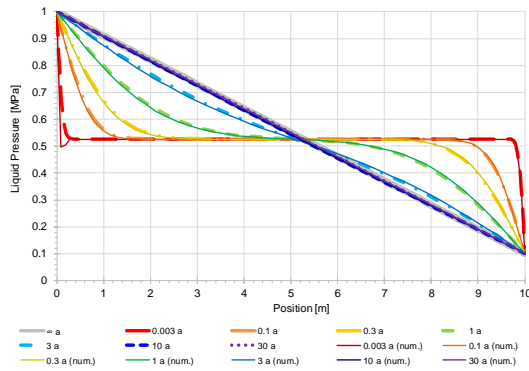

Fig. 4.15 Profiles of liquid pressure for model 1c

Fig. 4.16 Displacement profiles for model 1c

4.2.3 Scenario d – changed initial saturation

In natural and undisturbed state, the various host rocks have different hydraulic conditions: a claystone is mostly full saturated, a rock salt in Germany is considered to be dry and in crystalline rocks the rock matrix is nearly impermeable with respect to the water bearing fracture network. With interference in the natural state of the host rock due to excavation an affection of hydraulics and mechanics is induced. So, a claystone becomes unsaturated at the surfaces of the underground openings due to ventilation and a rock salt may become wet due to condensation of humidity entered by ventilation, both leading to partially saturated systems.

There are three components to be considered in an unsaturated medium: the solid, the liquid phase and the gaseous phase. As mentioned, due to the aim of starting very simple for ensuring the comparability with analytical results the gas phase was set constant and

only one-phase flow of the liquid phase is considered here. Therefore, this scenario provides changes in the initial degree of saturation and the applied stress state in comparison with the basic scenario. The system is partially saturated with a degree of 99.8 % which is very close to full saturation. The initial stress state is equal to atmospheric pressure, however, as boundary condition a stress and a liquid pressure of 7 MPa are applied (Fig. 4.17).

7 MPa

7 MPa

$\sigma_{tot,0}= 0.1013$ MPa $S_{l,0}= 0.998$ $S_l = 0.998$

Fig. 4.17   Initial and boundary conditions of model 1d examining the change of initial saturation degree

The processes considered here are closely linked to the basic scenario ones. With bringing up a mechanical stress an instantaneous reaction in liquid pressure and in strain is detected (Fig. 4.18, Fig. 4.19). Due to the very high initial saturation the model becomes fully saturated because of the mechanical compaction and a liquid pressure builds-up. Ongoing the shapes of the graphs are quantitatively like those of the basic scenario due to the mostly same occurring processes, however, under different boundary conditions. Considering the liquid pressure and strain curve in the middle of the model (x = 5 m) and comparing with the basic scenario ones, different slopes develop after 2 years. Here, the liquid pressure rises because the amount of liquid flowing into the model is higher than flowing out of the model which is the other way around in the basic scenario. The strain evolution follows the liquid pressure change.

Of course, the raised pressure conditions cause higher displacements compared to the basic scenario. The maximal displacement is approximately one magnitude of order higher; it is about 5 mm (Fig. 4.21).

The steady-state of liquid pressure is reached after 30 years. Altogether the values for liquid pressure, strains and displacements are higher than in the basic scenario resulting from the higher pressures in boundary conditions.

There are discrepancies in the accordance of the numerical and analytical results. As mentioned above CODE_BRIGHT needs the specification of a retention curve due to its poromechanical approach. Hence, the liquid pressure is changing in dependence of saturation. The approach for this model is simplified due to a linear retention curve which

leads to small errors in the numerical simulation. However, the shapes of liquid pressure and strain curves are in good accordance with the analytical results. Regarding the displacements (Fig. 4.21) further inconsistencies are detected which are assumed to result from the retention curve approach, too.

Fig. 4.18   Liquid pressure evolution for model 1d

Fig. 4.19   Strain evolution for model 1d
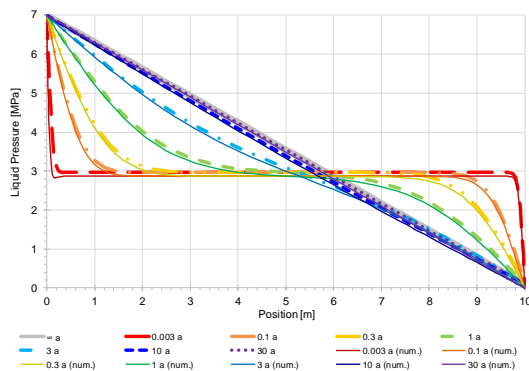
Fig. 4.20   Profiles of liquid pressure for model 1d
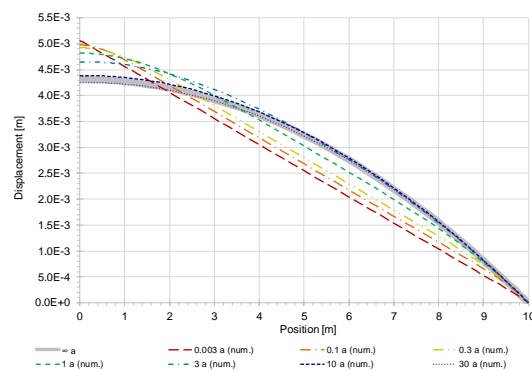
Fig. 4.21   Displacement profiles for model 1d

4.2.4   Scenario e – unified mesh discretization

For investigation of the basic processes, first, the implemented constitutive laws should be examined, however, there are further factors influencing the numerical results, e. g. the mesh discretization of the model. For an estimation of this factor, a unified discretization is defined (Fig. 4.22). The initial degree of saturation is set to 0.3 (p_l = -0.007 MPa) for a further investigation of partially saturated systems and the initial stress is equal to atmospheric pressure. The boundary conditions are the same as in scenario d, an applied stress and a liquid pressure of 7 MPa.
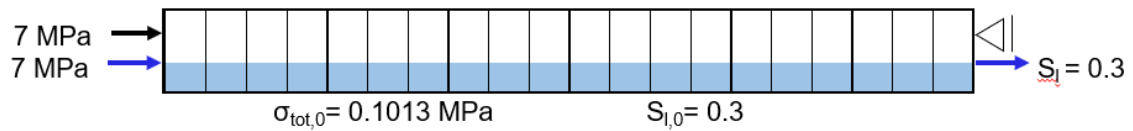
Fig. 4.22 Mesh discretization, initial and boundary conditions for model 1e investigating partially saturated systems using a unified mesh discretization

Because of the complexity in this scenario no analytical solution is available. Further, for a clearer investigation of the processes in the early time, additional plots with a time frame of 100 years are shown.

With bringing up the mechanical stress, the model gets instantaneous elastically compacted resulting in a rapid increase in strain to a value of $9*10^{-4}$ (Fig. 4.27, Fig. 4.28). The compaction and the inflow of liquid lead to an increase in saturation and to full saturation in the first three zones within of 100 years (Fig. 4.23). Due to the liquid flow from the left boundary there is a steady input of water which can pass the model only very slowly, as the permeability is very low. Hence, a liquid pressure builds up reducing the effective stresses followed by decreasing strains and displacements (Fig. 4.27, Fig. 4.28). The temporal dependence between liquid pressure increase and strain decrease can be modelled quite good (Fig. 4.25, Fig. 4.27). However, the progression of liquid pressure and strain happens stepwise which is a clear effect of the coarse mesh.

There is a clear temporal dependence between saturation and liquid pressure: if the pores inside a material are only partially filled with liquid the corresponding pressure for liquid is a suction stress, hence, a negative liquid pressure. When the pores are fully filled with liquid, the saturation degree is one and the liquid pressure becomes positive. Considering Fig. 4.24 and Fig. 4.26 this dependence could not be observed. The liquid pressure for the evaluation point $x = 0.75$ m becomes positive after 12 years, however, the saturation degree is about 65 %. This issue appears for all considered points. In CODE_BRIGHT the quantity liquid pressure is calculated in the nodes, whereas, the degree of saturation is calculated elementwise by averaging the nodal liquid pressures. Due to the very coarse mesh discretization, the liquid pressure gradient within an element is very large leading to a not neglectable failure in liquid saturation. A further discussion on this topic is to be found in Chapter 4.3.
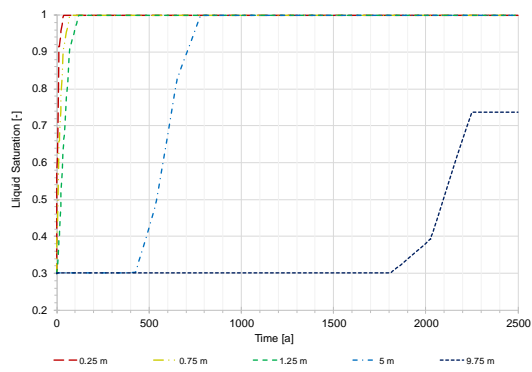
Fig. 4.23   Liquid Saturation for model 1e
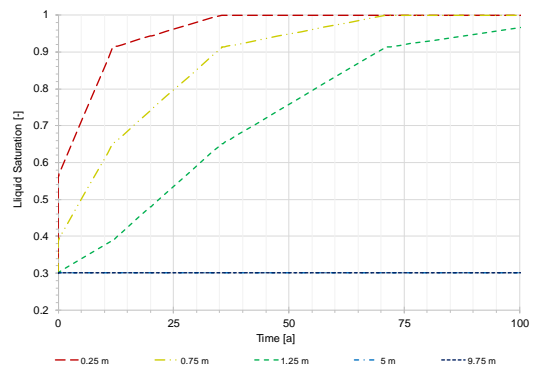
Fig. 4.24   Liquid saturation till 100 years for model 1e
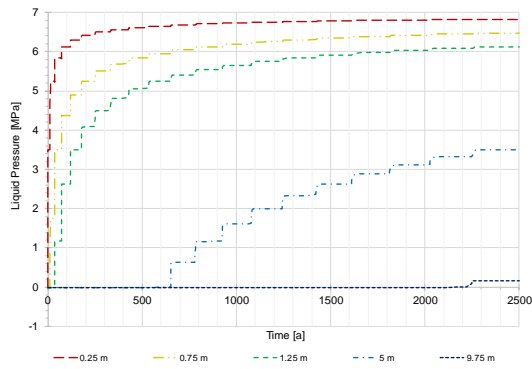
Fig. 4.25   Liquid pressure for model 1e
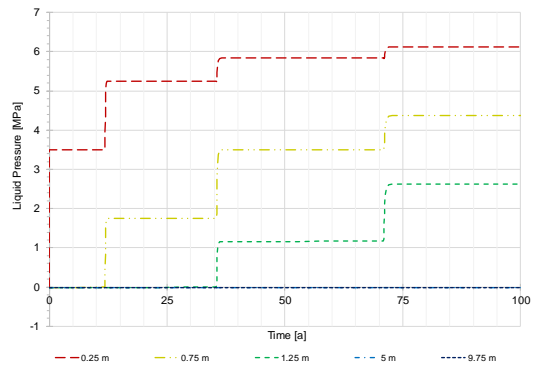
Fig. 4.26   Liquid pressure till 100 years for model 1e
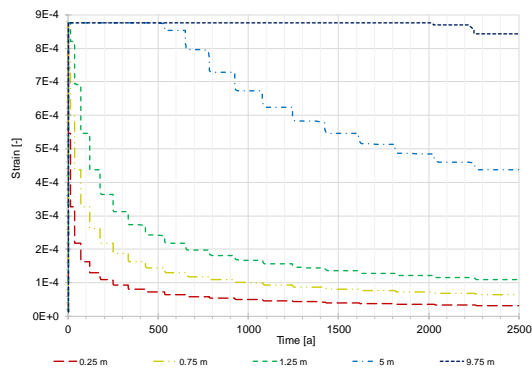
Fig. 4.27   Strain evolution for model 1e
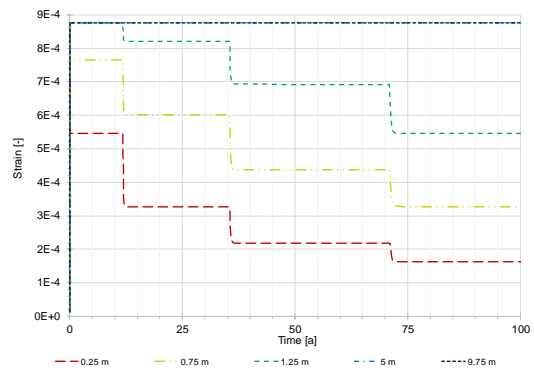
Fig. 4.28   Strain evolution till 100 years for model 1e

4.2.5 Scenario f – user-specified mesh discretization

In the previous scenario, a unified mesh discretization was used. To investigate a direct influence of the mesh discretization on the results this scenario is equal to the previous one, but with user-specified discretization. Fig. 4.29 shows the mesh discretization used by GRS which consist of 1,000 nodes and 1,000 elements. This very fine mesh discretization was chosen for having an effect as large as possible. The initial and boundary conditions are taken from the previous scenario (Fig. 4.22).

Nodes: 1,000   Elements: 1,000
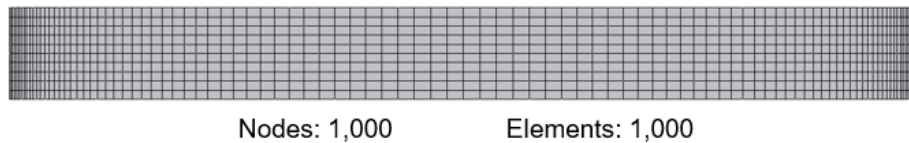
Fig. 4.29   GRS' mesh discretization for model 1f

In Fig. 4.30 - Fig. 4.32, the direct differences in numerical results due to mesh discretization are shown. Especially in the comparison of time evolutions for liquid pressure and strain, a smoothing of the curves with finer mesh discretization can be observed, thus, the steps in the graphs are clearly caused by the coarse mesh discretization. Qualitatively, the evolutions of liquid pressure and strain show good accordance between both scenarios.

There are clear differences between both developments of liquid saturation with time (Fig. 4.30). Whereas the model remains unsaturated in x = 9.75 m for the coarse mesh, a full saturation is reached with the finer mesh. Additionally, the points in time for the begin of saturation increase and reaching full saturation are different in all evaluation points. The deviations in liquid saturation results from the numerical calculation of this quantity in CODE_BRIGHT, however, they become smaller due to the diminished element sizes.

A closer discussion referring this topic is done in chapter 4.3. Altogether, there are obvious influences of the mesh discretization on the simulation results.
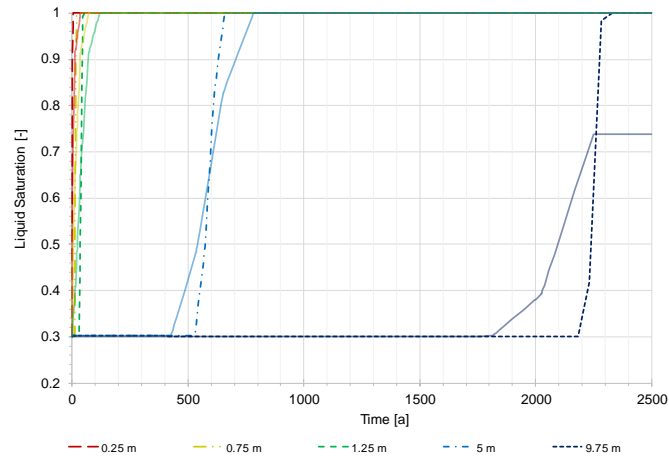
Fig. 4.30   Comparison for the liquid saturation evolution for scenario e with unified mesh discretization (continuous lines) and scenario f with user-defined mesh discretization (dotted lines)
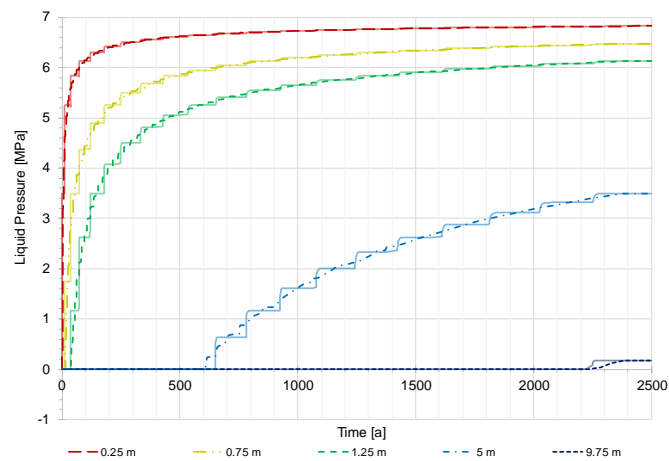
Fig. 4.31   Comparison for the liquid pressure evolution for scenario e with unified mesh discretization (continuous lines) and scenario f with user-defined mesh discretization (dotted lines)
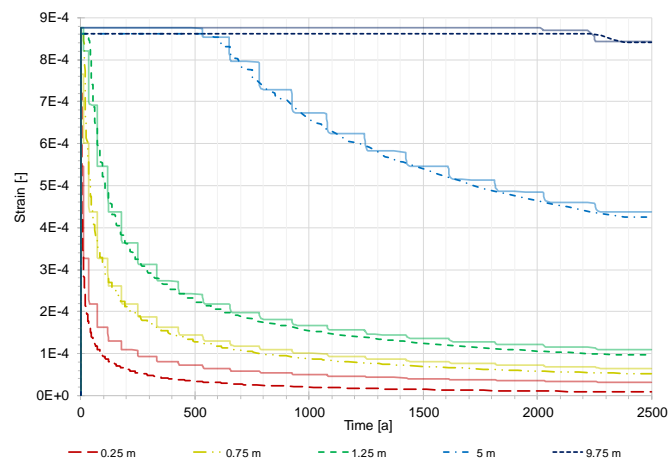
Fig. 4.32   Comparison for the strain evolution for scenario e with unified mesh discretization (continuous lines) and scenario f with user-defined mesh discretization (dotted lines)

25

4.2.6 Scenario g – including process couplings

As mentioned, GRS has to assume a retention curve due to problems in the application of CODE_BRIGHT referring the simplification of neglecting phase interactions. To give the possibility for GRS to calculate a scenario without this adoption, phase interactions are permitted here, and a retention curve is specified (Appendix A). For evaluating the effects, the same initial and boundary conditions as in scenario f should be considered, however, a gas phase is added (Fig. 4.33). For further comparability the same mesh discretization is chosen (Fig. 4.29).
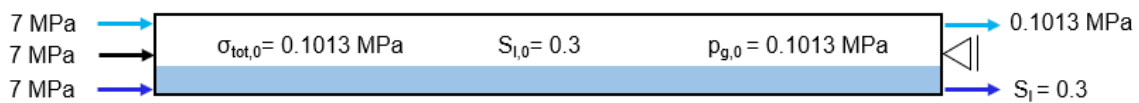
Fig. 4.33   Initial and boundary conditions for model 1g

First, a mechanical response to the instantaneous stress could be seen in the evolution of strains (Fig. 4.38) leading to a displacement of 0.005 m after 0.2 years (Fig. 4.39). Following the poromechanical approach, the initial saturation of 0.3 leads to a suction stress of -46.96 MPa. The positive fluid pressures on the left model border initiate inflow of liquid and gas in the model, thus the fluid pressure rises (Fig. 4.34, Fig. 4.35). With increasing amount of liquid, the saturation increases, too, resulting in a nearly full saturated model (Fig. 4.36, Fig. 4.37).

Following the basics of the poromechanical approach, a positive liquid pressure in a system is only possible, if it is fully saturated. In a partially liquid saturated system a negative liquid pressure, called suction, prevails, consequently the initial saturation of 0.3 leads to a suction stress of about – 46.96 MPa in the whole model. Due to the positive pressure on the left boundary, a liquid inflow is initiated, resulting in an increase in saturation and in liquid pressure (Fig. 4.34, Fig. 4.36). With time, the model becomes saturated, however, the constant saturation of 0.3 on the right model border leads to an outflow of liquid and consequently prevents a full saturation of the model (Fig. 4.37). Over time, the strains are decreasing due to relaxation and an increase in liquid pressure inside the model reducing the effective stresses. Due to the outflow boundary condition on the left border, there is still a partially saturated part. Since the capillary pressure is equal to zero for a full saturated state, the fluid pressures equalize and show the same values.
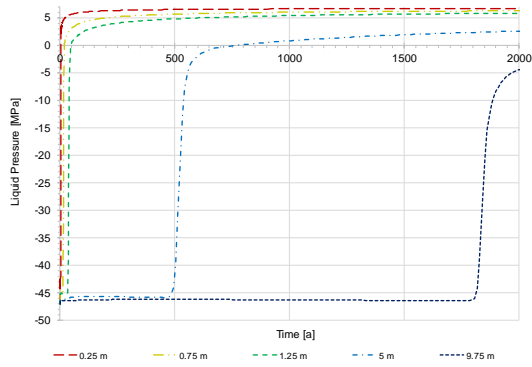
Fig. 4.34 Liquid pressure evolution for model 1g
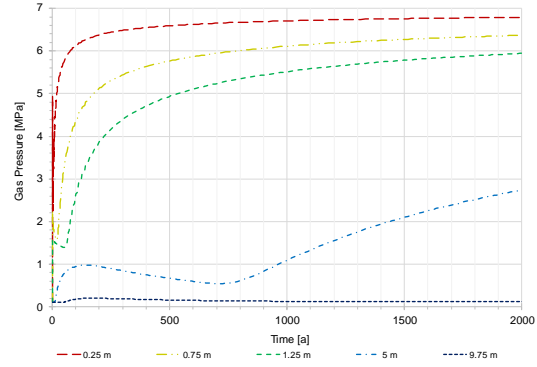
Fig. 4.35 Gas pressure evolution for model 1g
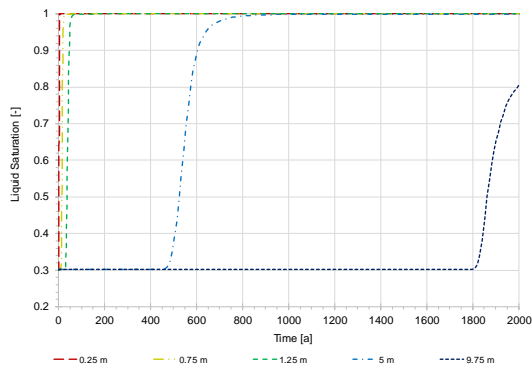
Fig. 4.36 Liquid saturation evolution for model 1g
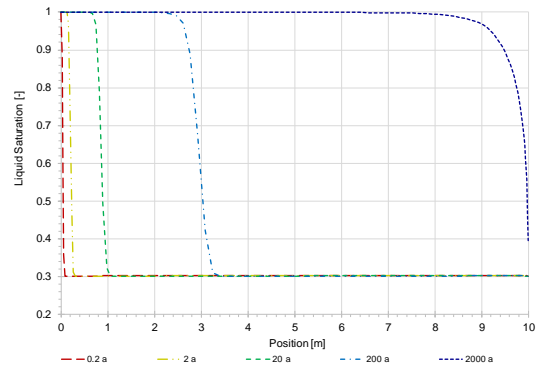
Fig. 4.37 Profiles of liquid saturation for model 1g
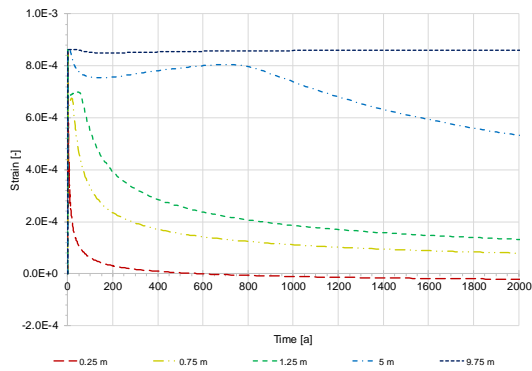
Fig. 4.38 Strain evolution for model 1g
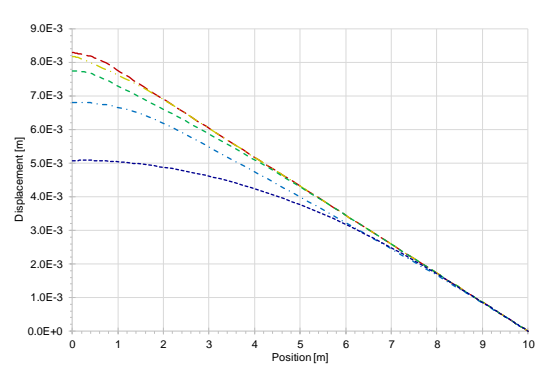
Fig. 4.39 Displacement profiles for model 1g

For a better comparison between the neglection and the examination of phase interactions the axis for the quantities dependent on time are adjusted in Fig. 4.40 - Fig. 4.42. The quantitative shapes of liquid pressures have a good agreement for the evaluation points 0.25 m and 0.75 m. For 1.25 m and 5 m there are some differences, especially in the steady-state which is lower for the simulation with phase interactions. Comparing the degrees of saturation for both simulations in Fig. 4.41, the saturation degree in point

27

9.75 m shows differences, hence, it is full saturated when neglecting phase interactions and still partially saturated including them. Additionally, the transition from nearly saturated to full saturated state is softer (point 5 m in Fig. 4.41). Other differences are shown by comparing the strain evolutions in Fig. 4.42. The reaction on the initial mechanical boundary condition is less distinctive in the first evaluation points for the simulation using a retention curve, since the maximum values are about $6.8*10^{-4}$ instead of $8.6*10^{-4}$. In x = 5 m, the strain evolution is totally different for both simulations as well as in the course and in the values. The maximal strain on the right model border is nearly equal in both simulations, however, there are small differences in the courses. The discussion about these differences can be found in chapter 4.3.
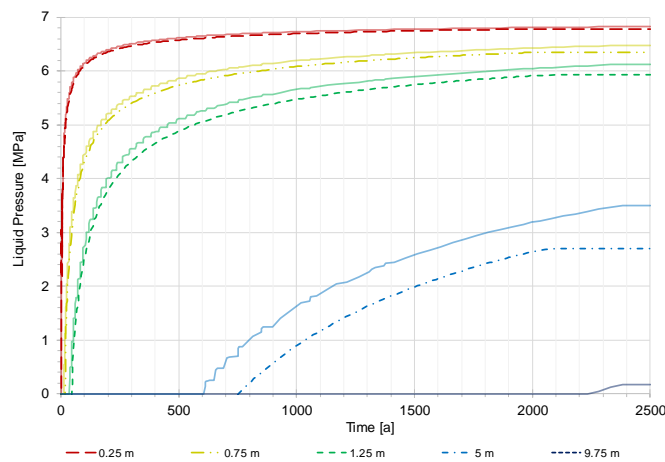
Fig. 4.40 Comparison of liquid pressure evolution for scenario f neglecting phase interactions (continuous lines) and scenario g including two-phase flow (dotted lines)
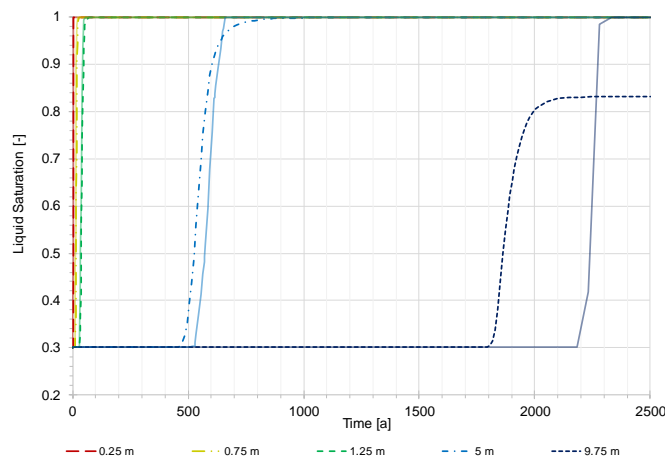
Fig. 4.41 Comparison of liquid saturation evolution for scenario f neglecting phase interactions (continuous lines) and scenario g including two-phase flow (dotted lines)
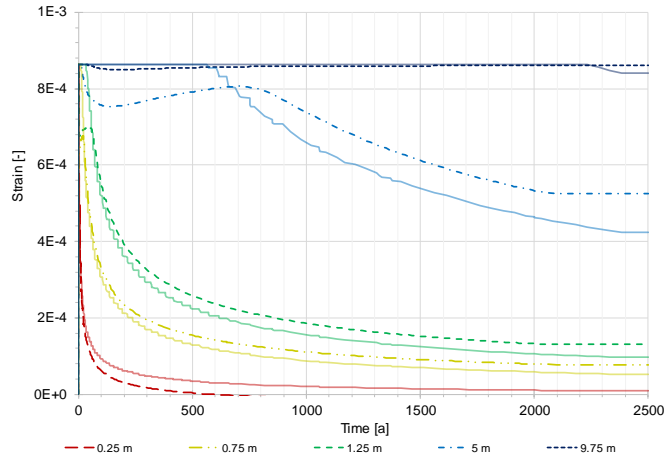
Fig. 4.42   Comparison of strain evolution for scenario f neglecting phase inter-actions (continuous lines) and scenario g including two-phase flow (dotted lines)

4.3   Discussion

In the previous chapter, all modelling scenarios for the first modelling phase are shown. Because of the simplified approach, GRS had to adopt a linear retention curve for nearly all scenarios, which may lead to inaccuracies in the simulation results.

For changing mechanical parameter, like Young's Modulus, the results are in good accordance with previous expectations. However, when changing the Biot coefficient CODE_BRIGHT provides no good results, firstly. Fig. 4.43 shows preliminary results for the liquid pressure distribution inside the model and

Fig. 4.44 shows the final results. In the first simulation of this scenario only the Biot coefficient in the linear elastic law was reduced. Decreasing the Biot coefficient leads to an increase in grain compressibility and further in a higher compaction due to the mechanical stress. Hence, the space for liquid in the pores becomes smaller and the liquid pressure is rising. However, an important part of Biot's theory is missing in this simulation: the reduction of the Biot modulus (3.11). It considers the interaction between liquid and increased grain compressibility in which the liquid pressure rises slower due to the higher grain compressibility. The hydraulic part of Biot's theory is not yet implemented for linear elasticity in CODE_BRIGHT, hence, an adaption over fitting the solid compressibility was done. This procedure is applicable because of the full saturation, however, is not useful for partially saturated systems.

29
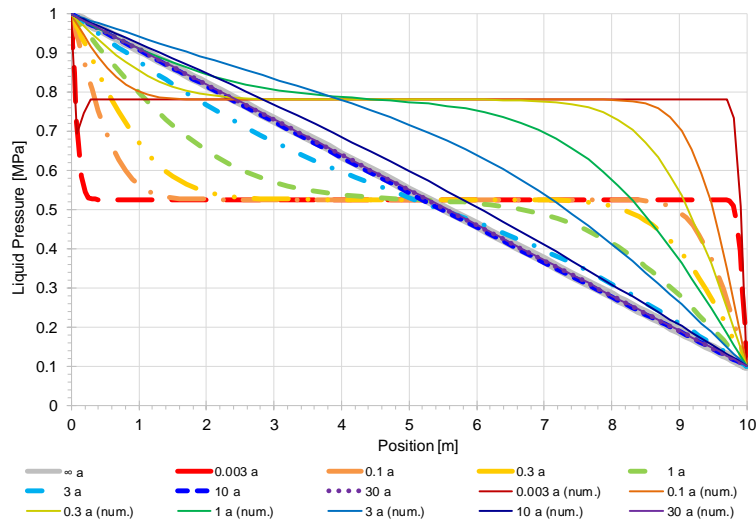
Fig. 4.43   Comparison of analytical solutions with numerical results (num.) for liquid pressure profiles in model 1c before adaption of Biot theory
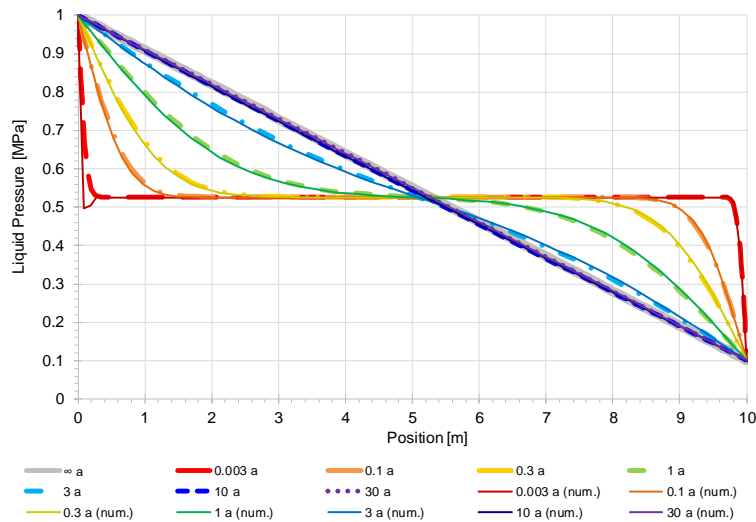
Fig. 4.44   Comparison of analytical solutions with numerical results (num.) for liquid pressure distribution in model 1c after adaption of Biot theory

In chapter 4.2.5, the influence of the mesh discretization on simulation results was investigated and clear impacts are found. The time evolution of liquid saturation is considered for a unified coarse discretization and a finer user-defined discretization (Fig. 4.30), therefore a different behaviour for the last evaluation point was detected. Since the saturation for the finer mesh was 100 %, it was only about 73 % for the coarse mesh. The similarity for the coarse and the fine mesh discretization is the saturation degree of 65 % for the last element, whereas the rest of the model is full saturated. The difference is dedicated to the location of the evaluation point x = 9.75 m related to the mesh discretization. For the simulation with unified mesh discretization the evaluation point lies in the

last element, whereas in GRS' mesh discretization the point is located in the 10th last element (Fig. 4.45).
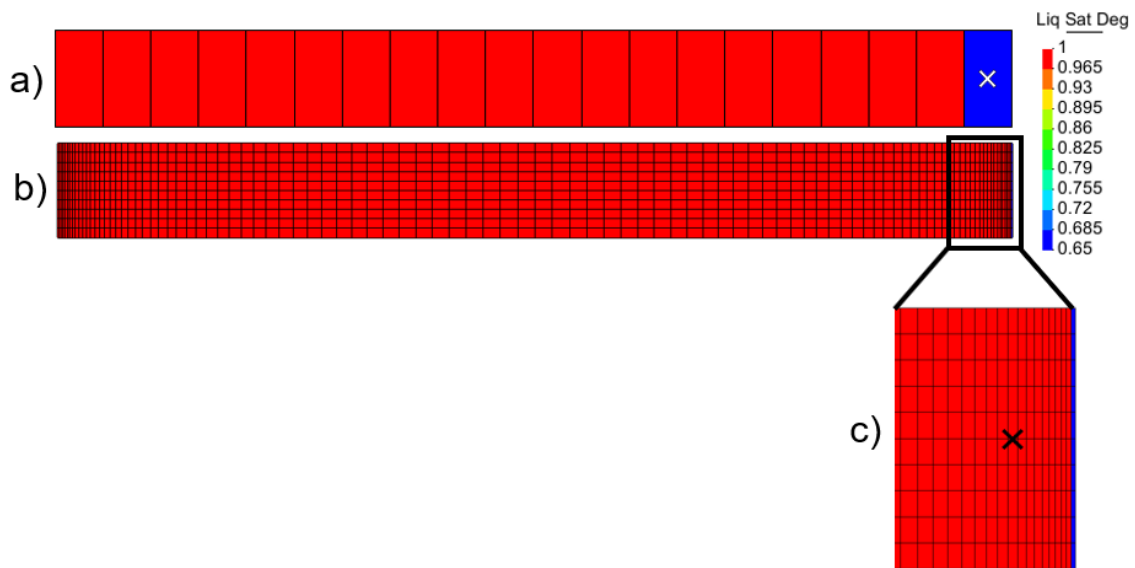
Fig. 4.45   Plots for liquid pressure distribution after 2,500 years in a) the model with unified mesh discretization, b) the model with GRS' mesh discretization and c) a detail of the right model border with GRS' mesh discretization and marked evaluation point in x = 9.75 m

In CODE_BRIGHT, liquid pressure is calculated as a nodal value, whereas liquid saturation is calculated element-wise due to averaging the nodal pressures corresponding saturations. Fig. 4.46 shows exemplary the calculation of saturation for the last element of the unified mesh discretization at 2,500 years. On the left border of the element a positive liquid pressure was calculated resulting in a saturation degree of 1. Contrary, on the right element border the hydraulic boundary condition prevails, fixing a liquid pressure of – 0.007 MPa leading to a saturation of 0.3. Averaging these saturation values for the evaluation point 9.75 which is located in the middle of the element results in a degree of saturation of 0.65. The same process is done for the last element of GRS' discretization, however the finer mesh leads to a more precise determination of the unsaturated area in the model.
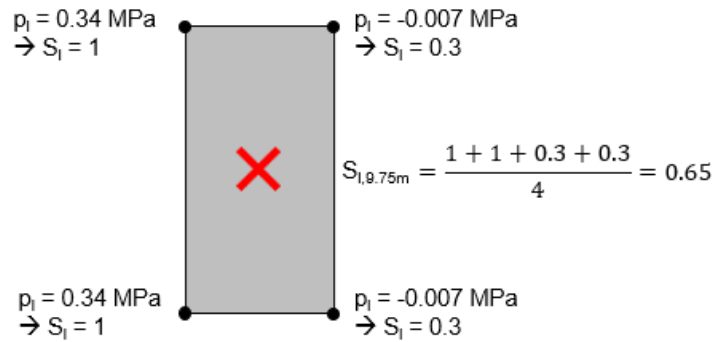
Fig. 4.46 Exemplary calculation of liquid saturation degree in CODE_BRIGHT for the last element of the unified mesh discretization at 2,500 years

Another comparison was done in chapter 4.2.6 due to correlating the simplified approach with the use of a van Genuchten retention curve. It has to be mentioned that conditions for a second fluid phase have to be added reducing the comparability of these two simulation scenarios. When using the linear retention curve the gas pressure is set to zero whereas in the van Genuchten approach a gas pressure was prescribed. A direct comparison of the initial conditions for the scenarios concerned is shown in Fig. 4.47. There are big differences in the negative liquid pressures applied, however, the modelling results are in good accordance as shown in Fig. 4.40 - Fig. 4.42 leading to the conclusion that a simplified consideration of fluid processes is suitable for a first estimation of results, but for a fundamental prediction the phase couplings have to be investigated.
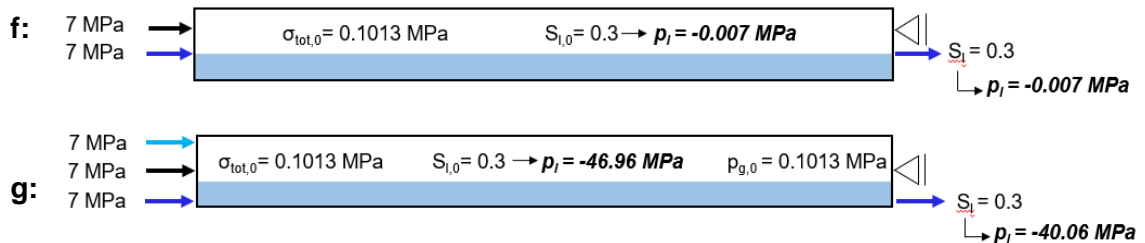
Fig. 4.47 Comparison of modelling conditions for scenario f and g in the first modelling phase

By comparing the simulation results with the project partners, differences in the calculation of strains and displacements are found for model 1g (Fig. 4.48). In CODE_BRIGHT the definition for effective stresses following Equation (3.12) is given for linear elasticity by default. In this benchmarking, the definition for effective stresses following Bishop (Eq. (3.9) was prescribed. When applying the default option, the model underlies a strong compaction in response to the instantaneous mechanical stress which is reduced with time. With applying the Bishop definition, the instantaneous compaction is the same and

compaction is also reduced with time, however, the model changes from compaction to extension meaning it is blown up by the fluids.
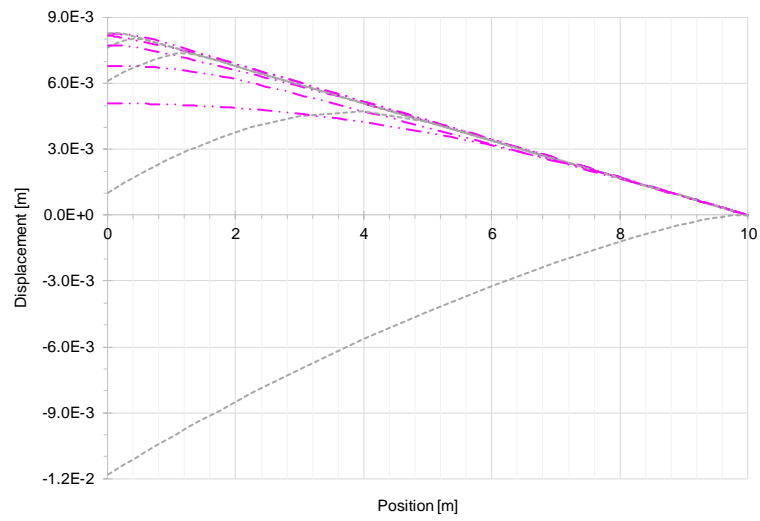
Fig. 4.48 Comparison of GRS' displacement profiles (pink) and project partner ones (grey) for model 1g at t = 0.2a, 2 a, 20 a, 200 a, 2,000 a.

5   2nd modelling phase – two phase flow

In the next stage of modelling work, a second fluid phase was added for becoming more realistic and simulating the interactions between gas and liquid phase inside the repository system. During the construction stage, the gas phase is assumed to be air, containing dry air and a certain proportion of dissolved water vapour, however, after disposal of radioactive waste there may be chemical processes in the repository, e. g. between the metal of the waste container and the host rock's porewater, leading to gas formation. Due to the additional gas volume a pressure may be build up, affecting the behaviour of the system and possibly causing fracturing of the host rock. Further, if there is a second fluid phase next to the liquid, a suction pressure exists, leading to a liquid flux.

Following the principle of investigating the basic processes, here, these phenomena are considered in a simplified way. Fig. 5.1 shows the geometry and processes of model no. 2 which are nearly equal to the previous model, however, the gas phase has been added.
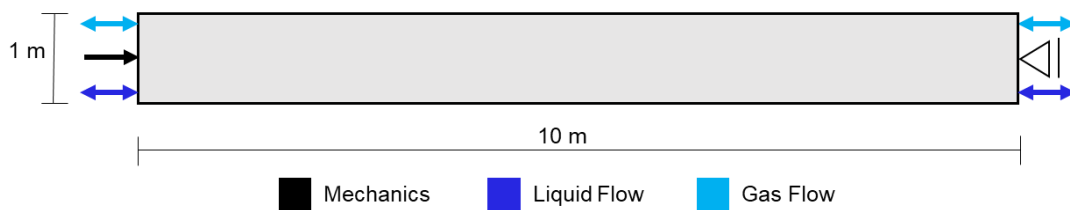
Fig. 5.1   Model geometry and considered processes in the 2nd modelling phase

Also, in this model, scenarios with the simplified approach of neglecting phase interactions were foreseen. Even if assuming a flat-linear retention curve was successful for the first modelling phase, this approach was not convenient for this stage that is why only models regarding a relationship between the two fluid phases due to a retention curve are simulated with CODE_BRIGHT and part of this report. The associated retention curve is shown in Appendix A. The evaluation points for the analysed quantities with time are equal to Fig. 4.3.

5.1   Basic scenario

In the basic scenario, simulation of two-phase flow was realized by assuming a partial saturated model and permeable boundaries. The hydraulic field is coupled with a me-

chanical stress applied on the right border of the model (Fig. 5.2). The material parameter, initial and boundary conditions are presented in Tab. 5.1. There is no change in boundary conditions over the simulation time of 100,000 years. The model is assumed to show backfill material inside a disposal drift.
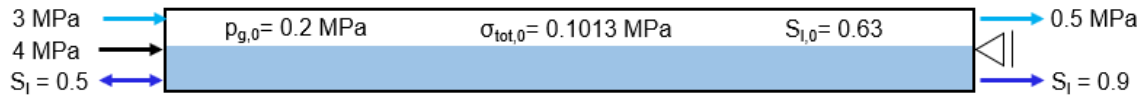
Fig. 5.2   Initial and boundary conditions for the basic scenario in the 2nd modelling phase

The assumptions for the initial state of the model are a liquid saturation of 63 % correlating to a suction pressure of -13.63 MPa, a gas pressure of 0.2 MPa and a mechanical stress of 4 MPa. At the left border of the model, a saturation of 50 % (p_l = -16.58 MPa), a gas pressure of 3 MPa and a mechanical stress of 4 MPa are assumed. The displacements on the right model border are not permitted, a gas pressure of 0.5 MPa is fixed and a saturation of 90 % (p_l = -4.89 MPa) is expected.

Tab. 5.1   Material parameters for the base scenario of the 2nd modelling phase

Parameters			
Young's modulus	E	650	[MPa]
Poisson's ratio	ν	0	[-]
Porosity	Φ	0.33	[-]
Intrinsic permeability	K	$2.5*10^{-21}$	[m^2]
Biot coefficient	α	1	[-]
Liquid viscosity	η	10^{-9}	[MPa*s]
Liquid bulk modulus	$\breve{K}_l$	2,200	[MPa]
Residual liquid saturation	S_{lr}	0.02	[-]
Residual gas saturation	S_{gr}	0	[-]
Van Genuchten parameter	λ	0.5	[-]
Van Genuchten pre-factor	$p_{cap,0}$	11	[MPa]
Pore connectivity parameters	$\tilde{\varepsilon}, \tilde{\gamma}$	0.5	[-]

Considering Fig. 5.3 and Fig. 5.5, in early time (<0.1 years) the specified initial conditions for gas pressure and liquid saturation are met. Due to the boundary conditions on the left model border an inflow of gas is initiated and gas pressure starts to rise in the first evaluation point (x = 0.25 m) after 0.2 years. With time the gas pressure increases in the whole model and reaches a maximum of nearly 3 MPa. The pressure behaviour in point x = 9.75 m is influenced by the right-hand side boundary condition inducing an outflow of gas which can be observed in Fig. 5.4 due to the high gradient in the right part of the

model. With gas entering the model and the additional saturation boundary conditions on the borders a liquid flow is induced from the right to the left border. With the outflow of liquid and the increasing fraction of gas, the liquid saturation is decreasing in the first three evaluation points. The liquid flow starts about 0.1 years later than the gas flow implicating the interaction between the two fluid phases. The saturation in the middle of the model remains nearly constant for about 200 years, then decreases slightly followed by a rapid increase. This behaviour can be observed in the first three curves, too. When gas pressure remains constant, the liquid saturation begins to equilibrate leading to an increase which could be seen in Fig. 5.6.

For showing the influence of the instantaneous initial stress in Fig. 5.8 a detail of the displacement evolution with time is presented. The deformation as a consequence of elastic material response is about $9*10^{-5}$ m which correlates to $9*10^{-6}$ %. The displacement of the model is negative which is suggested as an extension of the model due to the gas inflow. With time the extension to the left side increases till a maximum of $5.39*10^{-2}$ m is reached (Fig. 5.9).
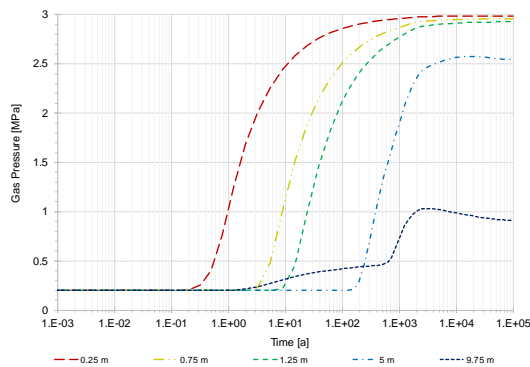
| **Fig. 5.3** | Gas pressure evolution for the basic model of phase 2 |
| **Fig. 5.4** | Profiles of gas pressure in the basic model of phase 2 |

| **Fig. 5.5** | Liquid saturation evolution for the basic model of phase 2 |
| **Fig. 5.6** | Profiles of liquid in the basic model of phase 2 |
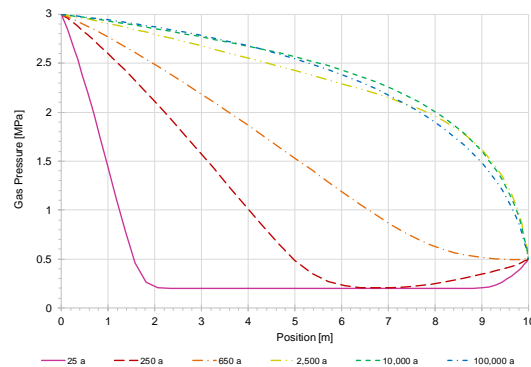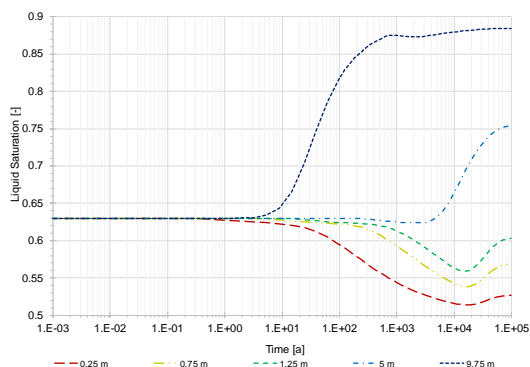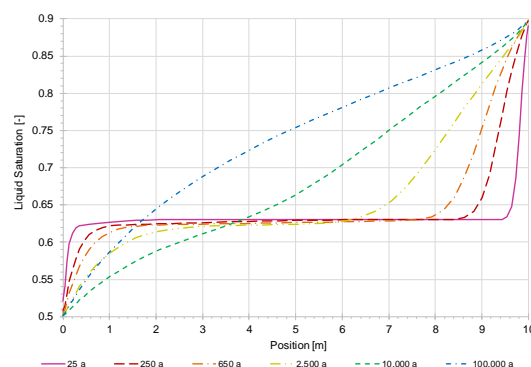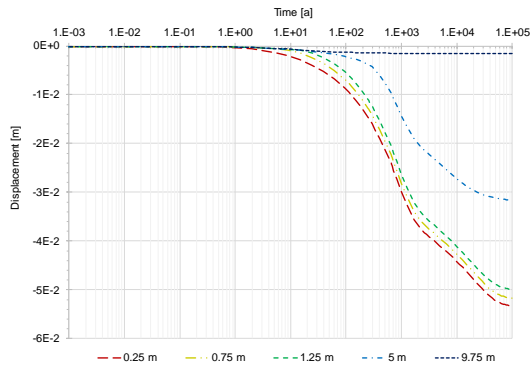
Fig. 5.7   Displacement evolution for the basic model for phase 2
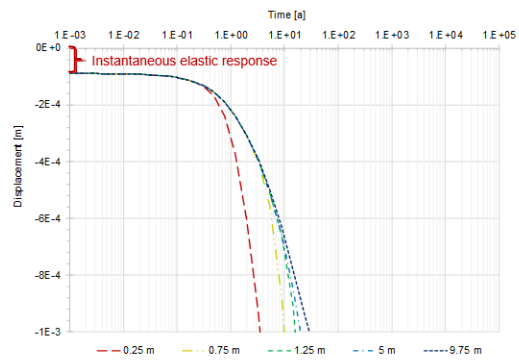
Fig. 5.8   Detail of initial model displacement for the basic scenario of phase 2
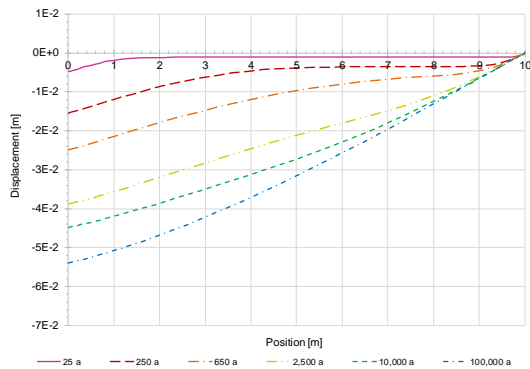
Fig. 5.9   Displacement profiles in the basic model of phase 2

5.2   Scenario variations

Three scenario variations are presented in the following section. For differentiation of the scenario variations the same procedure as in the previous chapter for modelling phase one was applied.

5.2.1   Scenario b – changed boundary conditions after 10,000 years

The conditions inside a repository system did not remain stable over the whole consideration period. During the construction phase, the drifts and shaft will be ventilated which leads to a desaturation of the near-field area in the host rock and a re-saturation after backfilling and closing. Due to chemical interactions between the metal of waste canisters and the host rocks pore water, gas is built up changing the gas pressure inside the system. The excavation of the repository area influences the primary stress state of the

host rock leading to instantaneous high stresses which are reduced with time due to stress rearrangements and later due to backfilling and closing.

In this scenario a change of conditions should be simulated exemplary, however, the addressed changes develop in situ over a longer time period and not as rapid as it is assumed here. The initial state of this model is equal to the basic scenarios (Fig. 5.2), however, the boundary conditions are changing after 10,000 years. Fig. 5.10 shows the changed boundary conditions.

Fig. 5.10   Boundary conditions after the change in model 2b

Having in mind the assumption to model a simplified backfill element, on the left model border, the gas pressure is reduced from 3 MPa to 2 MPa, the mechanical stress is decreased from 4 MPa to 3 MPa to model relaxation as a consequence of stress reorganisation and the liquid saturation is kept constant. Next to the right model border a disposal drift is assumed leading to a change of gas pressure from 0.5 MPa to 4 MPa due to assuming a pressure built up and the liquid saturation degree is reduced from 0.9 to 0.35 because degree of saturation will be reduced as a result of temperature increase due to the heat emitting waste.

The processes within the first 10,000 years are the same as in the previous scenario. In the time evolutions of the evaluated quantities, the rapid change in conditions could be seen very clear. Due to the change in gas pressure conditions, there is an increase in the right part of the model and a decrease in the left part inducing a gas flow reversal to the first (Fig. 5.11). Additionally, there is a second equilibration process of gas pressure inside the model.

The change of liquid saturation induces a reversal liquid flow followed by a rapid decrease in degree of saturation for the right model part creating a high gradient (Fig. 5.12). With time liquid flows out on both sides in frame of the equilibration process which is finished after about one million years and shows a linear steady-state distribution.

By reducing the stress on the left border, the mechanical resistance is reduced rapidly, and the extension is getting larger creating a maximum displacement of about $6.2*10^{-2}$ m

(Fig. 5.13). Due to the decreasing gas fraction in the left part of the model, the displacements and the extension decrease with time. In the end of simulation time, a maximum displacement in the left direction of $3.7*10^{-2}$ m is left.
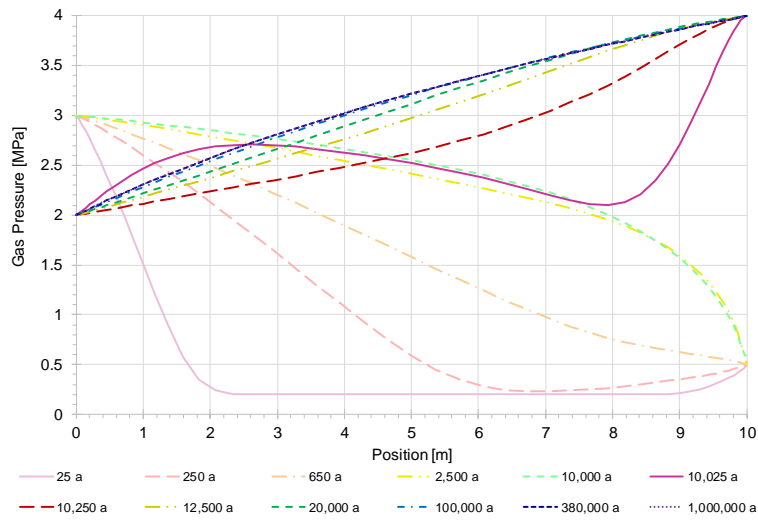
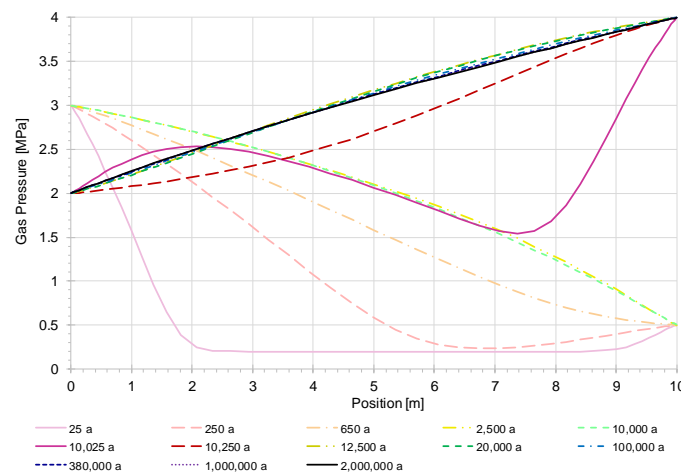**Fig. 5.11**   Gas pressure profiles for model 2b
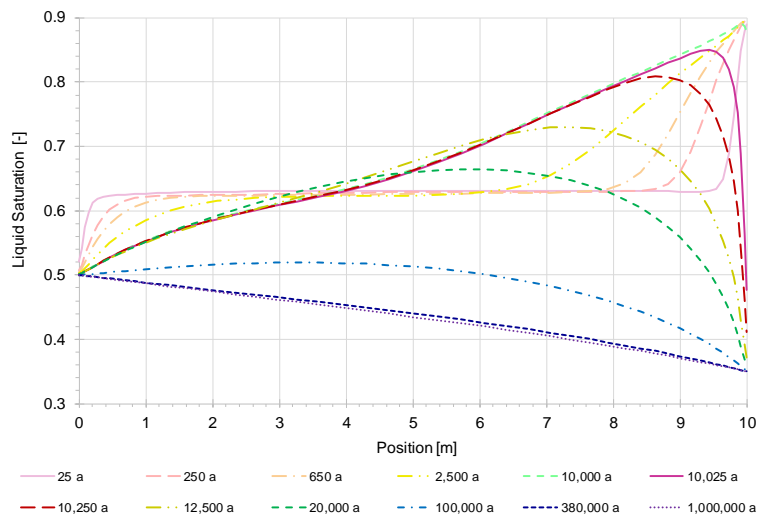
Fig. 5.12   Liquid saturation profiles for model 2b
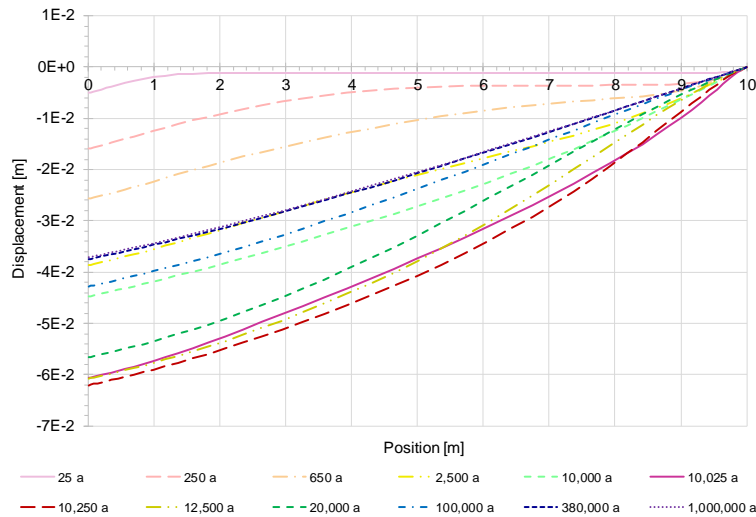
Fig. 5.13 Displacement profiles for model 2b

5.2.2 Scenario c – analytical boundary condition

In this simulation scenario, the liquid saturation boundary condition on the right model border is set to the value from the analytical solution. In Fig. 5.14, the initial and boundary conditions are presented at which the conditions are the same as in the basic scenario with exception of the red marked saturation condition.
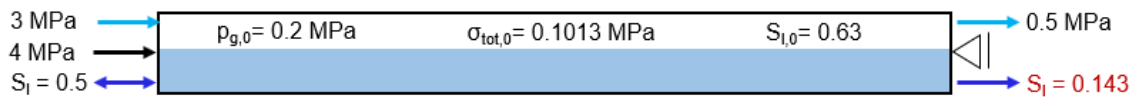
Fig. 5.14 Initial and boundary conditions for model 2c. The analytical boundary condition is marked in red.

Basically, the processes are the same as in model 2a, however, their evolution is slightly different. Due to the inflow of gas, the pressure rises in the first three points of time reaching nearly the same values as in the basic scenario (Fig. 5.15). Clear differences are to be seen in the pressure evolutions from 2,500 years on. In comparison, the gas pressures maximum in the middle of the model is about 0.5 MPa less than in the basic scenario, and the pressure near the right model border is less, too. Due to the lower degree of saturation, there is more space for the gas phase resulting in less pressure build-up. Additionally, the time to reach steady-state is much longer in this scenario since 1,000,000 years are needed instead of 100,000 years.

41

As expected, the decrease of the saturation boundary condition influences the distribution inside the model (Fig. 5.16). Over time, the initial saturation is decreased due to outflow of liquid on both model borders. With decreasing liquid saturation, the mass fraction of liquid in the model is reduced and there is more pore space for the gas.

By comparing the results for displacements, a different behaviour can be observed from 250 years on (Fig. 5.17). Instead of an ongoing extension in left direction, the displacement is reducing and finally the model is in full compression. Going back to the gas pressure distribution inside the model (Fig. 5.15), the steady-state distribution is lower than in the basic scenario leading to a different relation between fluid pressures and mechanical stress (Eq. (3.9)). The fluid pressures are decreasing resulting in a higher influence of total stresses and followed by a compression of the model.
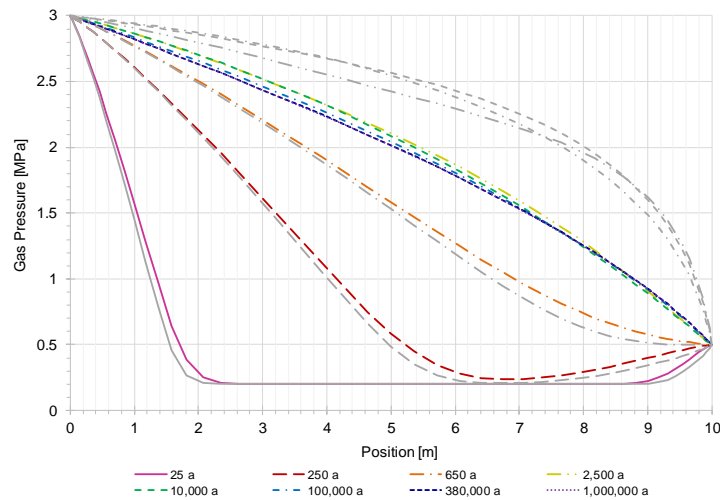
Fig. 5.15 Comparison of gas pressure profiles for model 2c (coloured lines) and model 2a (grey lines)
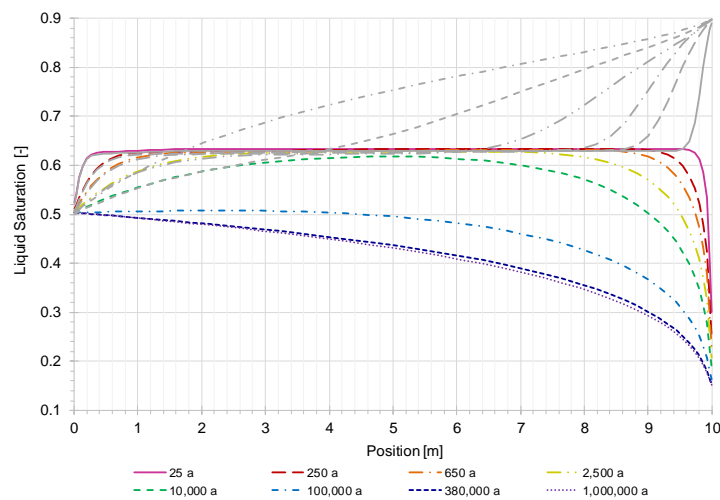
Fig. 5.16 Comparison of liquid saturation profiles for model 2c (coloured lines) and model 2a (grey lines)

42
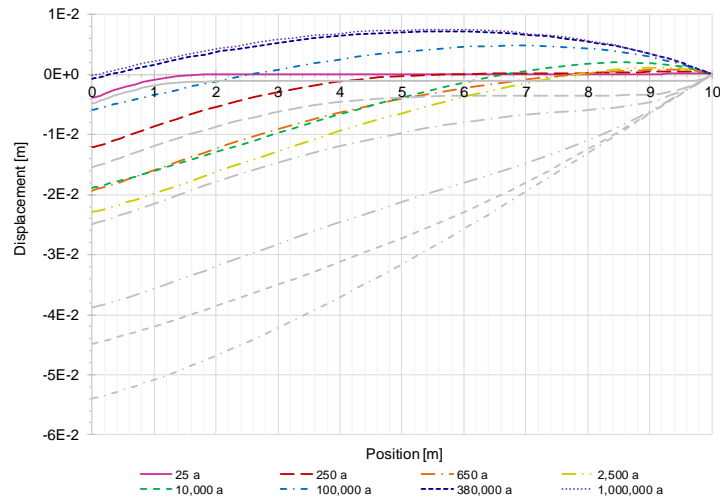
Fig. 5.17   Comparison of displacement profiles for model 2c (coloured lines) and model 2a (grey lines)

5.2.3   Scenario d – analytical boundary conditions and change of conditions after 10,000 years

Following the fact that the conditions inside a repository did not remain stable over time, this scenario combines the analytical solutions for the boundary saturations with the change in conditions after a specified time. Within the first 10,000 years the boundary conditions are equal to scenario c (Fig. 5.14). Afterwards the saturation is changing on the right border from 0.143 to 0.35 and on the left from 0.5 to 0.212 indicating resaturation and desaturation, respectively. Additionally, the mechanical and gas pressure conditions are changing the same way as in scenario b (Fig. 5.18).
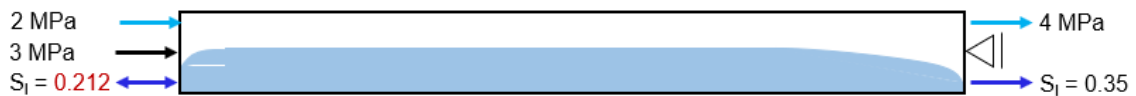
Fig. 5.18   Boundary conditions for model 2d after the change

The comparison for the first 10,000 years of simulation between the basic and the analytical saturation boundary conditions are already done in chapter 5.2.2, thus, only the results up to 10,000 years are discussed here.

The gas pressure on the left border is reduced from 3 MPa to 2 MPa, whereas on the right border it is increased from 0.5 MPa to 4 MPa indicating a pressure build up in the disposal section (Fig. 5.19). This leads to a change in gas flow direction. Comparing the

43

pressure evolution in time with scenario b (Fig. 5.11, Fig. 5.19), differences in the courses can be observed, e. g. in the smoothing. However, the values for the steady-states are in good accordance and differ only in the first decimal place.

The conditions for liquid saturation changes from 0.5 to 0.212 on the left and from 0.143 to 0.35 on the right. The courses for liquid saturation degree showed already big differences within the first 10,000 years (chapter 5.2.2) which is a logical consequence resulting from the different setup of analytical solutions. The evolutions for liquid saturation up to 10,000 years are hardly to compare with scenario b. In this scenario a desaturation on the left side and a saturation on the right side is set, whereas in scenario b the saturation is constant on the left and decreasing on the right side. Hence, only the effects due to the condition change are described now.

Due to the instantaneous change of saturation conditions on the model borders, high gradients are occurring leading to outflow of liquid in both directions (Fig. 5.20). Consequently, the saturation in the whole model decreases with ongoing time till a nearly linear steady-state is reached after about 2 million years.

With changed conditions, the model suffers further extension induced by the changed relations of fluids and their influence on the effective stresses (Fig. 5.21). Therefore, a maximum displacement of 0.05 m is reached. While before 10,000 years there was a part of the model in compaction, now the full model is in tension. With ongoing equilibration, the displacements become smaller, thus the extension is reducing, and in the end the model is extended of about 0.023 m.

Fig. 5.19   Gas pressure profiles for model 2d
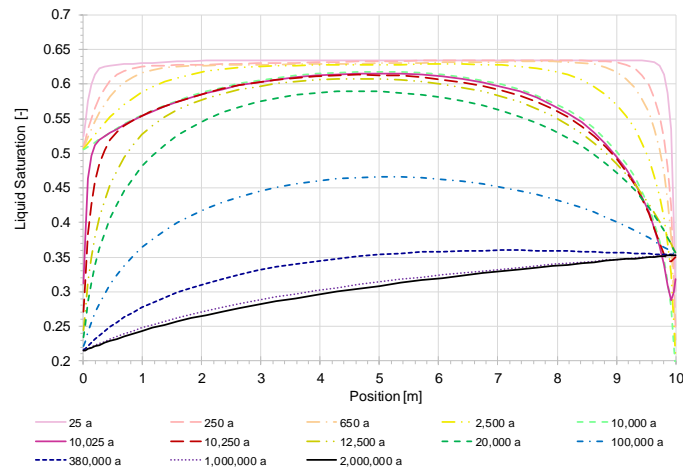
Fig. 5.20 Liquid saturation profiles for model 2d
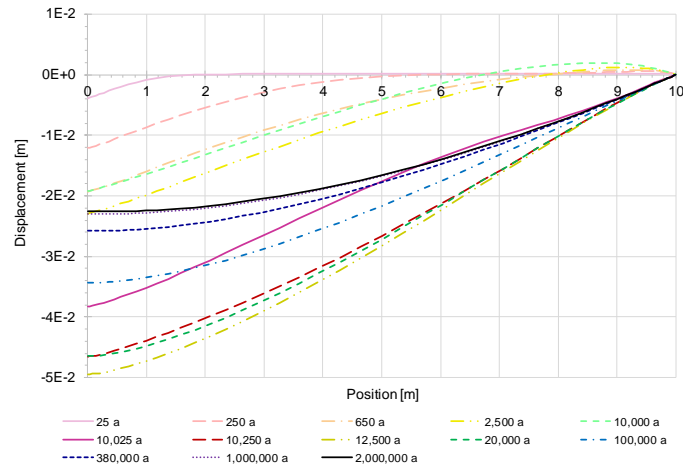
Fig. 5.21 Displacement profiles for model 2d

5.3 Discussion

During the modelling work, a discrepancy in the use of the gas phase relative permeability law was observed, hence, the van Genuchten approach (Eq. (3.6) was not available in CODE_BRIGHT. Instead a default law was specified following Equation (3.7) which is one minus the liquid phase relative permeability. Fig. 5.22 shows both, the liquid and gas phase relative permeabilities in dependence of the effective saturation for the van Genuchten approach and the default laws in CODE_BRIGHT. For the liquid phase the specification of relative permeability in CODE_BRIGHT follows the van Genuchten approach. However, for the relative permeability of the gas phase differences appear due to the diverse approaches. The default law in CODE_BRIGHT results in a very high gas

relative permeability for a wide range of effective saturation leading to a faster gas flow compared to the van Genuchten approach. The faster gas flow effects the gas pressures within the model. In collaboration with the code developer, the van Genuchten approach for relative gas permeability was implemented in CODE_BRIGHT and was used for the simulation of the second modelling phase and ongoing phases.
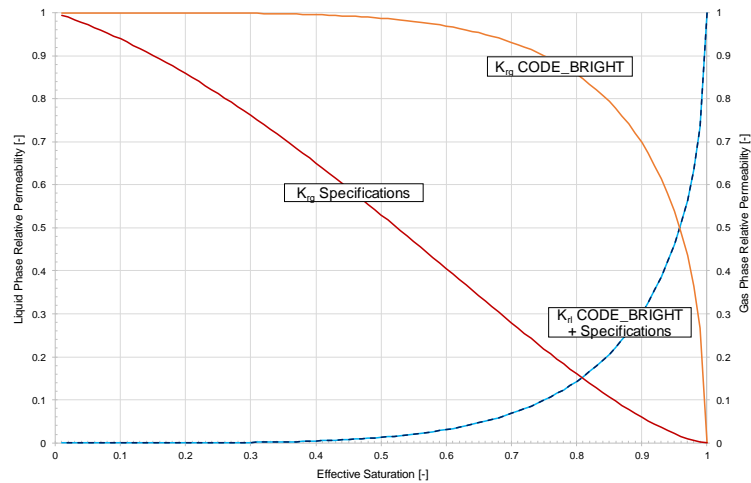
Fig. 5.22   Comparison of relative permeability following van Genuchten and the default law specified in CODE_BRIGHT. X-axis: effective saturation. Primary y-axis: Liquid phase relative permeability. Secondary y-axis: Gas phase relative permeability.

Within the simulation process, a further discrepancy was figured out in the gas pressure evolutions inside the model by comparing the results with the project partners. Fig. 5.23 represents a first comparison of all project partner results for the basic scenario simulating two-phase flow. The results from GRS Braunschweig are highlighted and show deviations from the other curves, especially in the right part of the diagram.
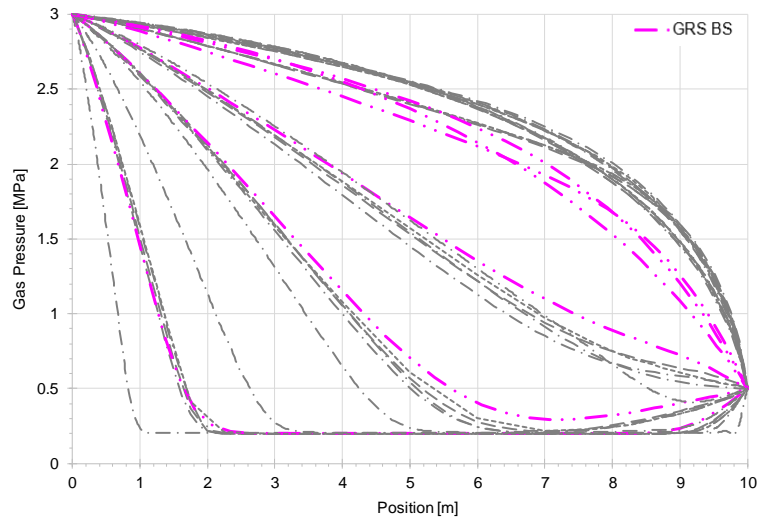
Fig. 5.23   Preliminary results of gas pressure profiles for the basic scenario of the second modelling phase. Evaluation times: 25 a; 250 a; 650 a; 2,500 a; 10,000 a; 100,000 a.

For the calculation of the gas density in CODE_BRIGHT, the ideal gas law and Henry's law are used, therefore, as default a Henry constant of $H = 10^4$ MPa is given. In the working progress, the Henry constant was set to $H = 10^8$ MPa leading to a decreased solubility of air in the liquid phase. Fig. 5.24 presents the direct contrast in the GRS results for the constant change. The new results have a much better agreement with the project partner ones (not shown in the figure) since a few of them are simulating without consideration of gas solubility processes in liquid.
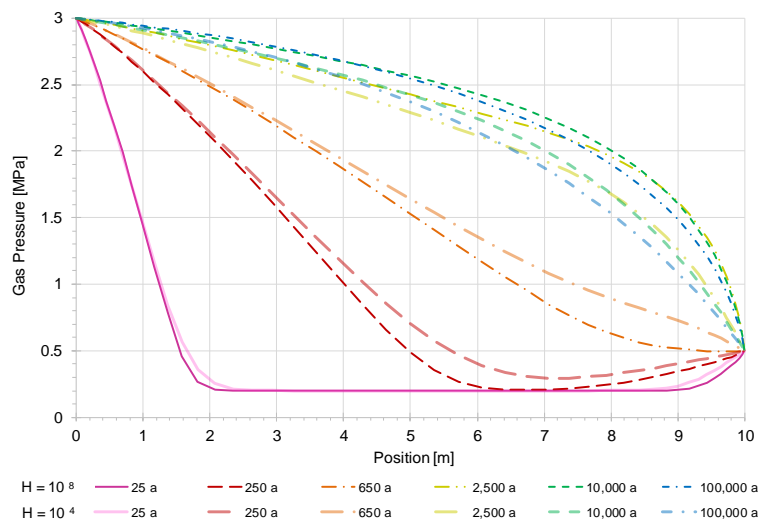
Fig. 5.24   Comparison of gas pressure profiles before and after the adaption of the Henry constant

47

6   3rd modelling phase – backfilled and sealed drift

An often-considered option for the disposal of radioactive waste is the storage in horizontal drifts. The cavities around the waste containers are backfilled with a suitable material depending on the type of host rock and afterwards the drifts are sealed with a plug, mostly composed of cementitious materials. Finally, the access drifts and shafts must be backfilled and sealed, too. For a repository in rock salt the backfilling is done with crushed salt and the sealing with a salt concrete or magnesia concrete plug depending on the mineralogical composition of the rock salt. In clay and crystalline rock, the most common solution for backfilling is bentonite and for sealing a concrete plug is used, too. Remembering not to explicitly to focus on a host rock type, the material parameters are chosen according to a repository in clay.

The simplified concept of drift disposal should be considered in this third modelling phase including two-phase flow and mechanical stresses. Therefore, the model geometry is extended to present a section of a disposal drift including the drift seal element and the backfilling of the cavities (Fig. 6.1). The retention curve for this modelling stage could be found in Appendix A.

Fig. 6.1   Model geometry and considered processes for the third modelling phase

As done in the previous modelling phases, the evaluation of the quantities is done due to considering the quantity evolution in the model section for different time steps and an additional consideration of time evolutions in specified positions in the model. Especially, the quantity evolutions with time near the material transitions are interesting (Fig. 6.2).
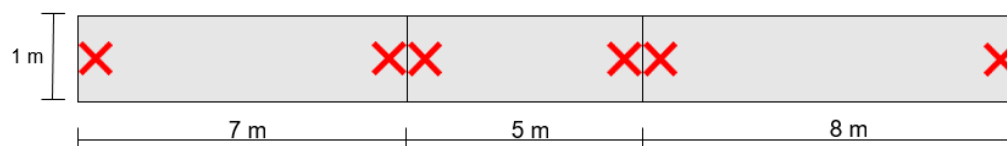
Fig. 6.2   Points for time evaluation of analysed quantities in the third modelling phase. X-coordinate for the points with increasing distance to the left boundary of the model: 0.25 m, 6.75 m, 7.25 m, 11.75 m, 12.25 m, 19.75 m. Y-coordinate for all points: 0.5 m

6.1 Basic scenario

The basic scenario includes a partially saturated model where two-phase flow is coupled with mechanical stress. In general, the entry of moisture in a repository should be avoided because of the advancement of possible chemical reactions, like container corrosion, or accelerated radionuclide transport due to liquid flow. So, the backfill material is emplaced mostly dry resulting in a very low degree of saturation (Fig. 6.3). The sealing elements are planned to consist of cementitious materials which need moisture for the hardening process leading to a relatively high initial degree of saturation. The right border is mechanically fixed, and the overall total stress is set to 5 MPa. The initial gas pressure in the model is 0.2 MPa and 0.25 MPa, respectively, however, a hydraulic pressure of 4 MPa is set on the left model border. The material parameters are presented in Tab. 6.1.
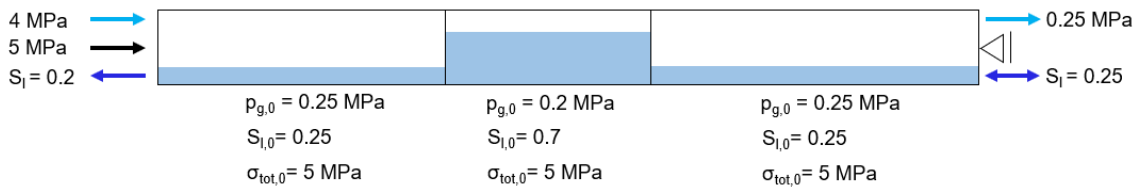
Fig. 6.3   Initial and boundary conditions for the basic scenario of the third modelling phase

Tab. 6.1   Material parameters for the base scenario of the third modelling phase

Parameter		Backfill	Drift Seal	
Young's modulus	E	200	600	[MPa]
Poisson's ratio	ν	0	0	[-]
Porosity	Φ	0.4	0.3	[-]
Intrinsic permeability	K	$2*10^{-19}$	10^{-20}	[m^2]
Biot coefficient	α	1	1	[-]
Residual liquid saturation	S_{lr}	0.01	0.05	[-]
Residual gas saturation	S_{gr}	0	0	[-]
Van Genuchten parameter	λ	0.47	0.37	[-]
Van Genuchten pre-factor	$p_{cap,0}$	15	34	[MPa]
Pore connectivity parameters	$\tilde{\varepsilon}, \tilde{\gamma}$	0.5		[-]
Liquid viscosity	η_l	10^{-9}		[MPa*s]
Liquid bulk modulus	$\breve{K}_l$	2,220		[MPa]
Liquid density	ρ_l	1,000		[kg/m^3]
Gas viscosity	η_g	$1.8*10^{-11}$		[MPa*s]

The model is being compacted due to the initial stress and gas pressure conditions leading to an increase in gas pressure (Fig. 6.4). In the left backfill material, the gas pressure reaches a nearly constant value close to 4 MPa which is the boundary conditions after ~ 60 years. The high pressure gradient in the early time is diminished to a value close to zero (Fig. 6.5). Within the drift seal and the right backfill, a pressure gradient builds up and increases with time. The gas pressure in the right backfill is ruled by the 0.25 MPa boundary condition, however, the left-hand side gas pressure condition has a strong influence on the whole model.

The reaction of the liquid phase occurs time-delayed to the stress and slower than the gas pressure reaction. The first change in liquid saturation in course of the applied conditions is detected after 0.01 years (Fig. 6.6), whereas gas pressure starts to increase after 0.003 years (Fig. 6.4). The liquid saturation applied on the left model border is lower than the initial saturation in the left backfill inducing a liquid flow out of the model leading to a smoothing of the gradient (Fig. 6.7). In the left backfill element, the liquid saturation remains more or less stable. Simultaneously, both backfill elements are influenced by the high liquid saturation of the drift seal. By attempting to equalize the gradient in the model, the liquid flows out of the drift element on both sides, resulting in saturation decrease in the drift seal and increases in the backfill elements near the transitions. The equalization process is not finished after the final simulation time of 630,000 years

Due to the instantaneous loading, the model gets compacted which is to be seen in the displacements in Fig. 6.8, meaning compaction is negative displacement and extension is positive. The trend of deformation changes after reaching steady-state gas flow. The liquid saturation in the drift seal continues to decrease, hence, the influence of gas pressure rises in the frame of the effective stresses (3.9) leading to a reduction of effective stress and simultaneously of displacement ending in extension of the sealing element. As a result, the left backfill element is shifted in left direction.
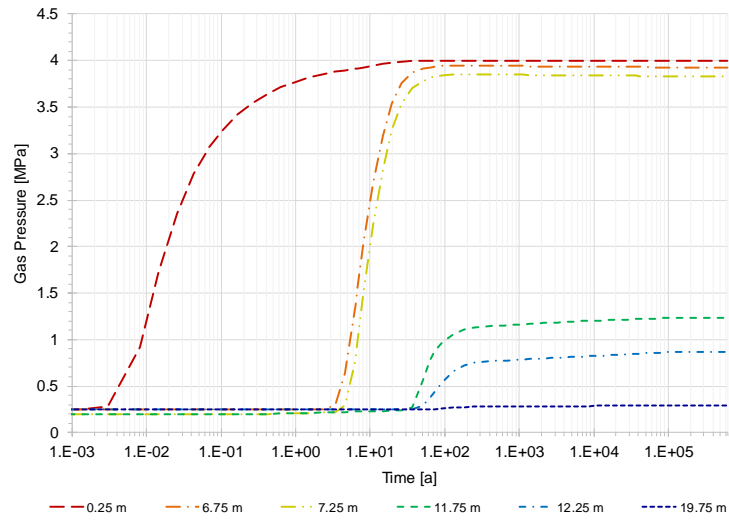
Fig. 6.4   Gas pressure evolution (model 3a)
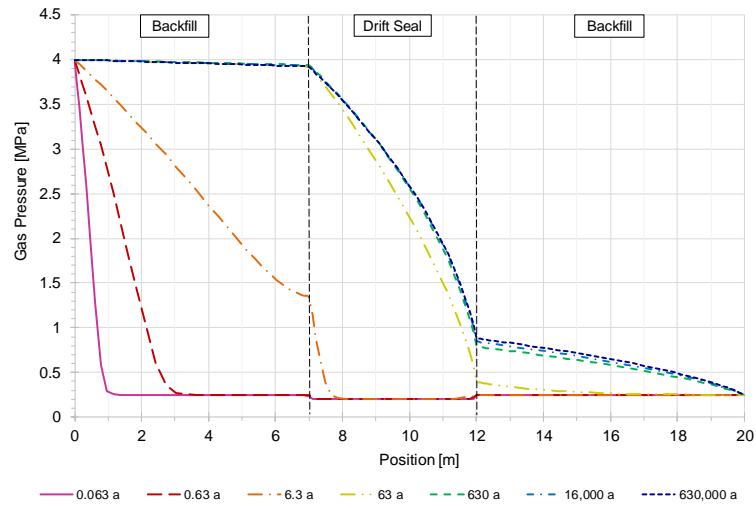
Fig. 6.5   Gas pressure profile (model 3a)
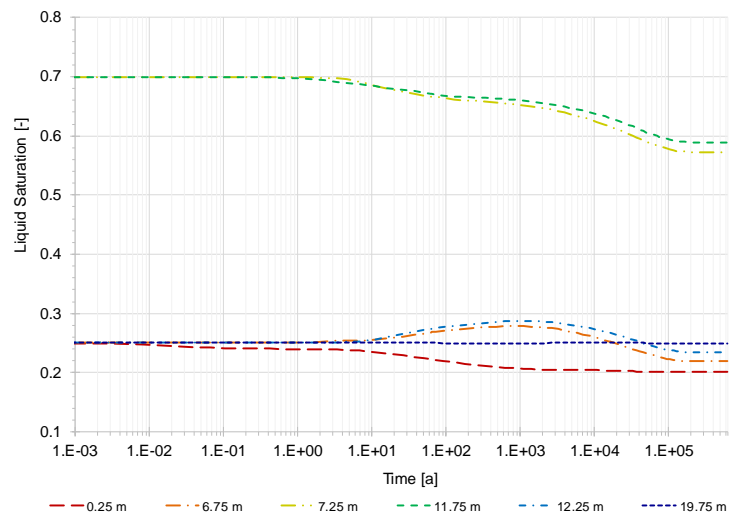
Fig. 6.6   Liquid saturation evolution (model 3a)
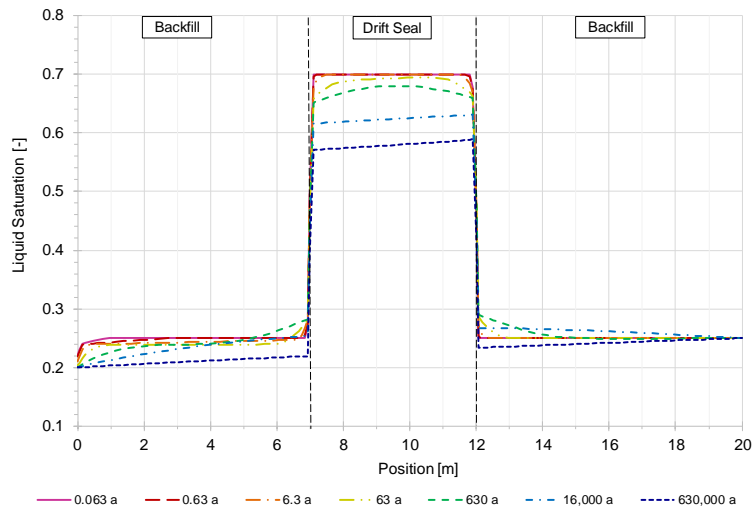
Fig. 6.7   Liquid saturation profile (model 3a)
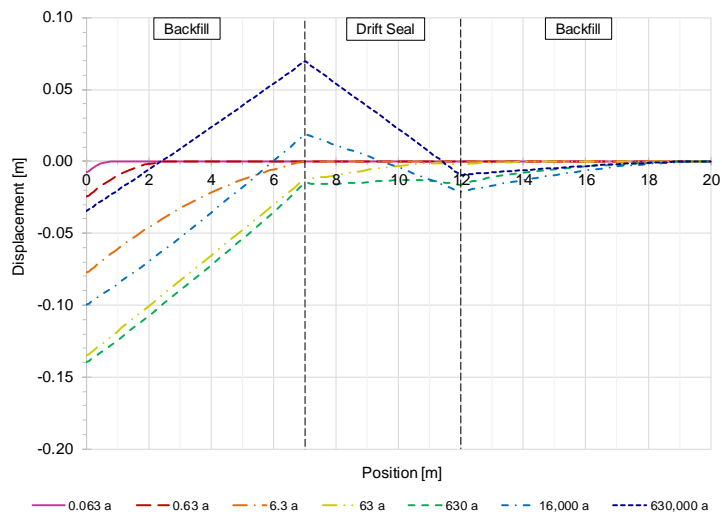
Fig. 6.8   Displacement profile (model 3a)

6.2   Scenario variations

In this modelling stage a large range of scenario variations are presented. They can be decided roughly in changes of mechanical parameter and changes of hydraulic parameter. For the evaluation of results only the most important ones are shown in the following, additional diagrams can be found in Appendix C.

6.2.1   Scenario b – no mechanics

In the basic scenario, hydraulic-mechanical coupled processes are considered. This includes important interactions like the reduction of porosity induced by mechanical compaction accompanied by a decrease of permeability and closing of flow paths. With reduction of pore space, there might be an increase in pore pressure which affects the effective stresses and further the strains.

For evaluating the influence of the mechanical aspects on the flow processes, here, the mechanical processes are neglected, and a pure hydraulic simulation is done (Fig. 6.9). The effect of hydraulic becomes clear due to the comparison of results with the basic scenario, also called model 3a.

| 4 MPa → | | | | → 0.25 MPa |
| S_l= 0.2 ← | | | | ← S_l= 0.25 |

$p_{g,0}$ = 0.25 MPa $p_{g,0}$ = 0.2 MPa $p_{g,0}$ = 0.25 MPa
$S_{l,0}$= 0.25 $S_{l,0}$= 0.2 $S_{l,0}$= 0.25
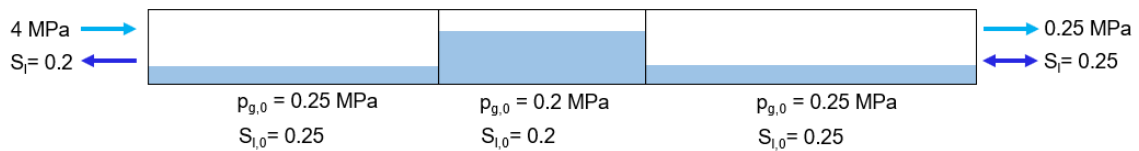
Fig. 6.9   Initial and boundary conditions for model 3b

By comparing the temporal evolutions of gas pressure no differences between this scenario and the basic scenario a can be observed (Fig. 6.10) leading to the conclusion that the compaction does not affects the gas flow. However, an influence of mechanics is to be seen in the liquid pressure evolutions in the left backfill material (Fig. 6.11). Because of the relatively small distinctions, a detail of the liquid pressure is displayed in Fig. 6.12. Clear deviations can be seen in points 0.25 m and 6.75 m which are both located in the left backfill material. The decrease of liquid saturation in point 0.25 m is delayed due to the missing compaction in the beginning. The pore space did not get compacted instantaneous squeezing out the liquid, but the liquid is replaced by the increasing gas pressure.
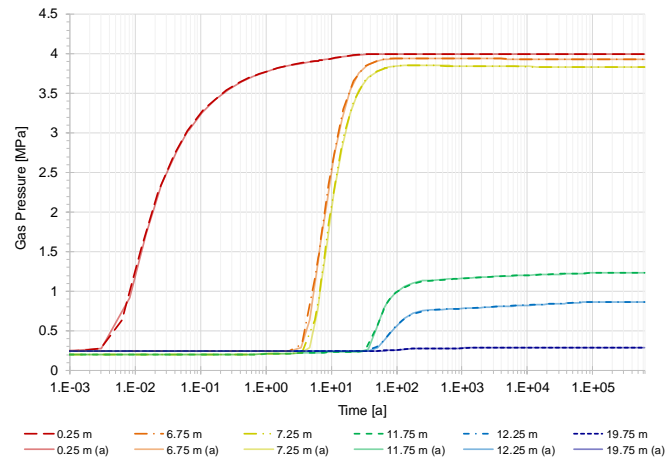
Fig. 6.10 Gas pressure evolution for model 3b (dotted lines) in comparison with model 3a (continuous lines)
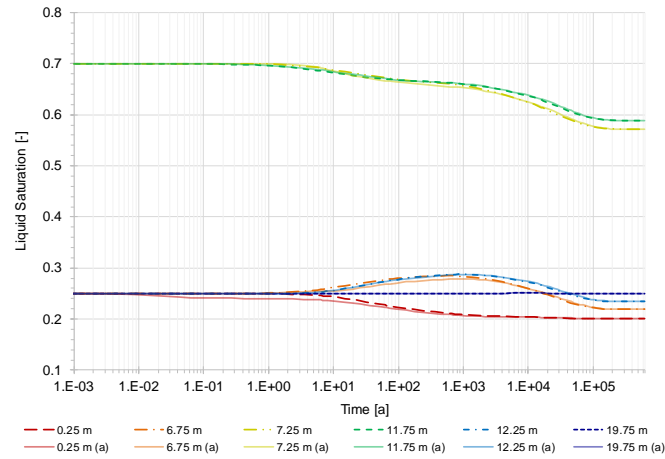
Fig. 6.11 Liquid Saturation evolution for model 3b (dotted lines) in comparison with model 3a (continuous lines)
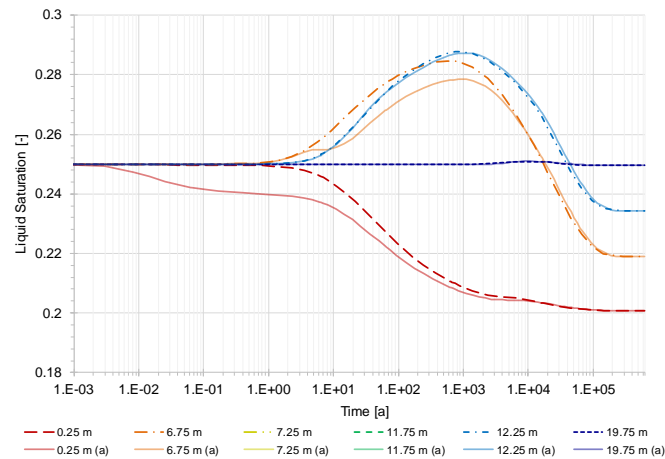
Fig. 6.12 Detail of the comparison in liquid saturation evolution for model 3b (dotted lines) and model 3a (continuous lines)

6.2.2 Scenario c – completely fixed boundaries

By setting a stress boundary condition on the left model border, extension of the material in left direction is possible. Thus, the stress condition assumes a further material next to the backfill. Since there might be no additional repository component with relatively small stiffness, but host rock with high stiffness at the end of a drift, the displacements are very low or equal zero. Due to restricting the displacements on the left model border, a very stiff material, e. g. the host rock, is simulated and the mechanical behaviour has to rearrange in the model (Fig. 6.13).

4 MPa →				0.25 MPa
$S_l = 0.2$ ←	$p_{g,0} = 0.25$ MPa	$p_{g,0} = 0.2$ MPa	$p_{g,0} = 0.25$ MPa	$S_l = 0.25$
	$S_{l,0} = 0.25$	$S_{l,0} = 0.7$	$S_{l,0} = 0.25$	
	$\sigma_{tot,0} = 5$ MPa	$\sigma_{tot,0} = 5$ MPa	$\sigma_{tot,0} = 5$ MPa	
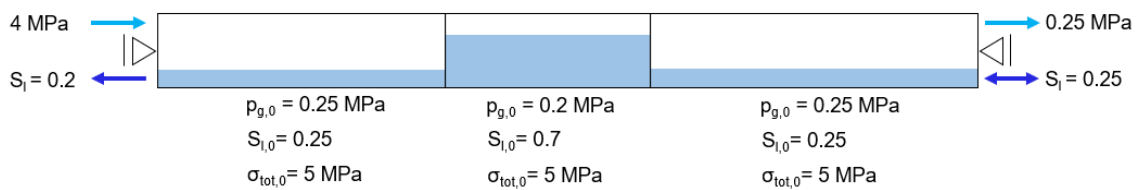
Fig. 6.13   Initial and boundary conditions for model 3c

The fixing of both model borders has strong influences on the mechanics. In contrast to the basic scenario where the stress is constant over the whole time, here, it increases in the first 200 years reaching a maximum of 6.5 MPa followed by a decrease (Fig. 6.14). The gas inflow through the right border will lead to expansion of the model, but due to the restricted boundary displacements expansion is forbidden and total stress rises as a result. By cause of the high gas inflow, the liquid is displaced, and a liquid flow is induced resulting in relaxation of the model, so, in decreasing total stress.

The restriction of displacements causes an expansion of the right backfill material against the drift seal which is in opposition to the expansion in left direction in the basic scenario (Fig. 6.15, Fig. 6.8). Additionally, the left backfill gets compacted in this scenario contrary to the expansion in the basic scenario. The mechanical behaviour with time of the drift seal is different in both simulations, however, the amount of compaction is similar in its final state.
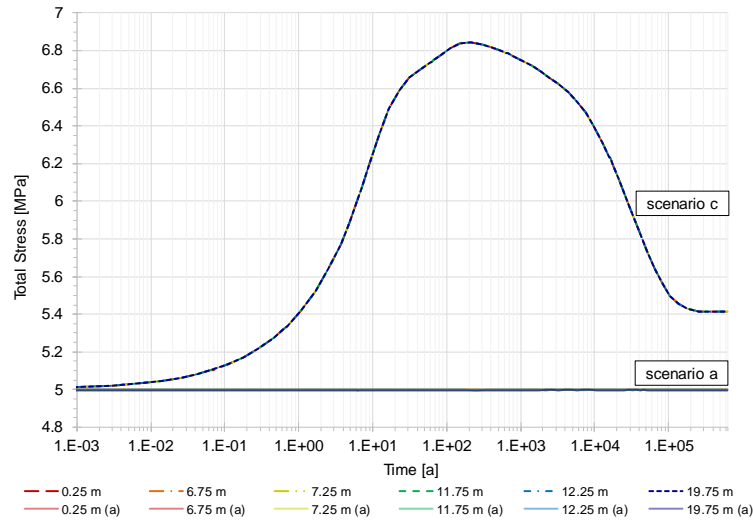
Fig. 6.14   Comparison of total stress evolution for model 3a and model 3c
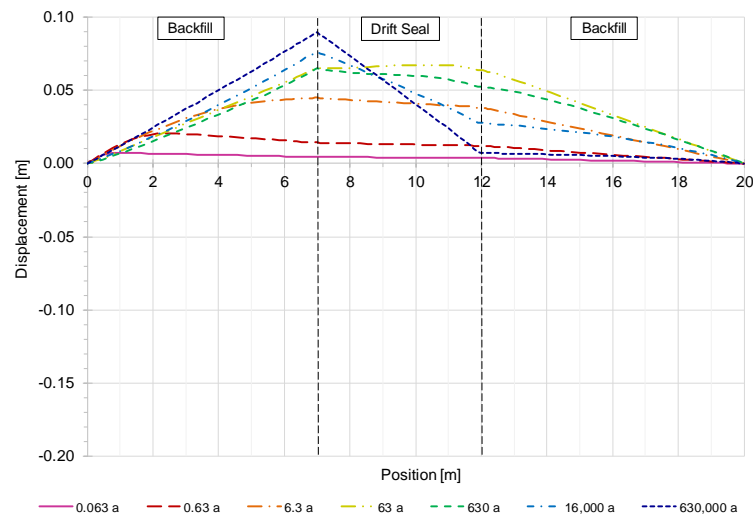
Fig. 6.15   Profiles of displacements (model 3c)

6.2.3   Scenario d – variation of effective stress definition

During the simulation work, a discussion about the definition of effective stress started (Chapter 4.3). The implemented definition of effective stresses for linear elasticity in CODE_BRIGHT is different from the prescriptions leading to differences in the results. In CODE_BRIGHT the total stress is reduced by the maximum fluid pressure which is the gas pressure in a partially saturated system. In the model predictions for this project, the total stress is subtracted by an averaged fluid pressure. For having a comparison in

the application of both definitions and for a direct comparability, here, the default definition in CODE_BRIGHT following Equation (3.11) is used. The conditions are equal to the basic scenario (Fig. 6.3).

The change of effective stress definition influences only the mechanical behaviour, thus, there are no changes in gas pressure and liquid saturation evolution compared with the basic scenario. In Fig. 6.16 and Fig. 6.8, the displacements of both simulations are shown. The evolutions for the first three time steps are similar, however, big differences started to develop afterwards. When using the maximum fluid pressure for the determination of effective stresses, the model gets compacted over the whole length and simulation time, reaching a steady-state for displacements after 630 years with a maximum value of 0.167 m. In contrast, the prescribed definition leads to a stop of compaction after 630 years and an extension of the drift seal. From 630 years on, the gas pressure is in a steady-state, but there is still liquid flow equilibrating the gradient in liquid pressure. In the drift seal element, the change in liquid pressure is relatively high which is not considered in the default definition in CODE_BRIGHT. A deeper discussion is done in chapter 8.
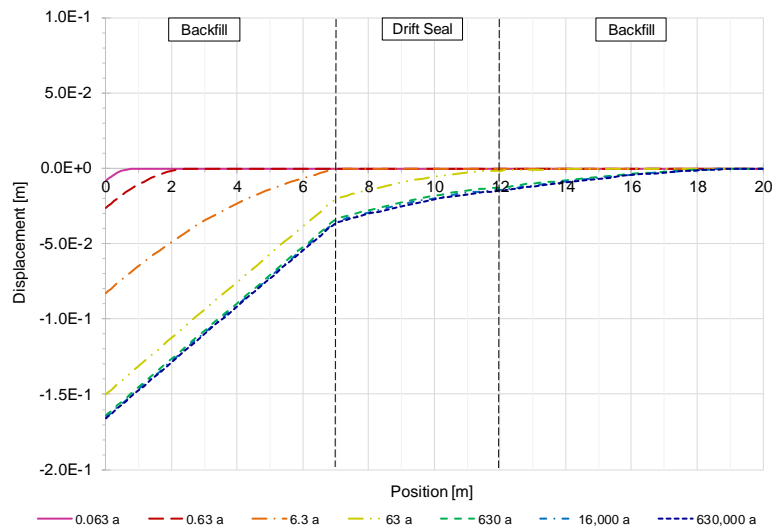
Fig. 6.16   Profile of displacements (model 3d)

6.2.4   Scenario e – softer backfill material

Depending on the repository concept different backfill materials are planned, thus with varying stiffness. For investigation of the interaction between the repository components in regard of the mechanical and the hydraulic behaviour, especially, dependent on the

mechanical stiffness of the backfill material, a lowered Young's modulus (E = 50 MPa) was chosen for backfill in this scenario. For comparability the initial and boundary conditions are like the basic scenario ones (Fig. 6.3).

The primary influence of the stiffness change affects the displacements of the model (Fig. 6.17). Because of the reduced Young's modulus, the mechanical resistance was lowered, and the displacements becomes bigger. Especially, the high gas pressure in the left backfill element leads to a maximal expansion of 0.5 m which is about 3.5 times higher than in the basic scenario. Another consequence is a lower compaction of the drift seal element.

Differences can be observed in the evolution of liquid saturation on the right model border, too (Fig. 6.18). The outflow of liquid out of the left backfill element happens much faster due to the high expansion and the resulting increase of pore space.
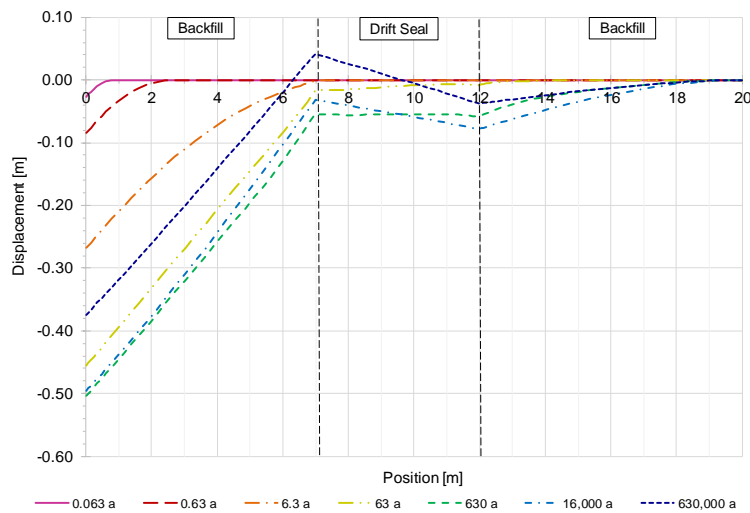
Fig. 6.17 Profile of displacements (model 3e)
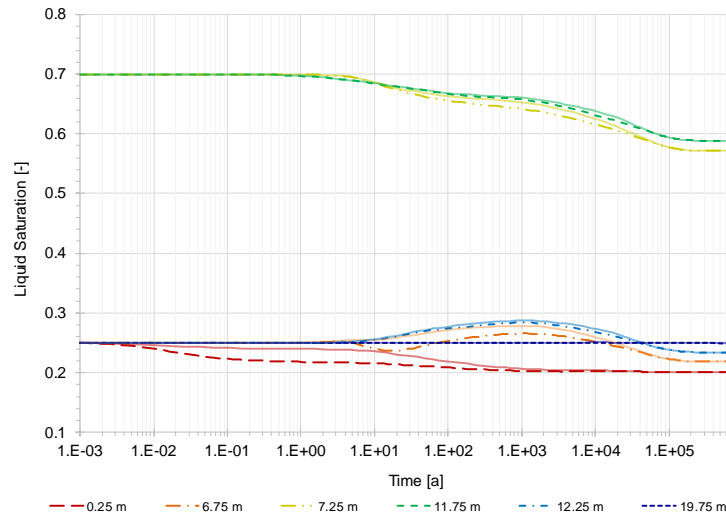
Fig. 6.18   Liquid saturation evolution (model 3e)

6.2.5   Scenario f – coarser backfill material

The initial porosity of the backfill material is an essential factor for the prevention of fluid flow and thus for radionuclide transport which depends on the construction method and the densification of the material. For evaluating the influence of backfills initial porosity on the fluid flow processes, the porosity is increased to 0.5. The initial and boundary conditions are similar to the basic scenario (Fig. 6.3).

Comparing the liquid saturations and the displacements with the basic scenario there are nearly no differences. However, deviations can be found in the gas pressure profile for 6.3 years. The gas pressure is about 0.5 MPa lower in the transition zone between the left backfill and the drift seal. A higher porosity is referred to more pore space in the medium which is filled with fluids. Since the pressure and saturation boundary conditions remain the same, the inflowing amount of gas is still the same, however, the gas pressure did not increase as much due to more pore space for the flowing gas phase.

The effect of porosity increase is very small in this example. However, the porosity in the backfill material is very high for both, model 3a and 3f.
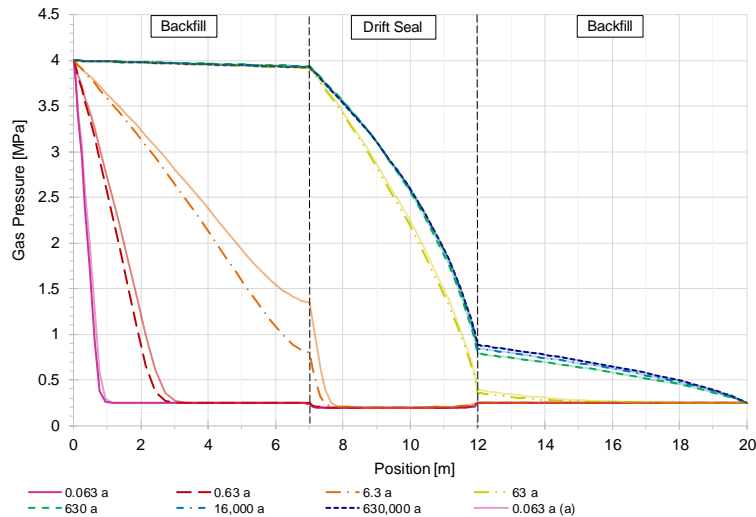
Fig. 6.19   Comparison of gas pressure profiles for model 3f (dotted lines) and model 3a (continuous lines)

6.2.6   Scenario g – perfectly mobile fluids

The intrinsic permeability of a porous media describes the rock specific permeability for a porous material which pores are completely filled with one fluid phase and the only dependence is on the specific properties of the material. When considering two phase flow, the two fluid phases mutually influence their respective permeabilities. Therefore, the effective permeability describes the permeability of one fluid in presence of another one, thus, the effective permeability is always smaller than the intrinsic permeability. The relative permeability of a fluid defines the relation between the effective permeability of the fluid and the intrinsic permeability of the porous media and is dependent on the degree of saturation for the fluid, respectively. Values for relative permeability can vary in a range of 0 to 1, implicating that for a relative permeability close to 1 the mobility of the fluid is very high. Frequently applied equations for the calculation of gas phase and liquid phase relative permeabilities arises from the combined Mualem/van Genuchten approach (3.5(3.6).

To investigate the mutual interactions between the fluid phases and their influence on the flow properties, the relative permeabilities of both, the liquid and the gas phase, are set to 1 indicating perfect mobility. The initial and boundary conditions are the basic scenarios ones (Fig. 6.3).

Because of the totally free movement, the fluid flow processes are faster compared to the basic scenario. The fluids flow much easier through the available pore space because of the neglected interactions between the effective permeabilities. For the gas pressure profile at 6.3 years, the gradient is much smaller in the left backfill and higher in the drift seal for the perfectly mobile fluids which illustrates the different intrinsic permeabilities of the materials (Fig. 6.5, Fig. 6.20). The permeability of the backfill is higher leading to a faster fluid flow. Even if the steady-state is the same for gas pressure, it is reached much earlier, in this scenario (630 years) than in the basic one (630,000 years). The same behaviour is to be seen in the liquid flow. It is much faster for perfectly mobility and the steady-state is reached quite early (Fig. 6.21).

The profiles of displacement show big differences in relation with the basic scenario (Fig. 6.8, Fig. 6.22). Due to the lowered gas pressures for the early times, the total stress is getting a higher influence leading to a stronger mechanical resistance against the expansion. Further, the lowered fluid pressures result in a compaction of the drift seal after 6.3 years which grows to a maximum after 63 years and finally ends in a steady-state equal to the basic scenario ones.

The fat grey lines in the diagrams show analytical solutions for this simulation problem. All in all, the numerical results show a very good accordance with the analytical ones.
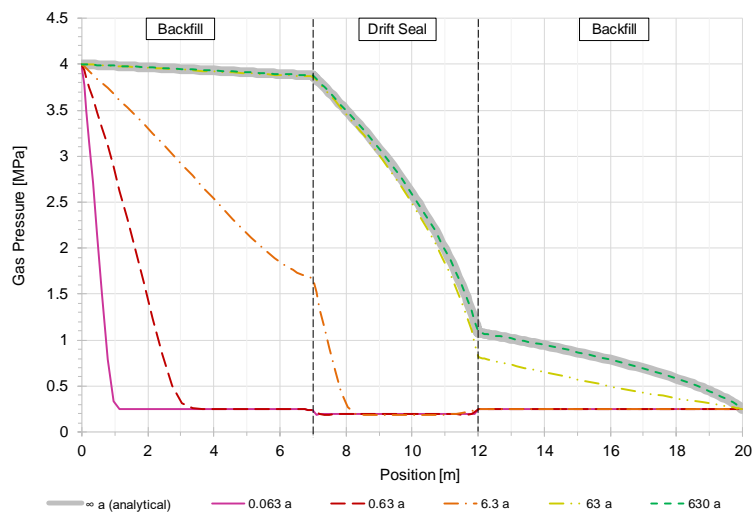
Fig. 6.20   Profiles of gas pressure (model 3g)
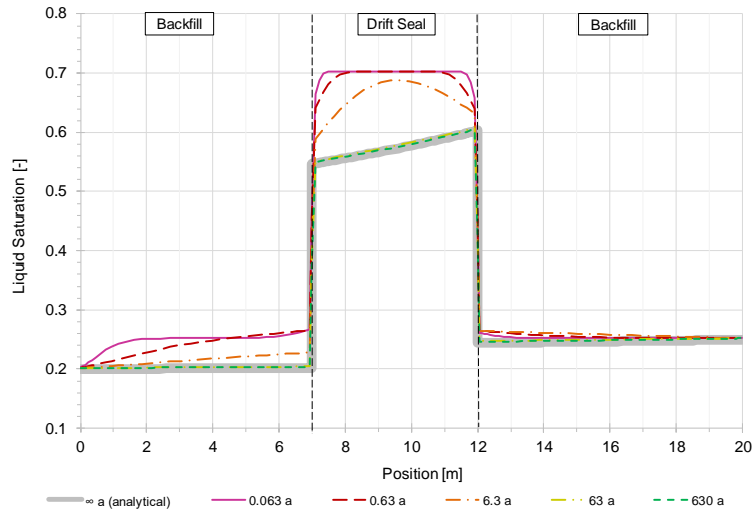
Fig. 6.21   Profiles of liquid saturation (model 3g)
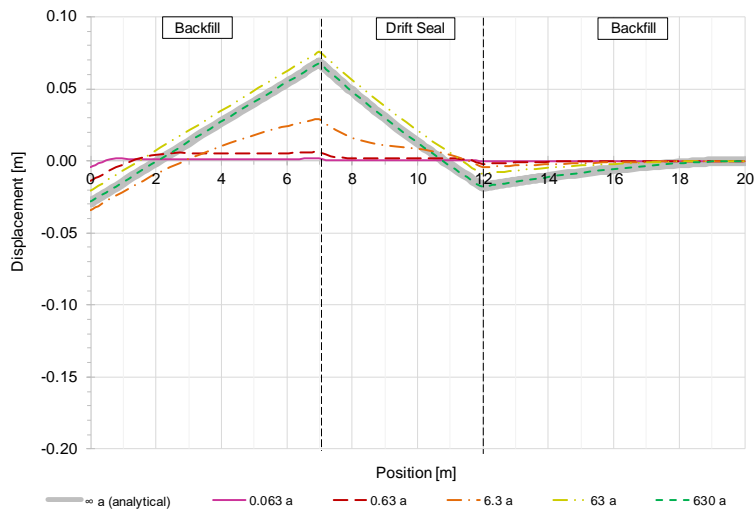
Fig. 6.22   Profile of displacements (model 3g)

6.2.7   Scenario h – homogenous retention curves

The retention curve specifies the relationship between the water content of a soil, here expressed by the saturation and the capillary pressure which is the difference in partial pressure between two fluid phases (Eq. (3.2). It reveals the whole saturation state of a soil from full saturation until its residual state and therefore, determines the corresponding suction pressure for the liquid phase.

The diverse materials in a repository differ in their retention curves which may lead to numerical inaccuracies due to an approximation in the transition between the materials.

For examination of this effect, both materials receive the same retention curve parameters, therefore, the backfill retention parameters are chosen. The retention curve can be found in Appendix B.3. Due to comparability, the initial and boundary conditions are equal to the basic scenario (Fig. 6.3).

A first indication for the performed modifications can be found in the evolution of liquid pressure (Fig. 6.24). The liquid pressure in the drift seal for the initial saturation of 0.7 is quite lower for the homogenized retention parameters corresponding to a decreased suction. The deviated evolution of liquid saturation is similar to the basic scenario for the first years (Fig. 6.23). From around 63 years on, the liquid saturation in the drift seal decreases due to outflow of liquid into both backfill elements which results from the increasing amount of gas. In contrast to the basic scenario, the drift seal has a lowered retention capacity for liquid, leading to an easier outflow. With time, the liquid saturation further decreases and finally a steady state is achieved in which the saturations in the backfill materials are nearly constant and adopted to the boundary specifications; and the gradient in the drift seal is a linear transition between both backfill elements.

Due to the changes in liquid flow behaviour and the correlating variations in liquid pressure, the displacements are affected (Fig. 6.25). By the facilitated liquid flow, the suction pressure is slightly decreased in the backfill materials meaning an increase in the absolute values of liquid pressure. Following Equation (3.9), the effective stress is decreased leading to higher extension of both backfills and lower compaction in the drift seal.
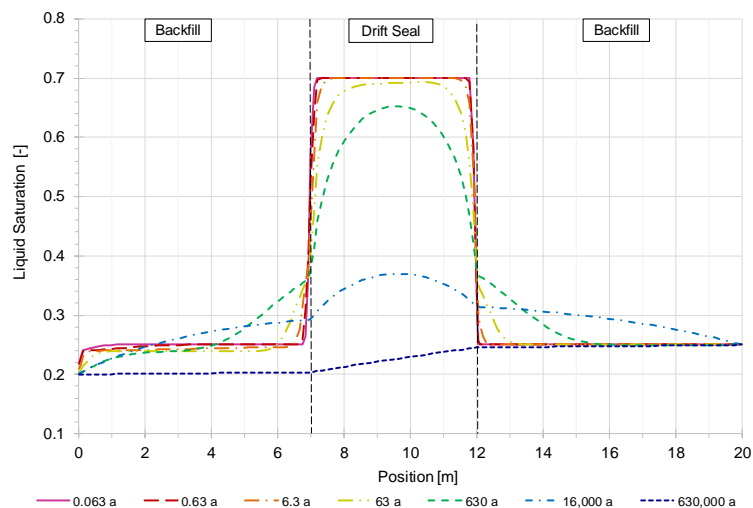
Fig. 6.23   Profiles of liquid saturation (model 3h)
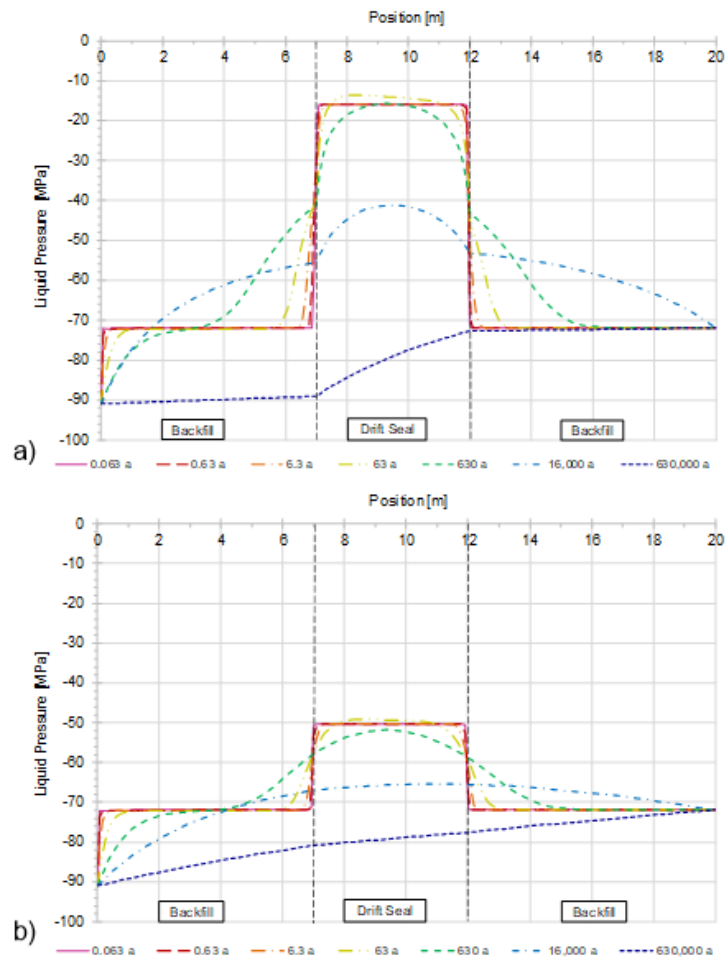
Fig. 6.24 Comparison between the liquid pressure evolutions for a) scenario h and b) scenario a
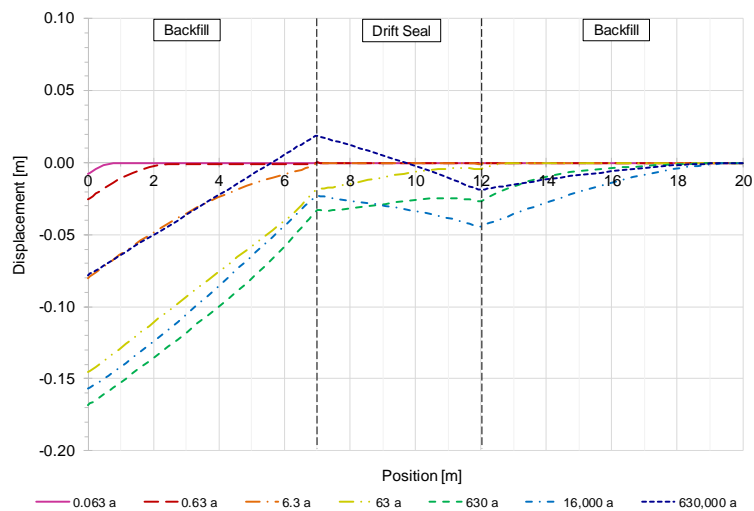
Fig. 6.25 Profiles of displacements (model 3h)

65

6.2.8   Scenario i – constant gas generation

Depending on the repository concept and the available resources, the waste canisters are made of steel or copper. The last is a quite expensive material with a very good resistance against corrosion, in contrast steel is cheaper but with a higher sensitivity for corrosion. The chemical process of corrosion produces gas which amount is dependent from the water and metal available. In this scenario, the gas generation in a repository should be examined in a simplified way due to applying a small constant gas production rate of $6*10^{-9}$ kg/s (Fig. 6.26).
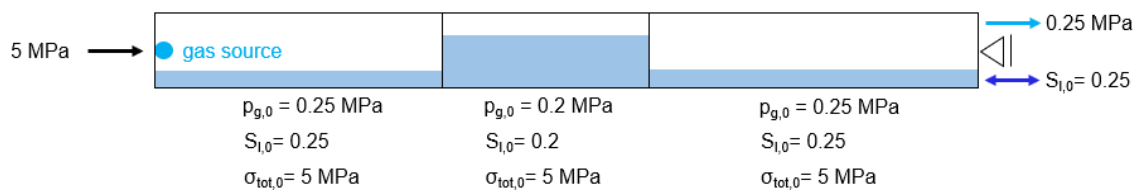
Fig. 6.26   Initial and boundary conditions for model 3i

The gas pressure rises with time because of the gas production till it reaches a final value of about 4.8 MPa (Fig. 6.27). The gas distribution in the left backfill material is quite homogenous in contrast to the other components. Especially in the drift seal, the gradient is getting relatively large with time, as gas flow is slower due to the lower permeability and the high liquid saturation. The pressure gradient in the right backfill is caused by the pressure in the drift seal and the boundary condition.

There are only minor changes for the liquid saturation in both backfill materials indicating that the liquid replaced by the gas in the drift seal flows into the backfills and out of the model (Fig. 6.28). Comparing the steady-state for liquid pressure with the basic scenario, it is slightly higher suggesting that less liquid is replaced by gas due to the slight increase of gas pressure, even if its value is higher. Additionally, there is no gradient for liquid pressure in the backfill materials.

During the first years, there is nearly no displacement in the model due to the corresponding small fluid pressures (Fig. 6.29). With gas pressure build up, the expansion of the backfill materials increases, whereas the drift seal gets compacted. The expansion of the left backfill is bigger than in the basic scenario due to the higher gas pressures. Since the value of gas pressure is quite close to the left stress boundary condition, the

expansion in left direction is higher than in the basic scenario leading to less compaction of the drift seal.
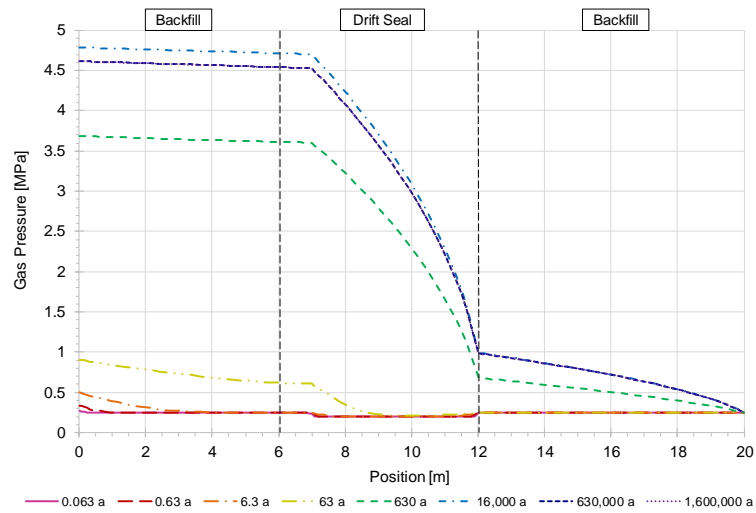
Fig. 6.27   Profiles of gas pressure (model 3i)
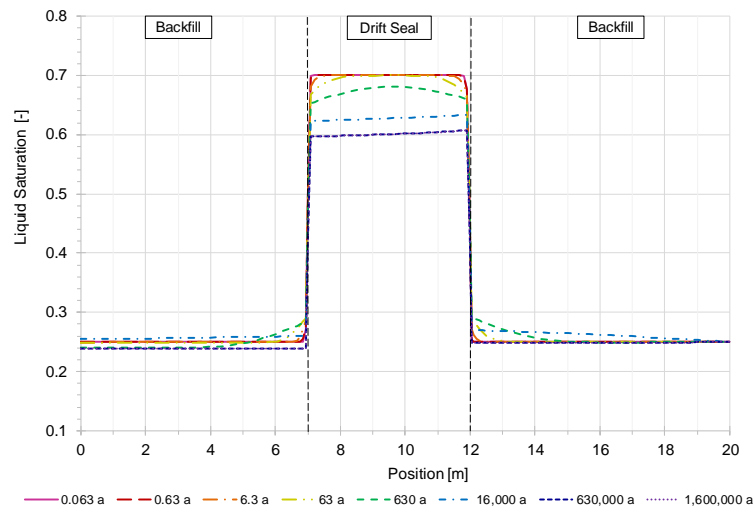
Fig. 6.28   Profiles of liquid saturation (model 3i)
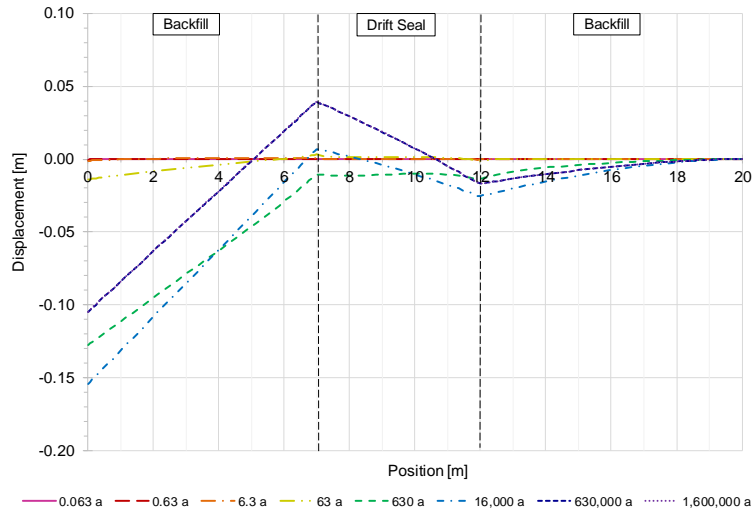
Fig. 6.29 Profiles of displacement (model 3i)

6.3 Discussion

In this modelling phase, the complexity of geometry was extended by adding a second material due to simulating a backfilled drift seal. The consideration of different materials can be challenging and deserves special attention, particularly for the numerical treatment of the transition zones between the materials. However, the basic processes observed are principally the same as investigated in the previous phases.

By comparing all partner results, one special point appeared which is not clarified yet. In scenario i, a point-shaped gas source was assumed in the left backfill material (Fig. 6.26). Due to the gas generation an increase in gas pressure is initiated which is quite similar for the first time points in all project partner results. However, with ongoing time differences appear in the maximum values of gas pressures, whereas, CODE_BRIGHT calculates the highest ones. For clarification of these differences, a closer consideration of the user-dependent implementation of the boundary condition and the numerical treatment of source terms in each simulator are needed.
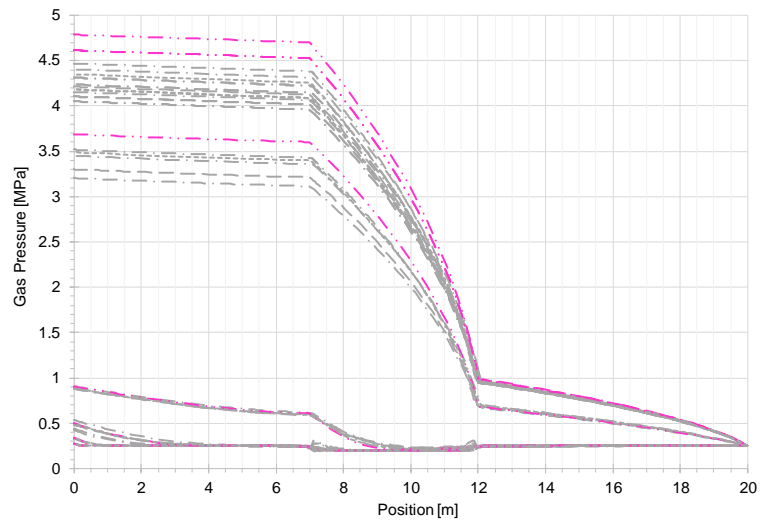
Fig. 6.30 Comparison of gas pressure profiles in model 3i for the project partner curves (grey) and the GRS curves (pink) for the time points: 0.063, 0.63, 6.3, 63, 630, 16,000, 630,000 and 1,600,000 years

In Section 6.2.5 it was shown that the effect of increased porosity is very small due to the high initial porosities. In a repository system, the fluid processes related to lower porosity ranges (< 20 %) are important to investigate, thus it should be mentioned ones more that these are results for a simplified theoretical investigation of numerical models and cannot be translated to the real system.

7 4th modelling phase – THM-coupled problem

After becoming more precise in the geometrical structure of a repository including different materials, the involved processes should be considered closer. Due to the radioactive decay of the waste to be stored, heat will be produced in a repository leading to coupled thermal interactions. The temperature increase produces thermal strains influencing the mechanical stress in the different components. The pore fluids will expand producing flow processes and affecting the effective stresses due to pressure build-up. Next to the thermal source, a gas source may exist resulting from corrosion of the waste containers. In many repository concepts, the waste canisters are made of steel which will corrode with time and in contact with liquid. The resulting gas production leads to an increase of gas pressure and induces gas flow.

For a final evaluation of a repository's safety, the thermal, hydraulic and mechanical processes must be considered in a full coupled way. However, for the proceed of numerical modelling a stepwise increase in complexity is chosen. First, a simple thermal-mechanical coupled model with a homogenous material is chosen for an initial investigation of the simulation code's thermal behaviour and additionally for proofing the accordance of the simulation codes solving elementary thermal problems. Second, the model becomes a more detailed geometry simulating an abstract disposal drift with two waste canisters, backfill material, a drift seal and the host rock. This model was first simulated TM-coupled and TH-coupled, extended to a THM-coupled simulation including the heat production and decay of the waste canisters and finally completed with adding the gas production

7.1 Pre-simulation: TM-coupled, homogenized model

In the previous modelling scenarios, the thermal aspects were not considered. For getting a first quick overview about the codes handling of thermal problems, a very simple TM-coupled model was simulated. Therefore, a generic drift with 1 m height and 40 m length containing two sections with thermal sources was assumed and a uniform set of material parameters was applied on the whole drift (Fig. 7.1). The parameters for the chosen material backfill can be found in Tab. 7.1.

Since the temperature evolution in a porous geological medium is strongly influenced by the specific heat capacity of the fluid phases, equivalent parameter should be used for a TM-coupled simulation in order to get realistic results which are comparable with a THM-

coupled simulation. These parameters include an equivalent density of 3.027 kg/m^3, a specific heat capacity of 1,640 J/(kg*K) and a thermal conductivity of 1.43 W/(m*K).
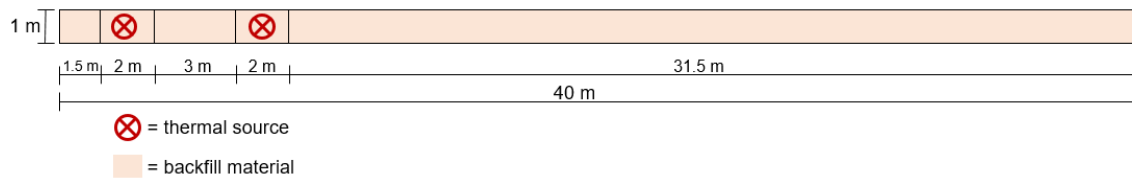
Fig. 7.1   TM-coupled homogenized model for practicing thermal implementation

The heat generation in the canister sections is assumed to be constant, therefore, each section generates a heating power of 1.5 Watt. The displacements on both ends of the model are permitted and for initial conditions a homogenous total stress of 8 MPa and an initial temperature of 25 °C is chosen.

The canisters heat output leads to a rising temperature in the whole model (Fig. 7.2, Fig. 7.3). The highest temperature increase is to be found on the left model border which acts like a reflexion axis. Thus, a maximum temperature of 98 °C is reached. Due to the fixing of both model borders the displacement reaches its maximum of about 2 mm in the middle of the model.

Altogether, the numerical results obtained with CODE_BRIGHT show a very good accordance with the analytical solutions, giving a small initial verification of the codes handling of thermal problems.
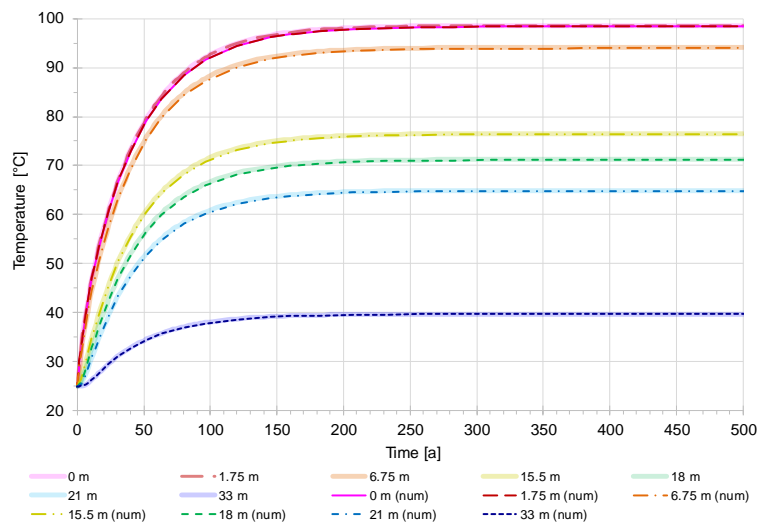
Fig. 7.2   Temperature evolution for the TM-coupled, homogenized simulation
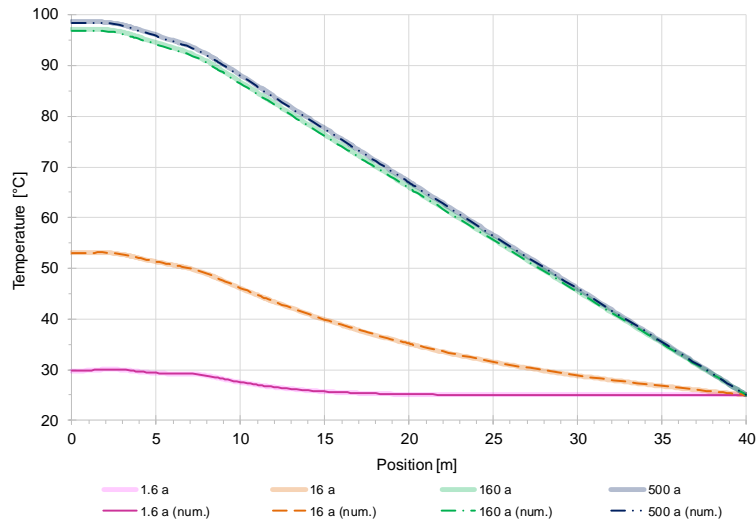
Fig. 7.3   Profiles of temperature for the TM-coupled, homogenized simulation
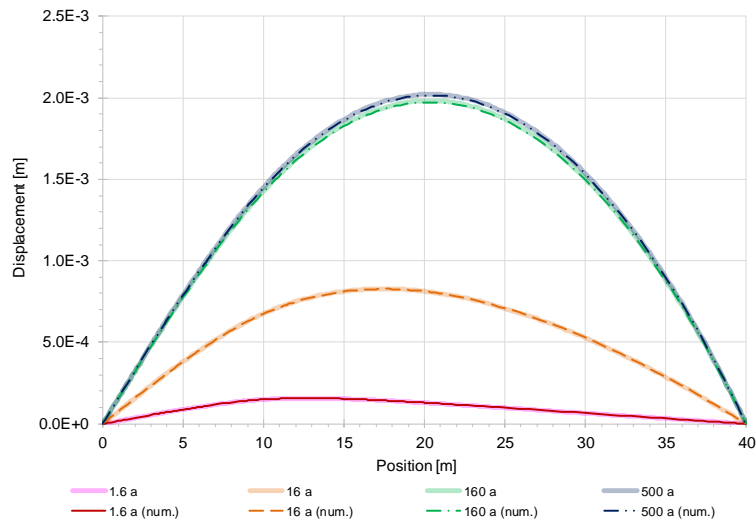
Fig. 7.4   Profiles of displacement for the TM-coupled, homogenized simulation

7.2   Modelling procedure

In the final modelling phase of this project, a generic drift is modelled containing two stored waste canisters, a drift seal as bearing, backfill material to close the underground openings and the host rock. The waste canisters are surrounded by backfill material, however, a detailed representation of individual canisters is not suitable for this application. Thus, the canister area is modelled as one section and receives averaged parameters resulting from the weighted amount of waste container and backfill material.

73

Fig. 7.5 Model geometry for the 4th modelling phase

The materials are approximated to strategies for a repository concept in clay rock (Tab. 7.1). Giving the canister section a heating power will simulate the heat entrance in the repository. The radioactive waste decay is simulated too, due to a linear decrease of heating power with time (Fig. 7.6a). Simulating heat flow in one dimension exhibits some restrictions, e. g. the vertical heat outflow into the host rock could not be reproduced leading to an overestimation of temperature inside the model. For this reason, the initial heat power is adapted to one dimension and therefore, far from the real heating power of a canister filled with high-level radioactive waste.

The simulation of gas production starts at 4,800 years with an increasing rate till a maximum input of $2.5*10^{-9}$ kg/(s*m^3) is reached (Fig. 7.6b). After, the gas production rate will decrease until it reaches zero at 14,000 years.
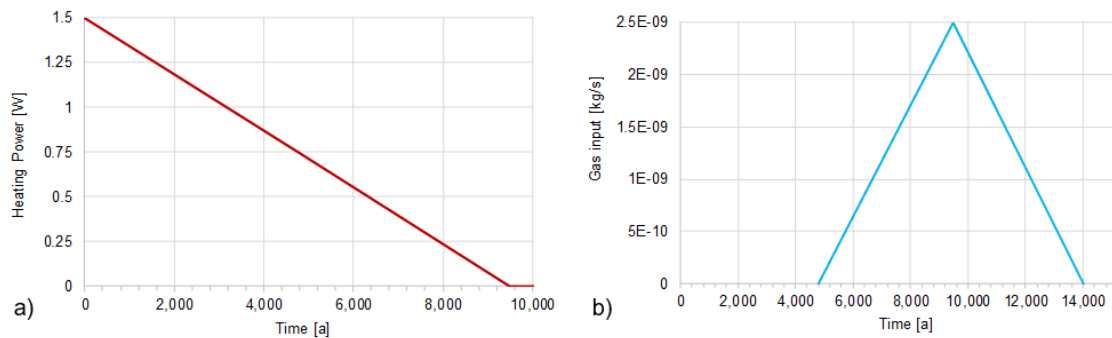
Fig. 7.6 Evolution for the simulation of a) heating power and b) gas generation

The final THM-coupled model including heat and gas production was derived by stepwise increasing complexity. Since the HM-coupling was investigated within the previous modelling phases, now, the coupling of thermal aspects with mechanics and hydraulics should be investigated individual. Thus, in Sections 7.2.1 and 7.2.2 a TM-coupled and a TH-coupled model were considered first before the assembly of all processes. Another intermediate step was done in Section 7.2.3 by simulating only the heat decay in a THM-coupled way before finally adding the gas generation in Section 7.2.4.

Tab. 7.1 Material parameter for the 4th modelling phase

Parameter		Backfill	Canister Section	Drift Seal	Host Rock	
Young's modulus	E	45	150	400	8,000	[MPa]
Poisson's ratio	ν	0	0	0	0	[-]
Porosity	Φ	0.42	0.37	0.35	0.17	[-]
Intrinsic permeability	K	$2*10^{-18}$	$1.75*10^{-18}$	$2*10^{-20}$	10^{-20}	[m²]
Biot coefficient	α	1	1	1	0.7	[-]
Residual liquid saturation	S_{lr}	0.03	0.03	0.1	0.16	[-]
Residual gas saturation	S_{gr}	0	0	0	0	[-]
Van Genuchten parameter	λ	0.5	0.5	0.3	0.28	[-]
Van Genuchten pre-factor	$p_{cap,0}$	12	12	26	30	[MPa]
Pore connectivity par.	$\tilde{\varepsilon}, \tilde{\gamma}$	0.5	0.5	0.5	0.5	[-]
Thermal conductivity	λ_{dry}	1.23	7.33	1.38	1.91	[W/(mK)]
	λ_{wet}	1.49	7.55	1.59	2.02	
Specific heat capacity	C_s	1,100	830	950	900	[J/(kgK)]
Density	ρ_s	2,500	3,450	2,500	2,700	[kg/m³]
Thermal expansion coeff.	α_{th}	$5*10^{-6}$	$5.9*10^{-6}$	$4*10^{-6}$	$3.6*10^{-6}$	[K⁻¹]
Liquid viscosity	η_l	$5*10^{-10}$				[MPa*s]
Liquid bulk modulus	$\breve{K}_l$	2,120				[MPa]
Liquid density	ρ_l	970				[kg/m³]
Liquid thermal conductivity	λ_l	0.65				[W/(mK)]
Liq. vol. therm. expansion	$\gamma_{th,l}$	$6*10^{-4}$				[K⁻¹]
Gas viscosity	η_g	$2*10^{-11}$				[MPa*s]
Gas thermal conductivity	λ_g	0.03				[W/(mK)]
Gas vol. therm. expansion	$\gamma_{th,g}$	$3*10^{-3}$				[K⁻¹]

7.2.1 Step a – TM-coupled model

With the application of a TM-coupled model the direct influence of temperature increase on the mechanical behaviour can be investigated. The displacements are caused by thermal strains only and with vanishing heating power the displacements should disappear, too. Further, the heat flow independent of changes in thermal conductivity can be observed and a first range of maximum temperature can be estimated. The initial and boundary conditions are displayed in Fig. 7.7. In the two canister sections, a thermal source with a power of 1.5 W per section is applied from on the beginning and is decreasing linearly till 9,500 years. For allowing a heat flow out of the model, the temperature on the right boundary is kept constant to 25 °C based on the non-restricted heat flow

into the host rock. Of course, equivalent parameters are used for ensuring the comparability with the THM-coupled simulations.
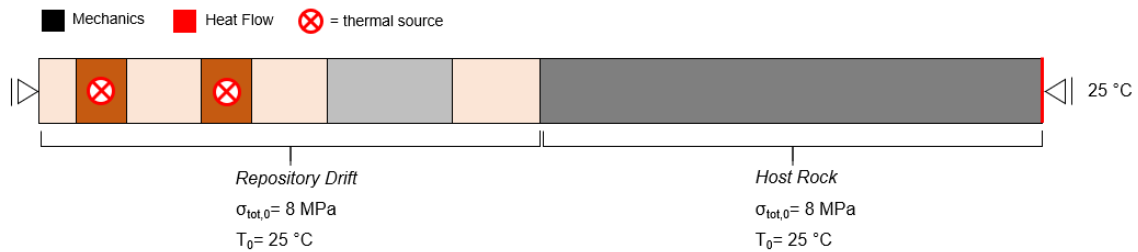
Fig. 7.7   Initial and boundary conditions for model 4a

In the beginning, the temperature rises rapidly due to the heat input from the waste canisters and reaches its maximum of ~81.4 °C after about 175 years (Fig. 7.8). According to the linear decrease of heating input, the temperature decreases linearly from the maximum point on reaching the initial value of 25 °C after 9,500 years. The area of maximum temperature is located at the left model border which acts like a reflection axis (Fig. 7.9). The temperature distribution inside the canister sections is nearly constant whereas it is linear in the other materials. The heat flow is faster in the repository part than in the host rock determinable by the gradients in temperature profiles.

The induced thermal strains lead to displacement of the different materials (Fig. 7.10). In the early time the whole repository area moves against the host rock. However, with time, the canister sections, the drift seal and the host rock expand leading to compaction of the backfill elements. The biggest extension can be found in the host rock; its left boundary moves about 1 mm against the repository section and as a result, the adjacent backfill experiences a strong compaction. Coherent with the temperature results, the highest displacements are reached after 175 years and with decreasing temperature the thermal strains are also becoming smaller till the initial state is reached after 9,500 years.
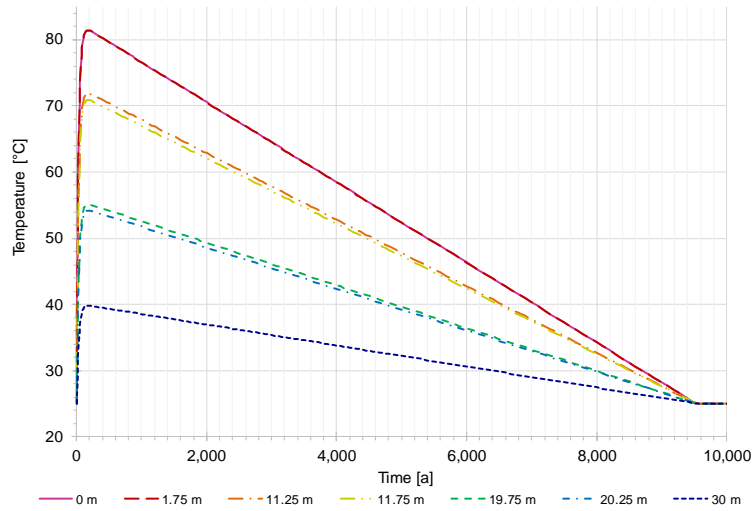
Fig. 7.8   Temperature evolution for model 4a
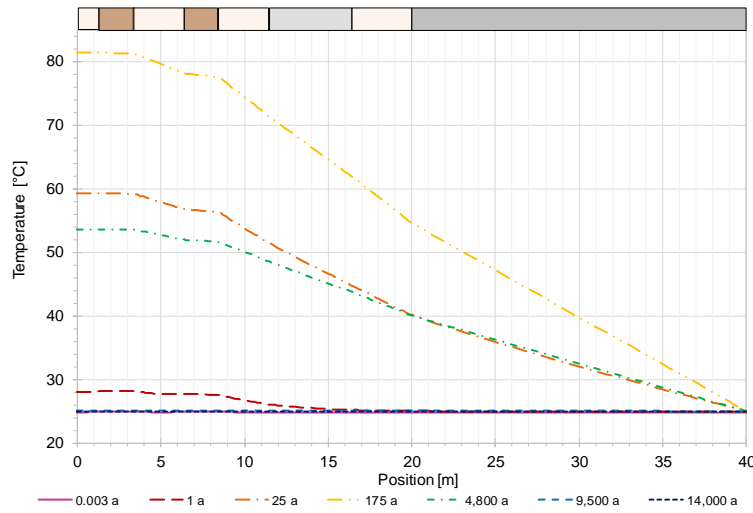
Fig. 7.9   Profiles of temperature for model 4a
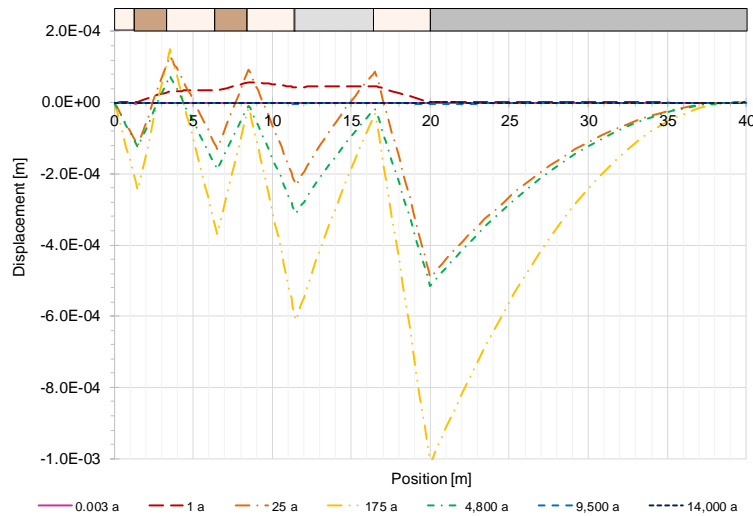
Fig. 7.10   Profiles of displacements for model 4a

7.2.2 Step b – TH-coupled model

Since the interactions between mechanics and temperature were examined in the previous chapter, here, the focus is on thermal and hydraulic interactions. For evaluation of the couplings between the thermal and hydraulic processes, both sources have to be considered. Fluid processes affect the heat flow processes e. g. due to changes in thermal conductivity with varying fluid saturation. The other way around, temperature variations lead to changes in fluid properties like viscosity.

Fig. 7.11 shows the model including the thermal and the gas source in the canister sections and the initial and boundary conditions. The host rock is assumed to be full saturated with fluid pressures of 4 MPa and the repository section has an initial saturation of 0.75. In its initial state the model has an initial temperature of 25 °C.

| Heat Flow | Liquid Flow | Gas Flow | ⊗ = thermal source | ⊗ = gas source |

Repository Drift
T_0= 25 °C
$p_{g,0}$ = 0.1013 MPa
$S_{l,0}$= 0.75

Host Rock
T_0= 25 °C
$p_{g,0}$ = 4 MPa
$p_{l,0}$= 4 MPa
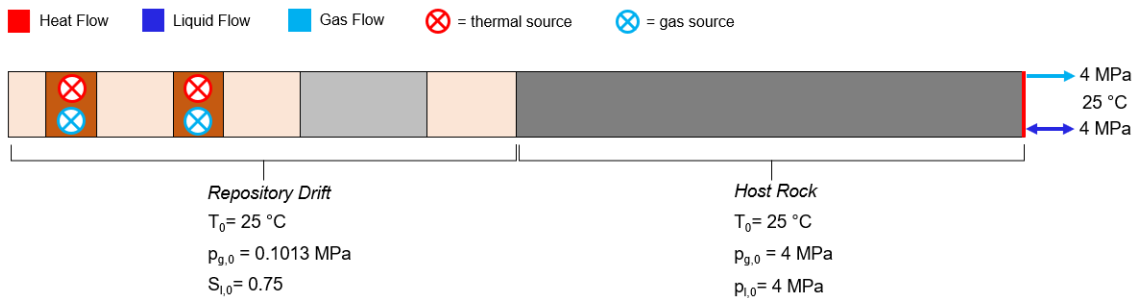
Fig. 7.11   Initial and boundary conditions for model 4b

The temperature evolution is very similar to the TM-coupled ones. The heat input leads to a strong increase in temperature reaching its maximum of 80.9 °C after about 163 years (Fig. 7.12). Thus, the maximum temperature is reached earlier, and its value is slightly smaller compared to the TM-coupled simulation (Fig. 7.8). Also, here, the temperature decreases linearly with heat input decreases till the initial temperature of 25 °C is reached.

The initial state of gas pressure distribution in the model provides a sharp transition between the host rock with 4 MPa and the repository section with atmospheric pressure (Fig. 7.13). With time the gas pressure begins to decrease in the host rock due to outflow of gas into the repository following the aim of equilibration. As a result, the pressure slightly increases in the repository section. With the start of gas production at 4,800 years, the gas pressure in the repository section, as well as in the host rock increases. The gas generation rate of $2.5*10^{-9}$ kg/(s*m³) leads to a maximal gas pressure of 21.7 MPa which is very high due to the fact of the one-dimensional model and the low

permeabilities. The profile for 9,500 years shows a homogenous pressure distribution in the repository section with exception of the drift seal where a gradient develops. In the host rock, there is also a gradient in gas pressure resulting from the influence of the right hand-side boundary condition. The gas outflow in frame of the boundary condition regulates the decrease of pressure with time. In the steady-state, a constant gas pressure of 4 MPa is reached in the whole model.

Considering the profiles for liquid saturation, first, it is referred to numerical inaccuracies due to the high gradient in the transition between the drift seal and the backfills (Fig. 7.14). Since the retention curves of the backfill and the canister is the same, there are no differences in suction pressure for these materials (Fig. 7.15). However, the drift seals retention curve shows higher capillary pressures for the whole range of saturation, leading to a higher suction stress for the initial saturation.

With ongoing heat input, the liquid saturation in the backfill, the canisters and in the host rock decreases, whereas it increases in the drift seal. The reason can be found by considering the liquid pressure evolution (Fig. 7.15). The increasing temperature induces a liquid flow into the direction of the outflow possibility, thus liquid flows from the backfills and canisters into the drift seal leading in an increase of liquid pressure which results in saturation increase. At the same time, the liquid pressure decreases in the host rock leading to a partially desaturation. When reaching the maximum temperature at 163 years, the liquid pressure in the repository section is nearly homogenous.

With start of the gas generation at 4,800 years, the liquid pressure and consequently the liquid saturation starts to increase due to the relationship between the fluid pressures in the pore space. The very high gas pressure at 9,500 years results from the high amount of produced gas which gets pressurized because of the restricted pore space and the low permeabilities. Since the fluid interacts inside the pore space, the high amount of gas pressurizes the liquid leading to a maximum liquid pressure of 15 MPa for a saturation of 87 %. When the gas generation rate becomes smaller, the fluids get relaxed due to outflow and the pressure decrease. For the steady-state, a liquid pressure of 4 MPa is reached which is equal to the gas pressure Additionally, in the steady-state the whole repository section is fully saturated resulting from liquid inflow from the host rock.
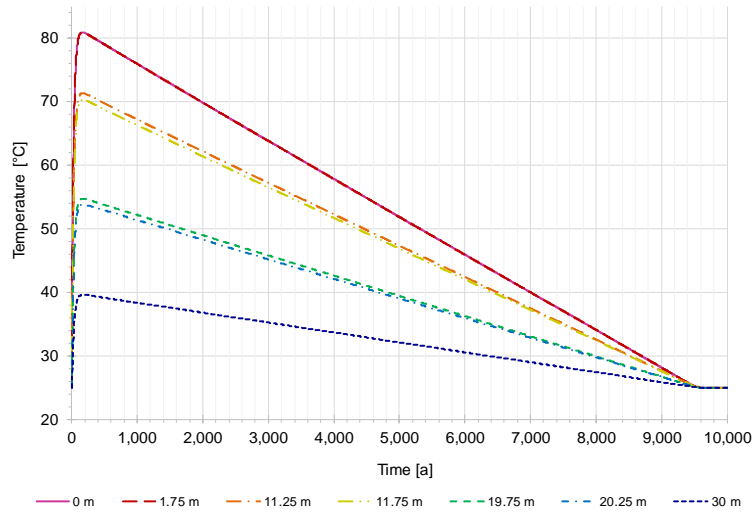
Fig. 7.12   Temperature evolution for model 4b
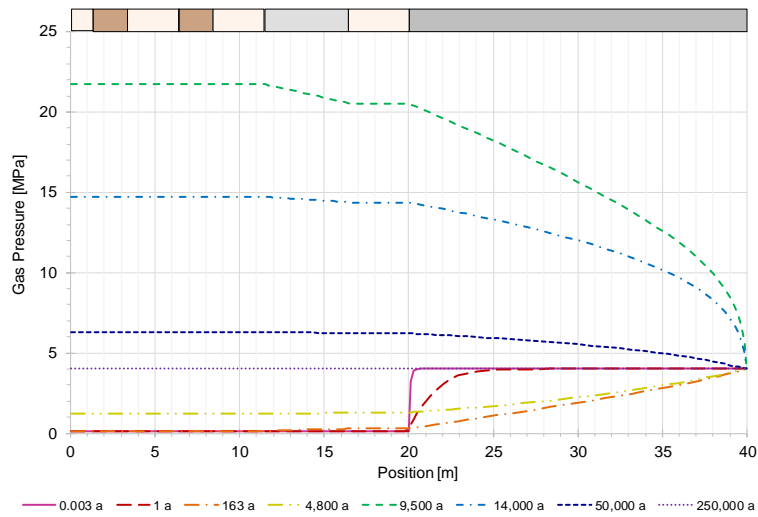
Fig. 7.13   Profiles of gas pressure for model 4b
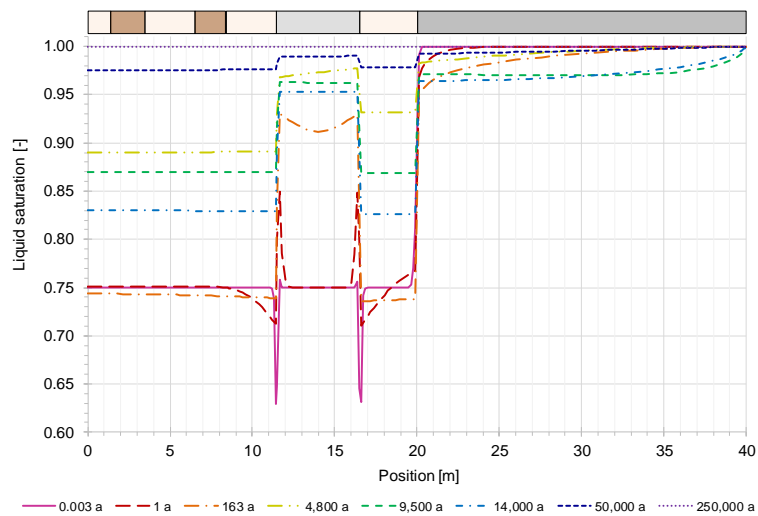
Fig. 7.14   Profiles of liquid saturation for model 4b
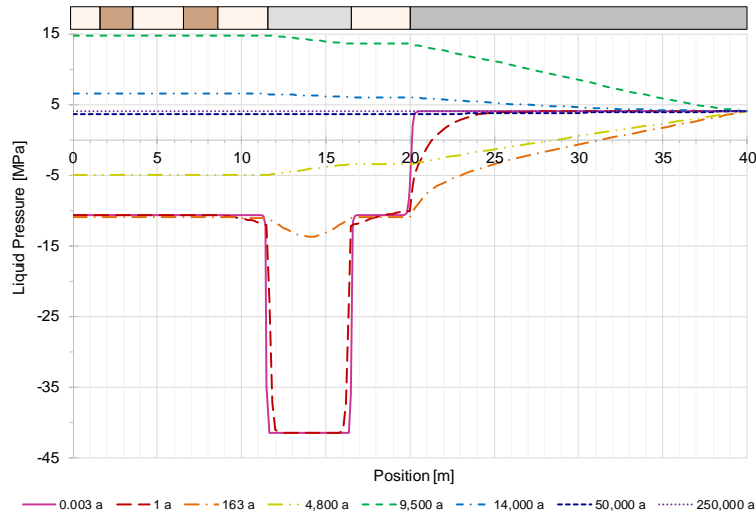
Fig. 7.15 Profiles of liquid pressure for model 4b

7.2.3 Step c – THM-coupled model with thermal source

After investigating the TM- and TH-coupled processes individually, in the next step, the thermal, hydraulic and mechanical aspects are merged, however, with the simplification of neglecting the gas source first. The initial and boundary conditions are equal to the previous two sections; thus, the host rock is considered as full saturated with a pore pressure of 4 MPa, the initial saturation of the repository section is set to 0.75 and the gas pressure is atmospheric (Fig. 7.16). Additionally, the initial stress state is set to 8 MPa, the initial temperature is 25 °C and the thermal source was implemented following Fig. 7.6a.
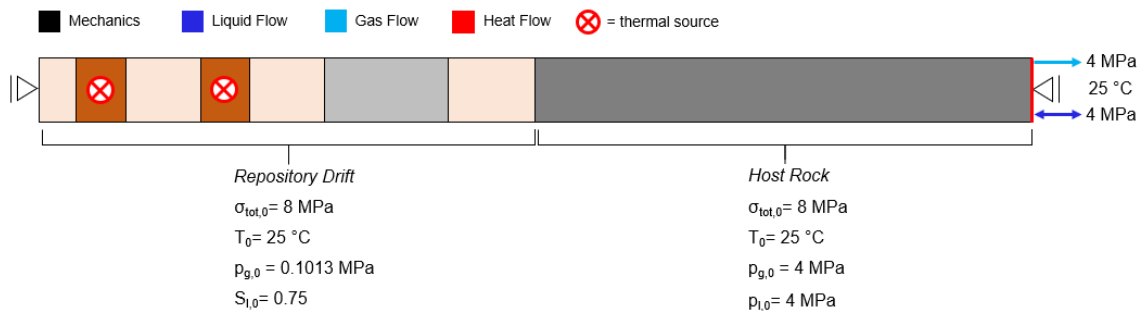
Fig. 7.16 Initial and boundary conditions for model 4c

Considering the temperature evolution, the results are quite similar to the previous simulations (Fig. 7.17). After a rapid increase, temperature reaches its maximum of 80.9 °C

81

at 163 years which is totally equal to the TH-coupled simulation (Fig. 7.12). In the further course, the temperature decreases linear till it reaches the initial temperature of 25 °C.

Until the beginning of the gas generation at 4,800 years, which is not considered here, the evolutions of fluid pressures and their saturations respectively are also similar to the TH-coupled simulation (Fig. 7.18, Fig. 7.19, Fig. 7.20). With increasing temperature, the fluid pressures rise due to the thermal expansion of both fluid phases leading to pore overpressures. Since the thermal expansion coefficients of all solid phases are of two or three orders of magnitude lower than the ones of the gas and the liquid phase, respectively, it leads to a pressurizing of the fluids due to differences in expansion velocity. After the end of heat generation, the gas pressure still rises to a maximum value of about 5.4 MPa. Simultaneously with decreasing temperature, liquid flow inside the repository is activated leading to an increasing saturation and gas pressure. In the steady-state, both fluid pressures are equilibrated to 4 MPa and the whole model is fully saturated.

For the profiles of liquid saturation, also numerical inaccuracies are occurring in the transition between backfills and drift seal (Fig. 7.19). In general, the same basic fluid processes as describes in Section 7.2.2 are occurring. With increasing temperature, the flow of liquid to colder areas is started, additionally the desaturation of the host is occurring, both leading to an increase of liquid pressure and liquid saturation in the drift seal. However, the drift seal does not reach a homogenous saturation, since the mechanical processes lead to expansion with increasing saturation.

Since the hydraulic processes have a very strong effect on the mechanical behaviour due to the definition of effective stresses, it is hard to compare the displacements for this simulation with the TM-coupled one in Section 7.2.1. However, the experience made with the TM-coupled simulation indicates a very low reaction on thermal strains in the early time (Fig. 7.10). In contrast to the TM-coupled simulation when only the backfill materials are compacted, here, all materials, except the drift seal, becomes compacted due to the increasing temperature (Fig. 7.21). Because of the fast-increasing amount of liquid inside the drift seal and the thermal expansion of the fluids, the drift seal underlies a strong expansion, compacting all the other materials.
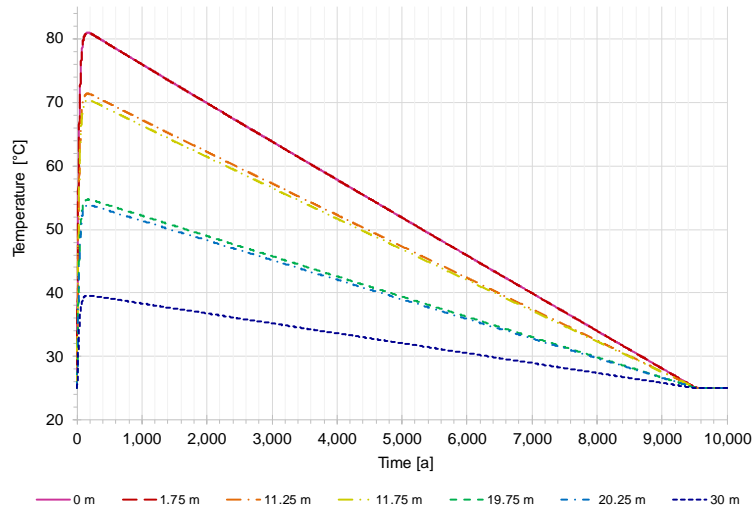
Fig. 7.17   Temperature evolution for model 4c
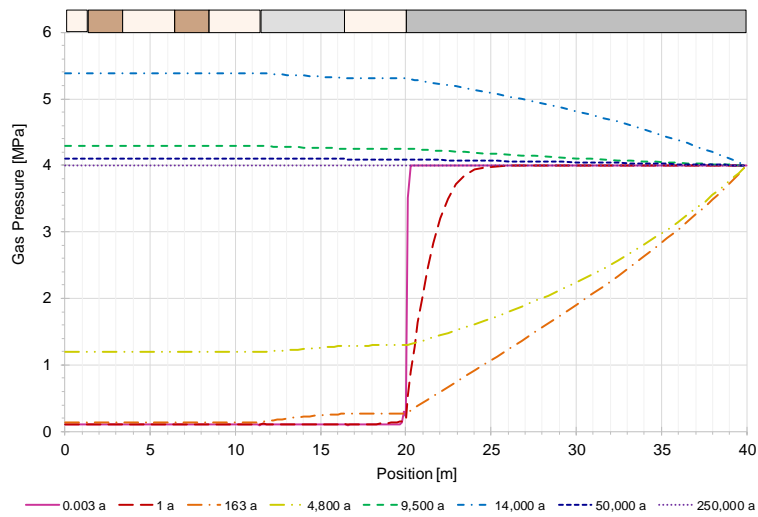
Fig. 7.18   Profiles of gas pressure for model 4c
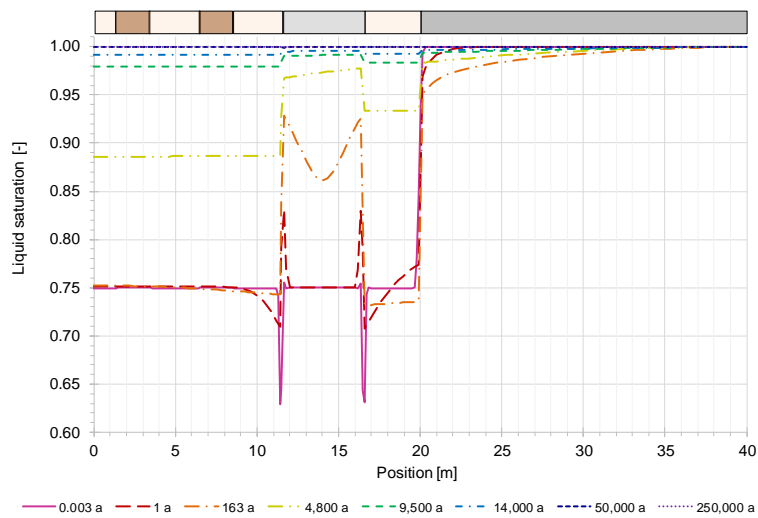
Fig. 7.19   Profiles of liquid saturation for model 4c

83
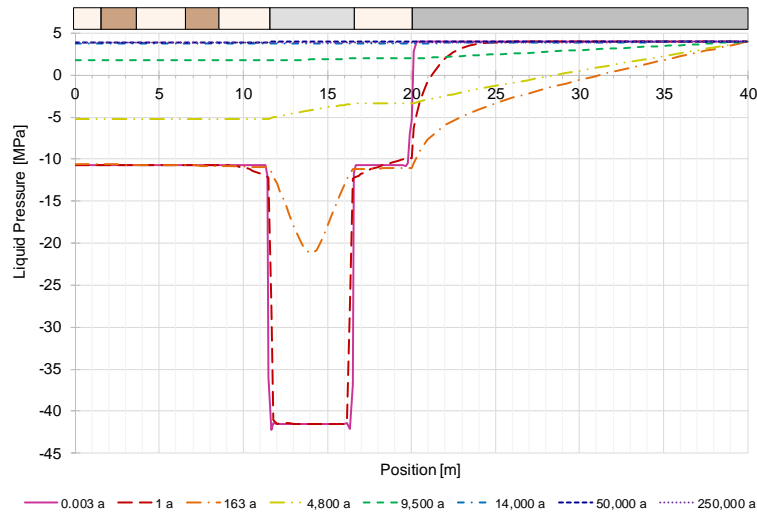
Fig. 7.20   Profiles of liquid pressure for model 4c
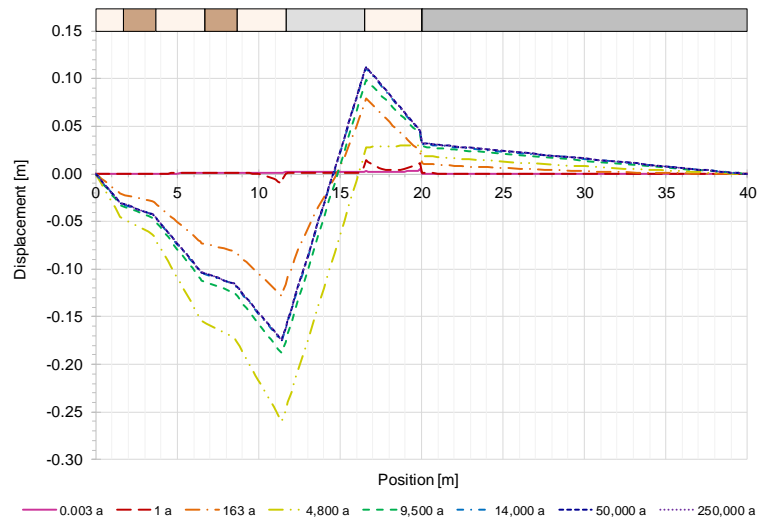
Fig. 7.21   Profiles of displacements for model 4c

7.2.4   Step d – THM-coupled model with thermal and gas source

In the final step, this scenario includes the full THM-coupled model with a linear decreasing heat input and the simulation of gas development inside a repository. The initial and boundary conditions are already explained in the previous sections and complained in Fig. 7.22. The heat and gas source are following the evolution shown in Fig. 7.6.
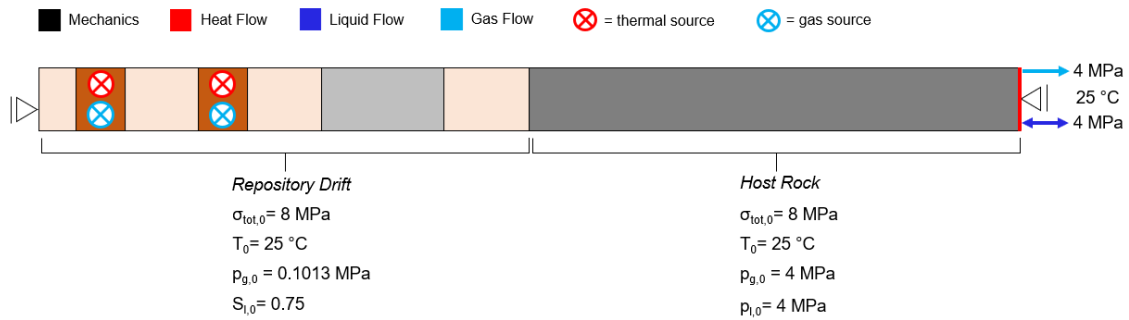
Fig. 7.22 Initial and boundary conditions for model 4d

Since the temperature evolution depends on the slight variation of thermal conductivity with degree of liquid saturation only, no differences can be determined by comparing the temperature evolution with the previous ones (Fig. 7.23). It reaches the maximum temperature of 80.9 °C after 163 years which is also the case for the TH-coupled and THM-coupled simulation neglecting the gas phase.

The gas pressure evolution is nearly the same as for the TH-coupled model leading to the conclusion that the occurring processes are the same and that the mechanics have no influence on the pressure build up as a result of the gas generation (Fig. 7.24).

In contrast, the evolutions of liquid pressure and saturation are similar to the THM-coupled model neglecting gas build up until the start of gas generation indicating a clear influence of mechanics on the liquid phase as described in Section 7.2.3. In the further course, the evolution is equal to the TH-coupled simulation, hence, the gas generation exerts a strong influence on the liquid phase (Section 7.2.2).

In general, the displacement profiles for both THM-coupled simulations looks quite similar (Fig. 7.21, Fig. 7.27). However, the influence of gas pressure build-up can be figured out clearly. For the peak of gas input at t = 9,500 years the strongly compacted repository area left-hand of the drift seal extends due to a blow-up and pushes the drift seal into the right direction resulting in a further compaction of the last backfill element. With diminishing gas production rate, the repository section moves back into left direction resulting in a relaxation of the last backfill element and a slightly re-compaction of the backfilled canister sections. In the long-term behaviour, the displacements reach the same steady-state which arises with neglecting the gas production.
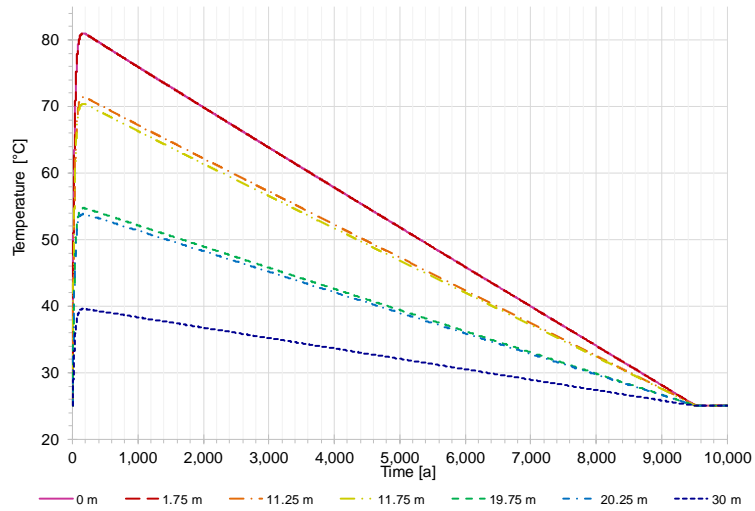
Fig. 7.23 Temperature evolution for model 4d
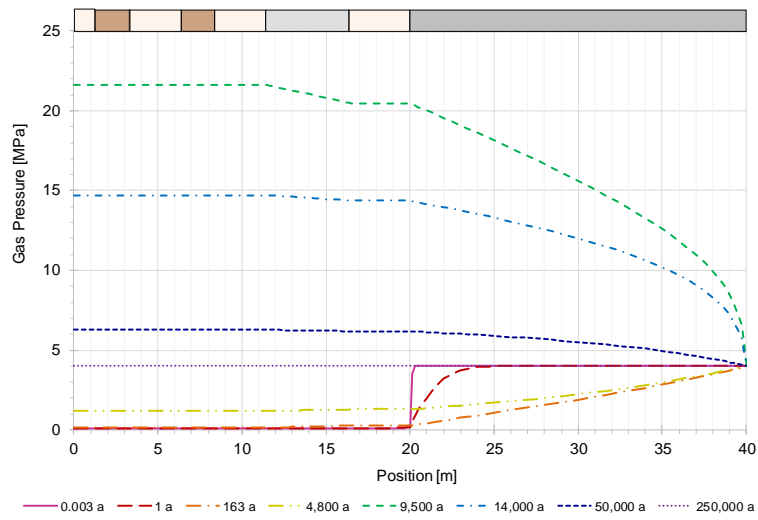
Fig. 7.24 Profiles of gas pressure for model 4d
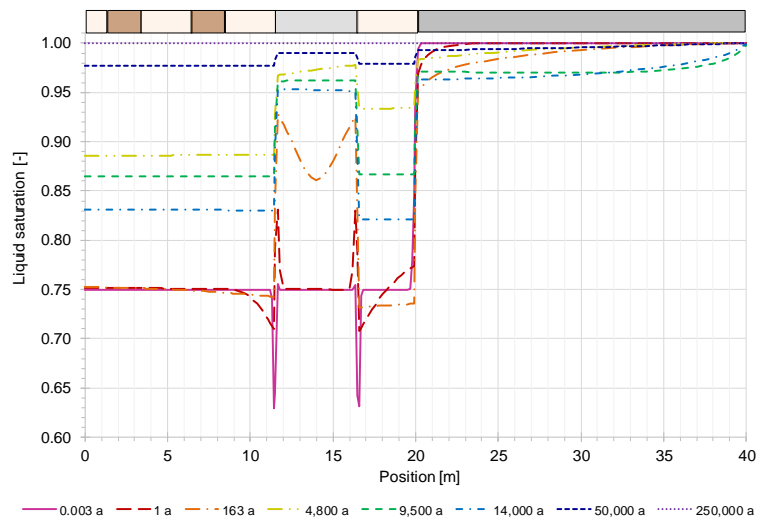
Fig. 7.25 Profiles of liquid saturation for model 4d
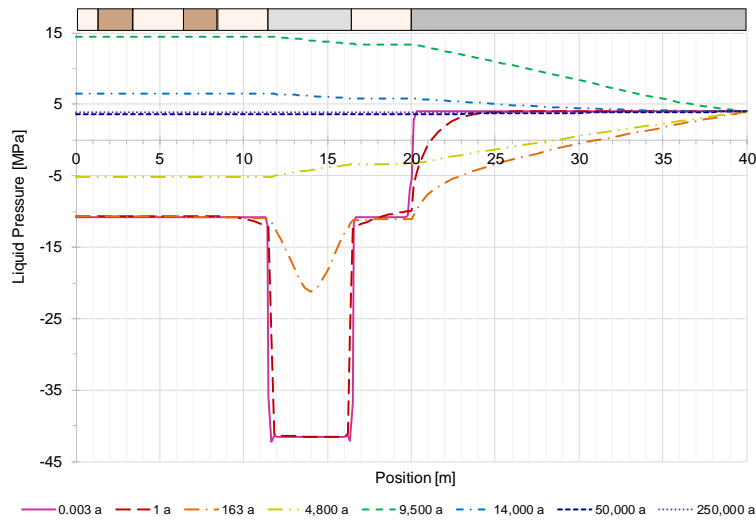
Fig. 7.26   Profiles of liquid pressure for model 4d
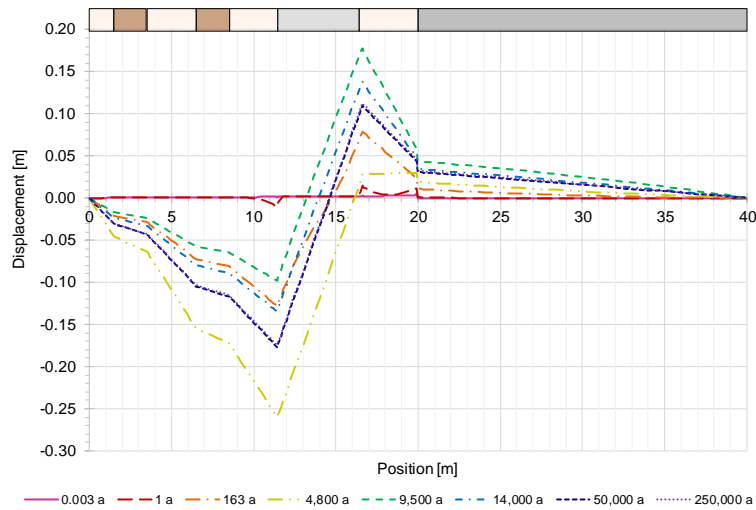
Fig. 7.27   Displacement profiles for model 4d

7.3   Discussion

In this last stage of modelling work, a comparison with project partner results was not possible yet. However, the presented results are plausible and explicative in the consecutive way. Therefore, first the accordance of numerical results with analytical ones for a simple thermal-mechanical coupled problem was shown in Section 7.1. With stepwise increasing complexity, it was exhibited that a TM-coupled problem in a partially saturated porous medium can be compared to a THM-coupled problem by using equivalent values for density and specific heat, since temperature distribution is strongly affected by the latter. Due to the detailed consideration of sequential processes and couplings a comprehensive understanding was achieved.

During the simulation process differences in the treatment of fluid properties, like density and viscosity, between the various simulation codes were exposed. Whereas the most simulation codes are capable to set the fluid properties constant, the dependencies on temperature and pressure could not be neglected in CODE_BRIGHT. There are different options implemented for the relation of fluid properties dependencies, thus in the future, it would be of interest to compare and investigate the fluid properties implementations in various simulation codes and their influence on the simulation results.

Another question appearing during the modelling work includes the handling of hydraulic processes in transition zones of materials with different retention curves. In the simulations including hydraulics, discontinuities in liquid saturation profiles could be observed in the transition between drift seal and backfills. Fig. 7.28a shows a plot of the liquid saturation distribution in the drift seal and the neighbouring backfills in early time. Mostly, the saturation is close to its initial value of 0.75, but the two elements of backfill which are directly located next to the drift seal show deviations. The corresponding liquid pressure distribution presents a high gradient in the transition due to the different retention curves (Fig. 7.28b). As already discussed in Section 4.3, the pressures are calculated as nodal values and the saturation are derived element-wise which causes numerical inaccuracies.
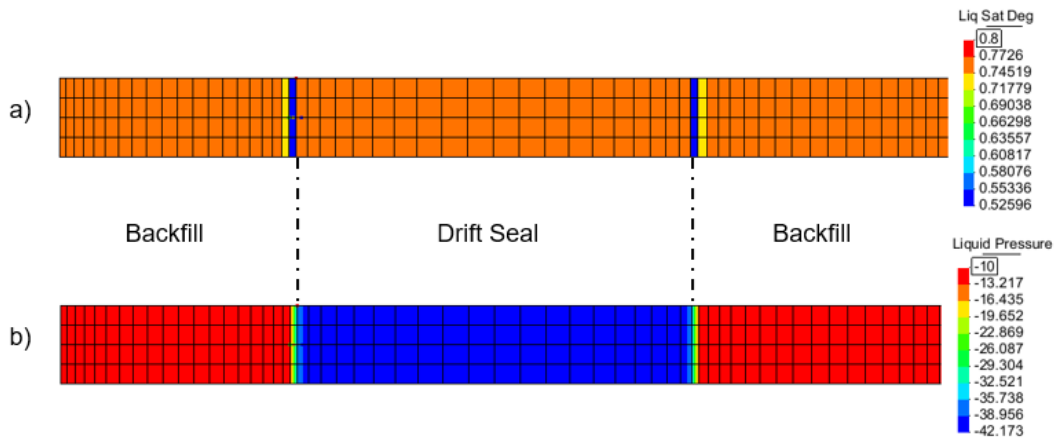
Fig. 7.28   Plot of a) liquid saturation distribution and b) liquid pressure distribution in the drift seal and the adjacent backfill elements for t = 0.003 a

By a closer consideration of the displacement profiles, discontinuities in the transition between the backfill and the host rock can be observed (Fig. 7.29). The compaction of the backfill element is not homogenous since its last 10 cm underlie a stronger compaction. This phenomenon can be observed in both THM-coupled simulation and its investigation will be part of future work in GRS.
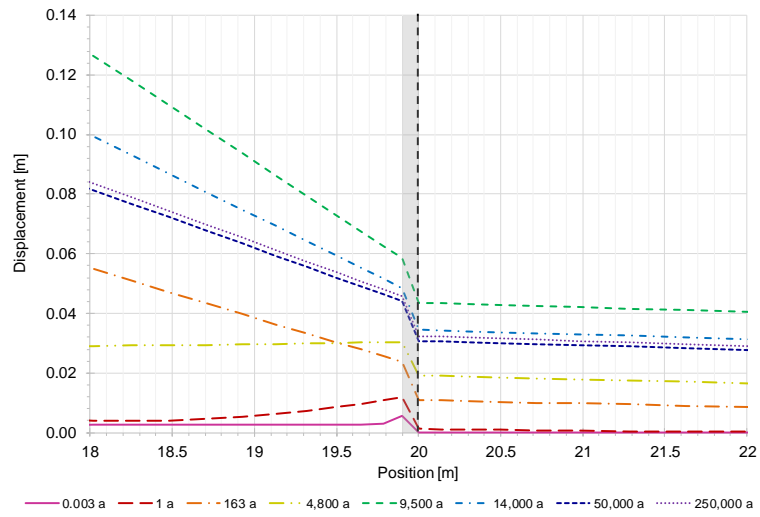
Fig. 7.29 Detail of model 4d displacement profiles focussing the transition between the backfill and host rock

8   Discussion and conclusion

The aim of this THM-coupled simulator benchmarking project was to apply well specified and simplified modelling tasks to investigate basic processes, especially flow phenomena, which are included in mostly all THM-coupled simulations in porous media. Therefore, different modelling phases were planned, starting with single phase flow coupled with mechanics extending to two-phase flow and finally reaching a full THM-coupled model. To have a clear focus on the model evolution and the influences of the various processes, it was started with a very simple one-dimensional model. With time the geometry complexity was increased by simulating a backfilled drift seal and finally assuming a generic repository drift, still in one-dimension. Due to the detailed exploration and comparison of various simulation codes, the project partners gained improvements of code understanding and advancement of their own code.

Within the project, comparisons of results for the first, second and third modelling phase were done. All in all, the final results show very good accordance between the different simulators, since there had been discussions and adaptions within the working progress.

In general, there had been a discussion about the definition of effective stresses, since the prescribed definition following Bishop stresses Eq. (3.9) is not included for simple linear elasticity in CODE_BRIGHT. The default definition for linear elasticity is following Eq. (3.12), hence, deformation is affected by the maximum fluid pressure which is the gas pressure for unsaturated media and the liquid pressure for full saturated media. The prescribed definition following Bishop includes a suction-induced compaction which is mostly applied for argillaceous materials and therefore implemented in the more complex mechanical model for describing argillite in CODE_BRIGHT. By comparing the first simulation results for the first modelling phase, the displacements of CODE_BRIGHT were in very good agreement with the project partners, because the differences in effective stress definition vanishes for full saturation. First when applying a partially saturated model the differences becomes clear. However, in the further course of the project, CODE_BRIGHT could handle simple linear-elasticity with the application of Bishop stresses.

Another issue appearing during the project lifetime was the application of Biot theory /BIO 57/. As already discussed in Section 4.3, the hydraulic part of the Biot theory which describes the change of fluid content with pore pressure increase in dependence of the

fluids and grain compressibility, is not implemented in CODE_BRIGHT. Thus, the mechanical influence of a different grain compressibility on the hydraulics is neglected. For a full saturated model, this mechanism can be simulated by an iterative adaption of grain compressibility in the solid phase. However, for a partially saturated system this proceeding is not suitable leading to deviations in fluid pressure evolutions.

In this benchmarking exercise the mesh discretization was not prescribed, but the influence of mesh discretization was investigated showing clear influences of mesh discretization on the simulation results. Especially, due to the element-wise calculation of some quantities in CODE_BRIGHT the mesh size and refinement affects the results.

It was shown in the third modelling phase in Section 6.2.8 that differences between gas pressure increase as a result of a gas source exist between the various simulators. The reasons are not clarified yet, hence, it is assumed that there will also be differences between the project partner results in the gas pressure evolution for the fourth modelling phase.

By adding the thermal aspects, a discussion about the influence of fluid properties dependences on pressure and temperature was initiated. Since it is not possible to set fluid properties constant in all simulation codes, the default values have to be compared and differences should be examined. However, this was not possible in the frame of this project and is therefore a need for future work.

Within the framework of this project, CODE_BRIGHT could be improved in cooperation with the code developers and discussions for further advancements have been induced. For example, the gas phase relative permeability relationship following van Genuchten was implemented and discussions about the necessity of constant fluid parameters and the implementation of the Biot theories hydraulic part were initiated. On basis of the project results, there are clear indications of further needs for investigations which are partly mentioned in the previous chapters. Due to the restricted project lifetime the thermal aspects and their coupling interactions could not be investigated adequately, and potential work is of future interest. After such detailed examination in one dimension, an increase in complexity by two and three dimensions should be another step further. Additionally, the increase in complexity referring mechanical material models and becoming more realistic or material specific could be material for future work.

References

/BIO 57/   Biot, M. A., Willis D. G., The Elastic Coefficients of the Theory of Consolidation. Journal of Applied Mechanics, pages 597 – 601, December 1957

/BIS 61/   Bishop, A. W., Donald, I. B., The Experimental Study of Partly Saturated Soil in the Triaxial Apparatus, Proceedings of the 5th International Conference on Soil Mechanics and Foundation Engineering; July 1961, Paris, France

/CIM 20/   International Center for Numerical Methods in Engineering (CIMNE), GiD Reference Manual, Barcelona, 2020

/COM 12/   COMSOL Inc., COMSOL Multiphysics 4.5, User's Guide, 2012

/HOE 12/   Müller-Hoeppe, N., Breustedt, M., Wolf, J., Czaikowski, O., Wieczorek, K., Intigrität geotechnischer Barrieren, Teil 2, Vertiefte Nachweisführung. Bericht zum Arbeitspaket 2, Vorläufige Sicherheitsanalyse Gorleben, GRS-288, Oktober 2012

/HOT 14/   Hotzel, S., Gasausbreitung in unverritztes Steinsalz – Hydro-mechanisch gekoppelte Modellrechnungen mit dem Simulationstool TFC, Report GRS-339, BMUB project 3610R03230, Cologne, Germany, 2014

/KOL 12/   Kolditz, O. Bauer, S., Bilke, L., Böttcher, N., Delfs, J.-O., Fischer, T., Görke, U.-J., Kalbacher, T., Kosakowski, G., McDermott, C.I., Park, C.-h., Radu, F., Rink, K., Shao, Hua, Shao, Haibing, Sun, F., Sun Y., Singh, A.K., Taron, J., Walther, M., Wang, W., Watanabe, N., Wu, Y., Xie, M., Xu, W., Zehner, B., OpenGeoSys: an open-source initiative for numerical simulation of thermo-hydro-mechanical/chemical (THM/C) processes in porous media, Environ. Earth Sci., 67(2), 589–599, 2012

/LUX 15/   Lux, K.H., Rutenberg, M., Seeska, R., Feierabend, J., Düsterloh, U..: Kopplung der Softwarecodes FLAC³D und TOUGH2 in Verbindung mit in situ-, laborativen und numerischen Untersuchungen zum thermisch-hydraulisch-mechanisch gekoppeltem Verhalten von Tongestein unter Endlagerbedingungen, Teil II: Physikalische Modellierung, Kopplung von FLAC³D und TOUGH2 sowie numerische Simulationen, Abschlussbericht zum BMWi-Forschungsvorhaben (02E11041), Lehrstuhl für Deponietechnik und Geomechanik, Technische Universität Clausthal, Clausthal-Zellerfeld, September 2015.

/LUX 18/   Lux, K.H., Rutenberg, M.: Vorprojekt – Internationales Benchmarking zur Verifizierung und Validierung von TH²M-Simulatoren insbesondere im Hinblick auf fluiddynamische Prozesse in Endlagersystemen (BenVaSim), Abschlussbericht zum BMWi-Forschungsvorhaben (02E11506), Lehrstuhl für Deponietechnik und Geomechanik, Technische Universität Clausthal, Clausthal-Zellerfeld, März 2018

/RIN 18/   Rinaldi, A.P., Rutqvist, J., Blanco-Martín, L., Hu, M., Sentis, M.L., 2018, Coupling TOUGH3 with FLAC3D for parallel computing of fluid flow and geomechanics, Proceedings of the TOUGH Symposium 2018

/RUT 18/   Rutenberg, M., Feierabend, J., Lux, K.-H., Maßmann, J., Lorenzo Sentís, M.L., Graupner, B.J., Hansmann, J., Czaikowski, O., Wieczorek, K., Friedenberg, L., Hotzel, S., Kock, I., Rutqvist, J., Hu, M., Rinaldi, A.P., 2018, BenVaSim – A Benchmarking of Simulators for Modelling TH2M Processes in the Context of Radioactive Waste Disposal. Proceedings of TOUGH Symposium 2018

/RUQ 11/   Rutqvist, J., 2011, Status of the TOUGH-FLAC simulator and recent applications related to coupled fluid flow and crustal deformations, Computers & Geosciences 37, 739 – 750

/TER 43/   Terzaghi, K., Theoretical Soil Mechanics. John Wiley and Sons, 1943

/UPC 20/   Universitat Politècnica de Catalunya, Department of Civil and Environ-
            mental Engineering, Division of Geotechnical Engineering and Geosci-
            ences: CODE_BRIGHT User's Guide, Version 8.4, Barcelona, September
            2018

List of figures

List of tables

A   General overview about the models

A general overview about the different modelling phases is given. Therefore, the basic scenarios are representative for the 1st – 3rd modelling phases, respectively, and the final THM-coupled model is displayed for the 4th phase.

1st modelling phase (s. Fig. 4.4):
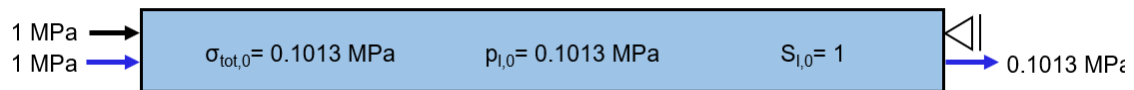
1 MPa →			
1 MPa →	$\sigma_{tot,0}$= 0.1013 MPa	$p_{l,0}$= 0.1013 MPa	$S_{l,0}$= 1

→ 0.1013 MPa

2nd modelling phase (s. Fig. 5.2):

3 MPa →
4 MPa →
S_l = 0.5 ←→

$p_{g,0}$= 0.2 MPa	$\sigma_{tot,0}$= 0.1013 MPa	$S_{l,0}$= 0.63

→ 0.5 MPa
S_l = 0.9

3rd modelling phase (s. Fig. 6.3):

4 MPa →
5 MPa →
S_l = 0.2 ←

→ 0.25 MPa
S_l = 0.25

$p_{g,0}$ = 0.25 MPa	$p_{g,0}$ = 0.2 MPa	$p_{g,0}$ = 0.25 MPa
$S_{l,0}$= 0.25	$S_{l,0}$= 0.7	$S_{l,0}$= 0.25
$\sigma_{tot,0}$= 5 MPa	$\sigma_{tot,0}$= 5 MPa	$\sigma_{tot,0}$= 5 MPa

4th modelling phase (s. Fig. 7.22):

■ Mechanics ■ Heat Flow ■ Liquid Flow ■ Gas Flow ⊗ = thermal source ⊗ = gas source

→ 4 MPa
25 °C
→ 4 MPa

Repository Drift	Host Rock
$\sigma_{tot,0}$= 8 MPa	$\sigma_{tot,0}$= 8 MPa
T_0= 25 °C	T_0= 25 °C
$p_{g,0}$ = 0.1013 MPa	$p_{g,0}$ = 4 MPa
$S_{l,0}$= 0.75	$p_{l,0}$= 4 MPa

107
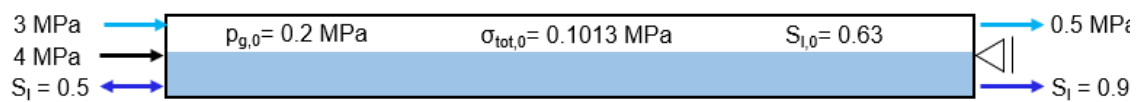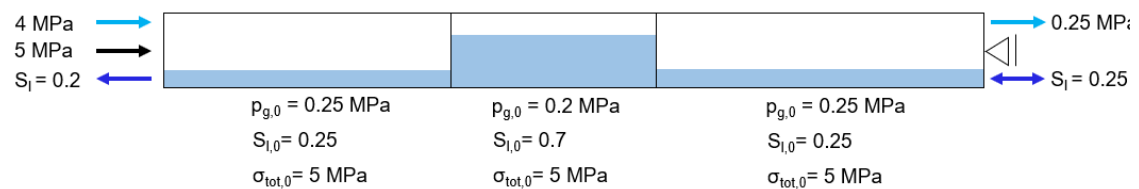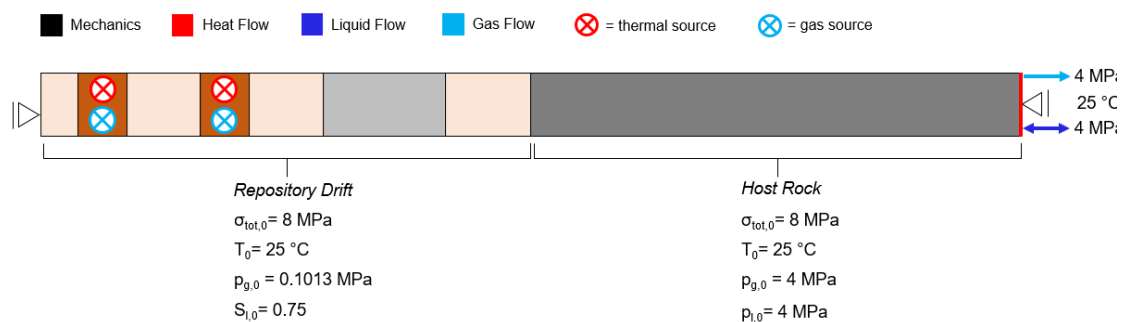
B   Retention curves

B.1   Retention curve for the 1st modelling phase

In the first modelling phase, the interactions between fluid phases should be neglected.
However, in scenario g they are considered, and a retention curve is specified:
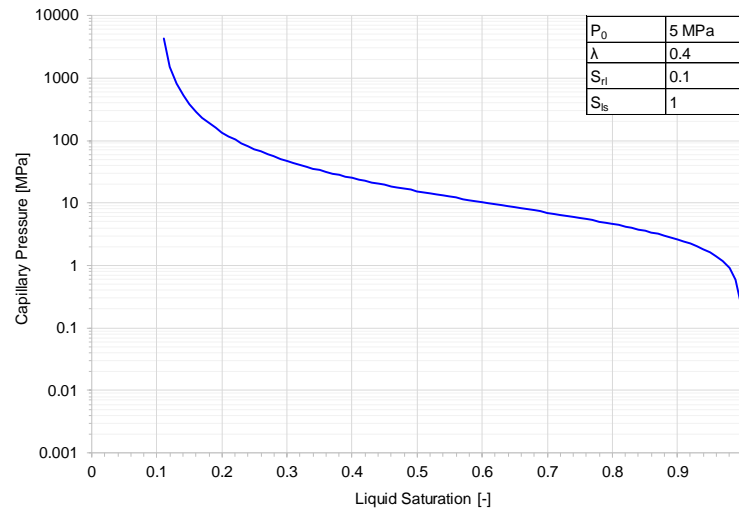
Fig. B. 1   Retention curve for scenario g of the first modelling phase

B.2   2nd modelling phase

Following, the retention curve for the generic material of the second modelling phase is
shown.
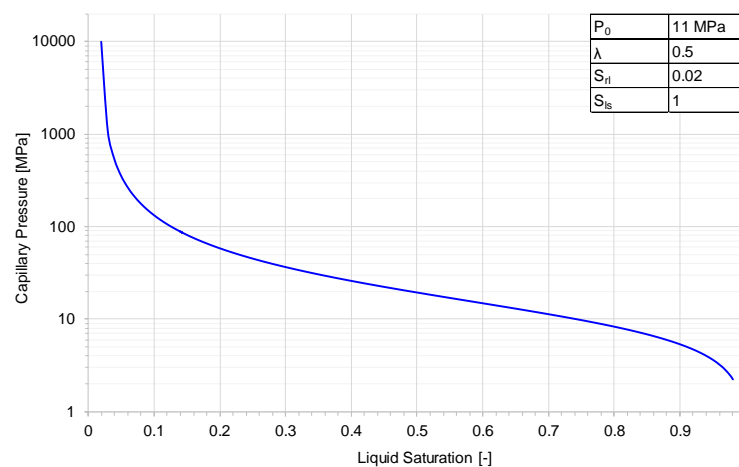
Fig. B. 2   Retention curve for the second modelling phase

B.3   3rd modelling phase

In the third modelling phase, two materials are considered. Therefore, the retention curves are presented in the following diagram.
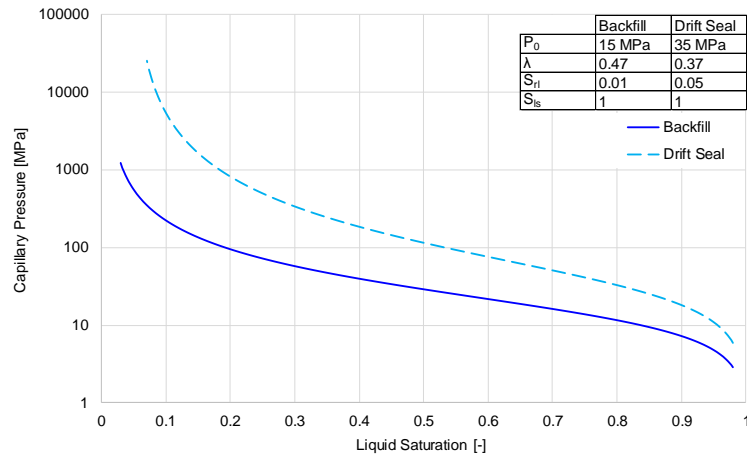
Fig. B. 3   Retention curve for the third modelling phase

B.4   4th modelling phase

Here, a generic repository drift was simulated assuming four different materials. Their retention curves are shown in the following diagram.
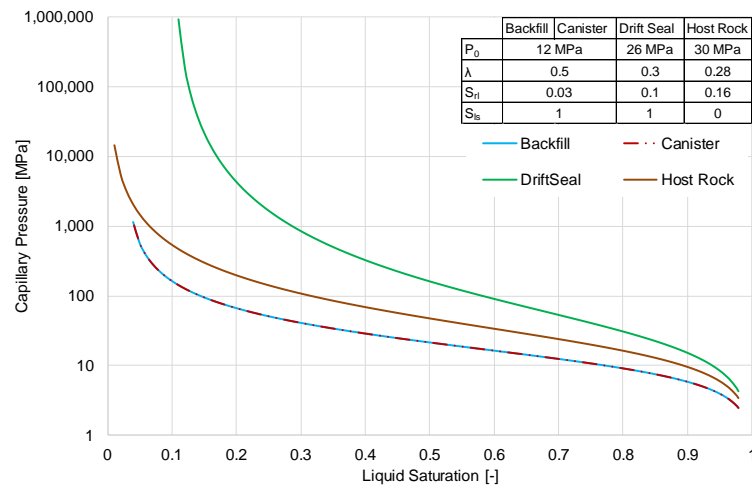
Fig. B. 4   Retention curve for the fourth modelling phase

C Supplements for the 1st modelling stage

Additional diagrams for the results of the 1st modelling phase could be found in the fol-
lowing.

C.1 Scenario e – unified mesh discretization
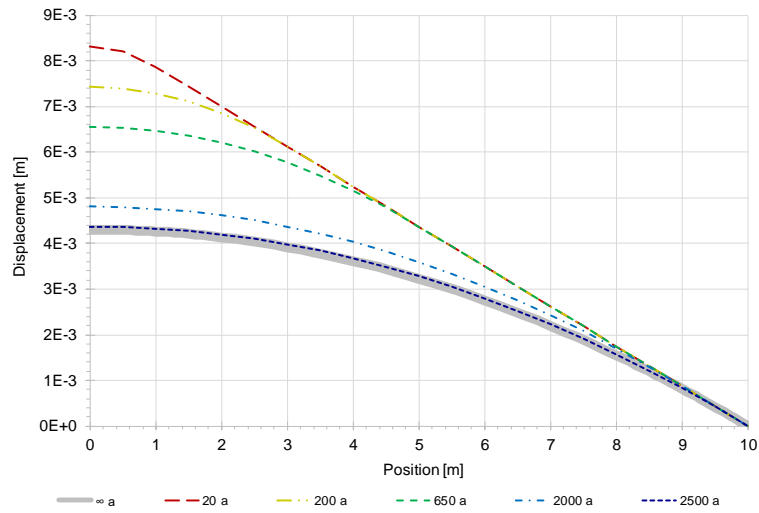
Fig. C. 1 Displacement profiles for model 1e
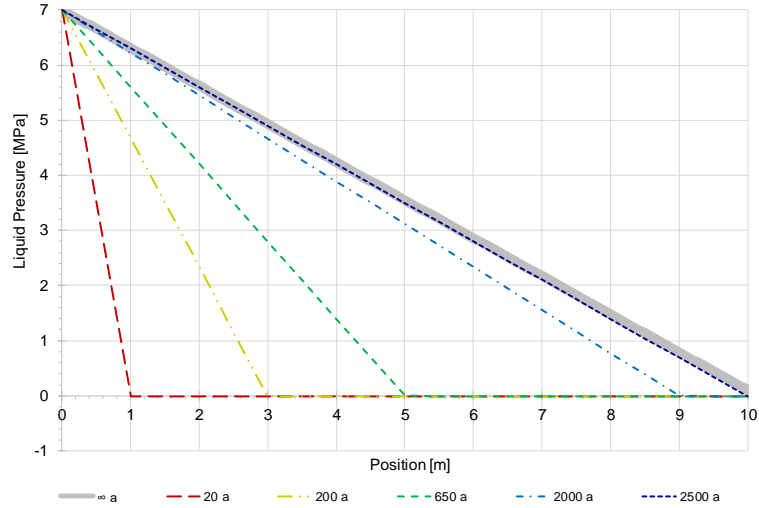
Fig. C. 2 Profiles of liquid pressure for model 1e

C.2 Scenario f – user-specified mesh discretization
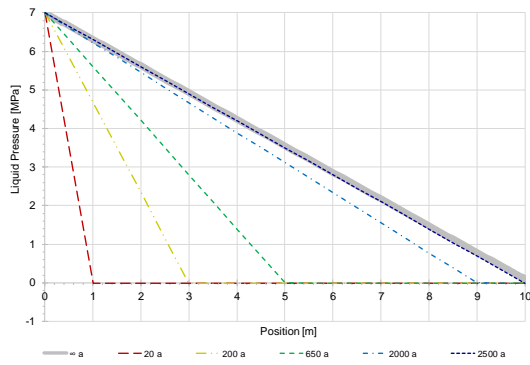
Fig. C. 3 Liquid Pressure distribution in model 1e with unified mesh discretization
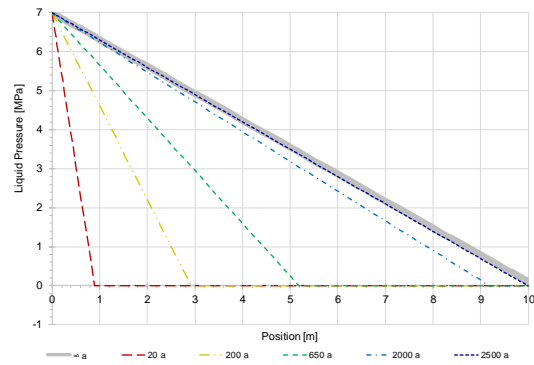
Fig. C. 4 Liquid Pressure distribution in model 1f with GRS' mesh discretization
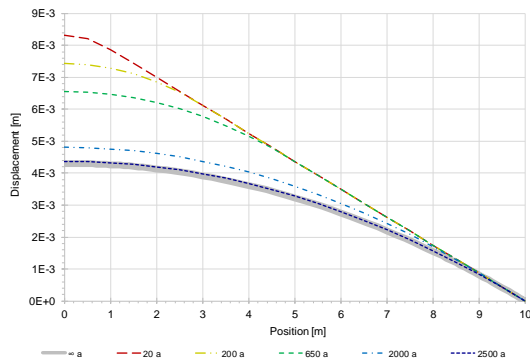
Fig. C. 5 Displacements in model 1e with unified mesh discretization
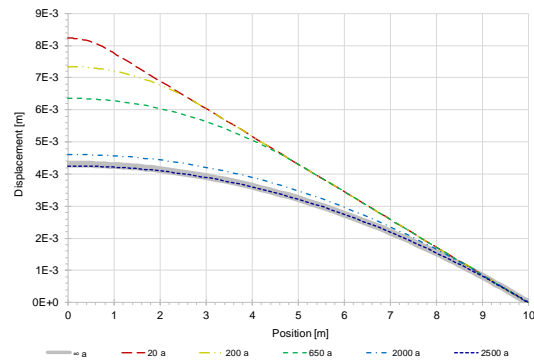
Fig. C. 6 Displacements in model 1f with GRS' mesh discretization

C.3 Scenario g – including process couplings
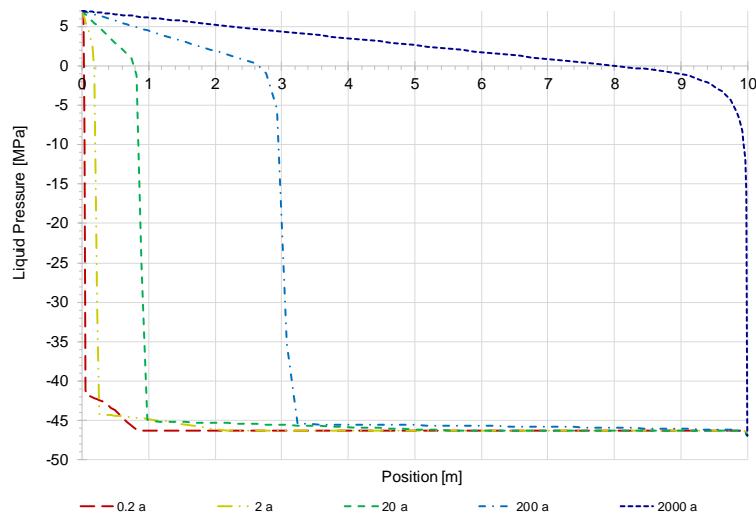
Fig. C. 7 Liquid pressure distribution in model 1g

D   Supplements for the 2nd modelling phase

Additional diagrams for the results of the 2nd modelling phase could be found in the following.

D.1   Scenario b – changed boundary conditions after 10,000 years
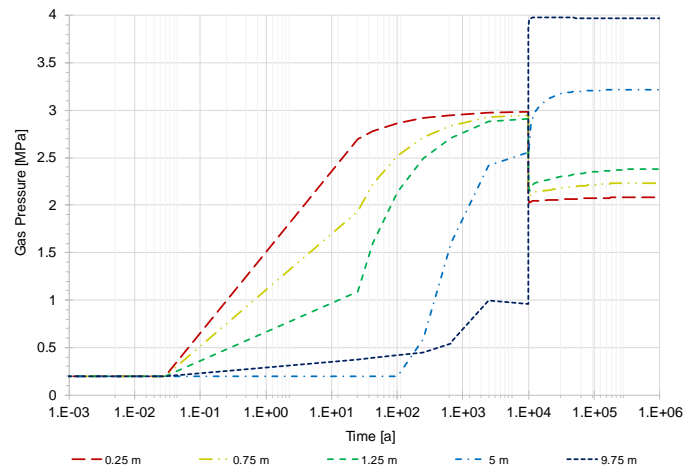
Fig. D. 1   Gas pressure evolution for model 2b
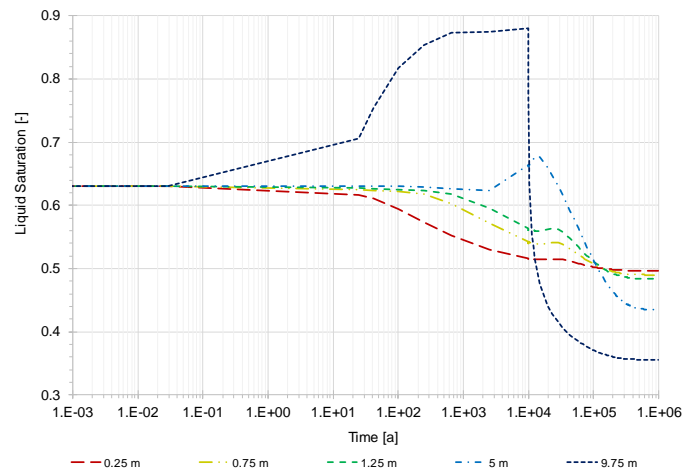
Fig. D. 2   Liquid saturation evolution for model 2b
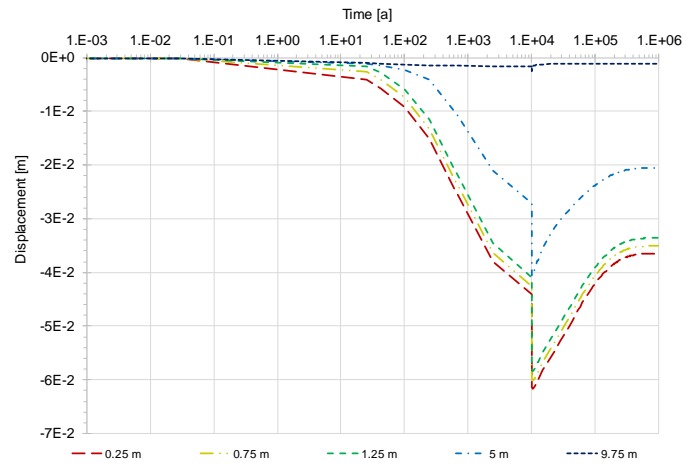
Fig. D. 3   Displacement evolution for model 2b

D.2   Scenario c - analytical boundary condition
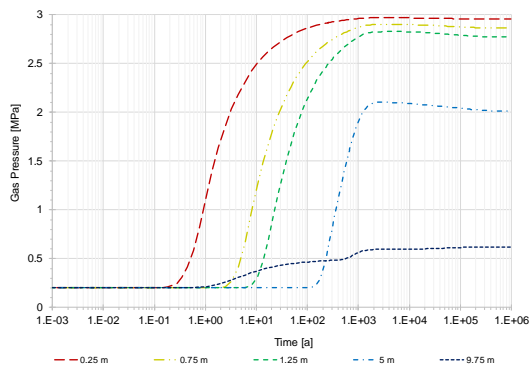
Fig. D. 4   Gas pressure evolution for model 2c
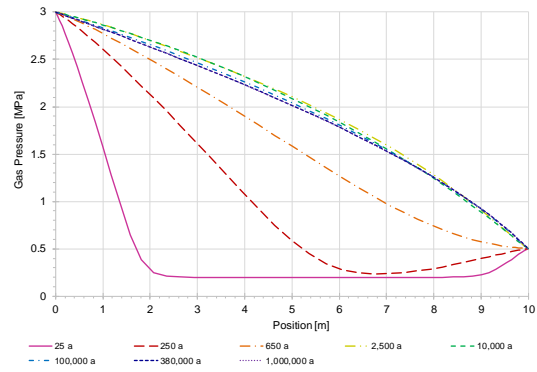
Fig. D. 5   Gas pressure profiles for model 2c
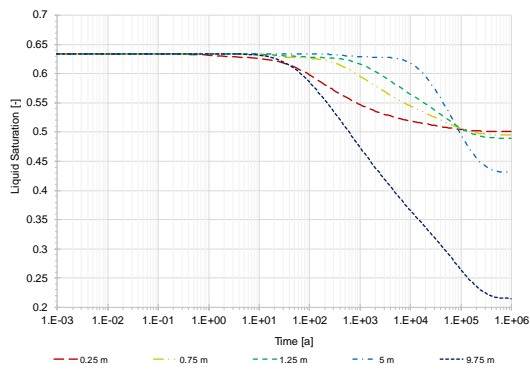
Fig. D. 6   Liquid saturation evolution for model 2c
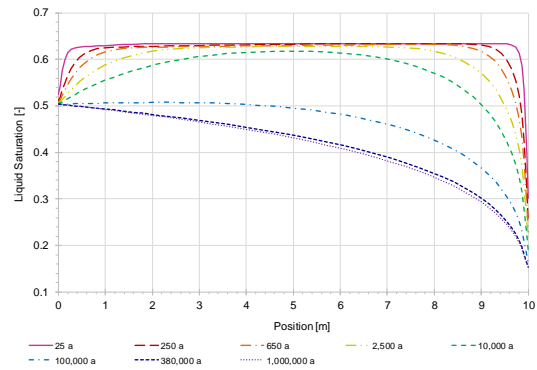
Fig. D. 7   Liquid saturation profiles for model 2c
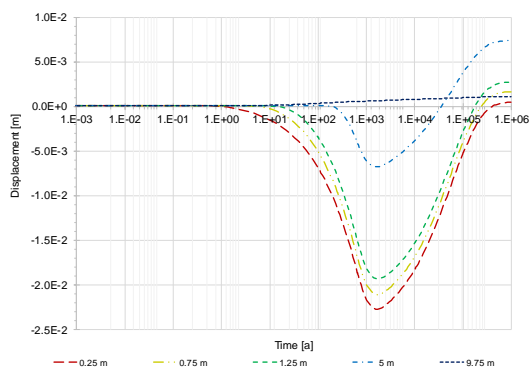
Fig. D. 8   Displacement evolution for model 2c
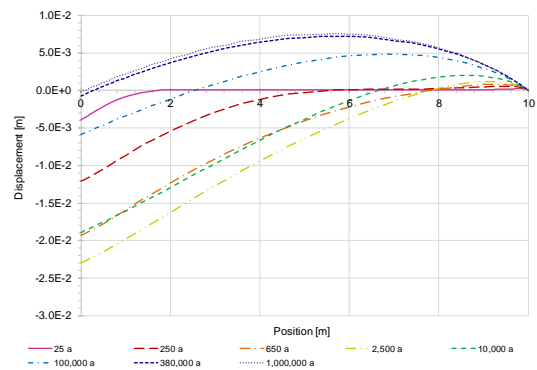
Fig. D. 9   Displacement profiles for model 2c

115

D.3 Scenario d – analytical boundary condition and change of conditions after 10,000 years
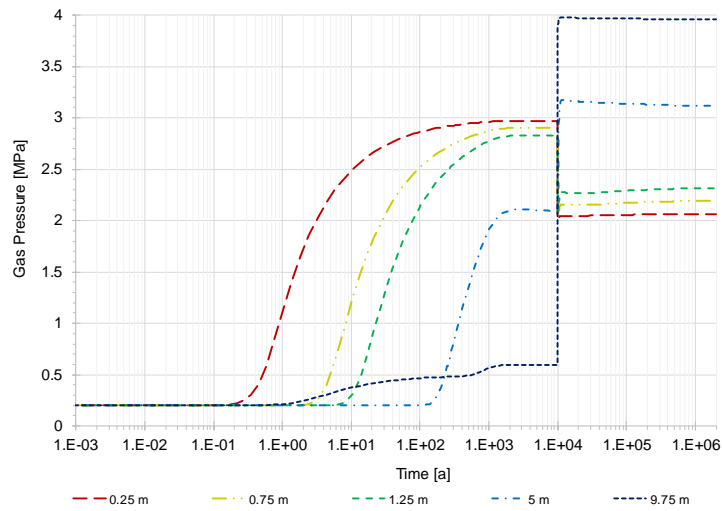
Fig. D. 10 Gas pressure evolution for model 2d
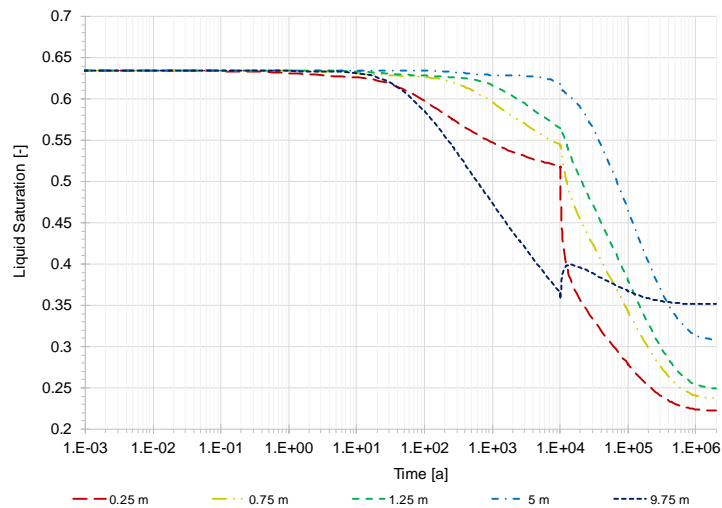
Fig. D. 11 Liquid saturation evolution for model 2d
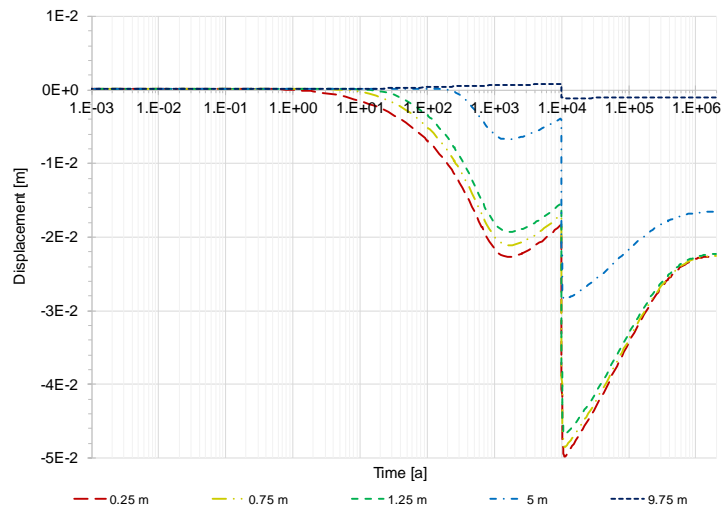
Fig. D. 12 Displacement evolution for model 2d

E Supplements for the 3ʳᵈ modelling phase

Additional diagrams for the results of the 3ʳᵈ modelling phase could be found in the following.

E.1 Scenario c – completely fixed boundaries
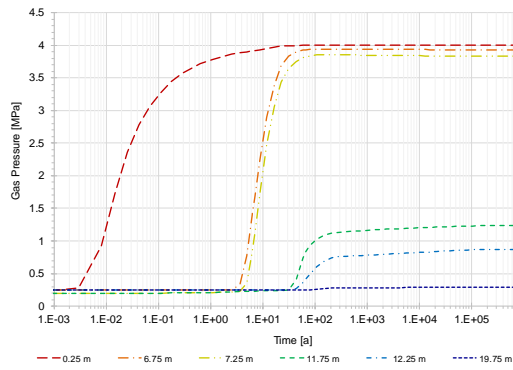
Fig. E. 1 Gas pressure evolution for model 3c
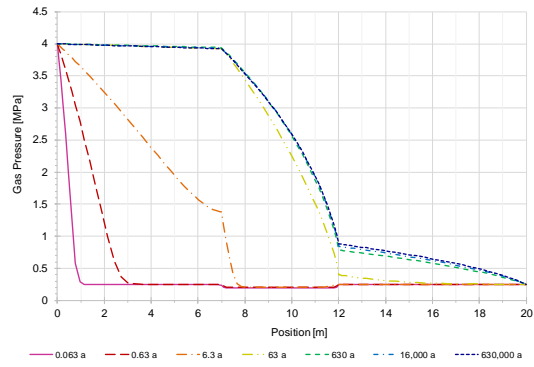
Fig. E. 2 Gas pressure distribution in model 3c
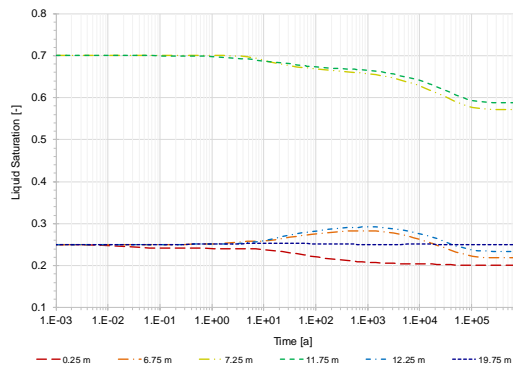
Fig. E. 3 Liquid saturation evolution for model 3c
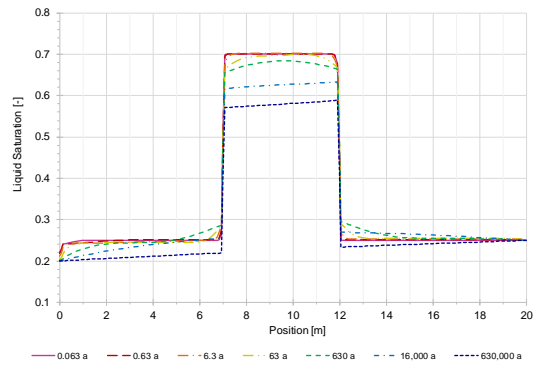
Fig. E. 4 Liquid saturation profile in model 3c

E.2   Scenario e – softer backfill material
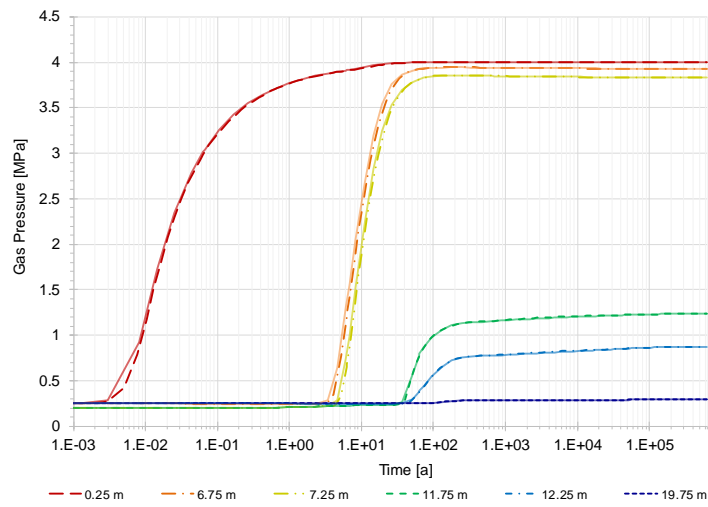
Fig. E. 5   Comparison of gas pressure evolution for model 3a and 3e
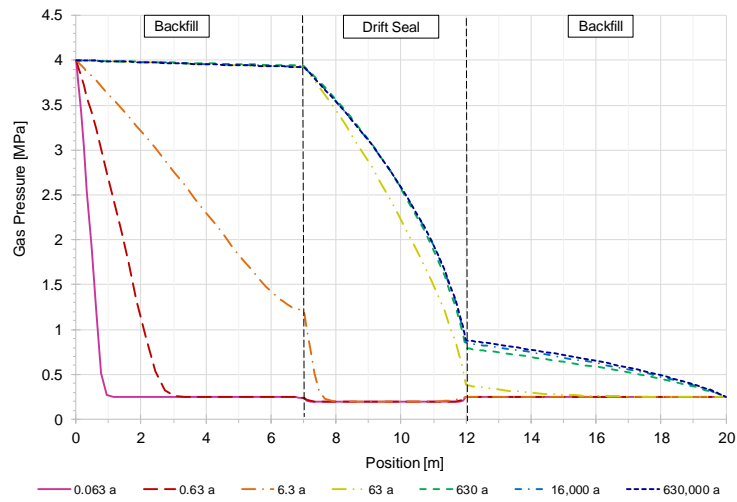
Fig. E. 6   Profiles of gas pressure for model 3e
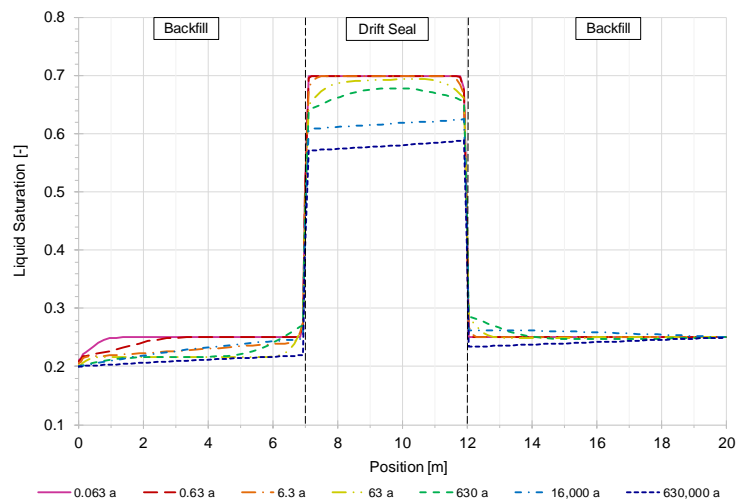
Fig. E. 7   Profiles of liquid saturation for model 3e

E.3 Scenario f – coarser backfill material
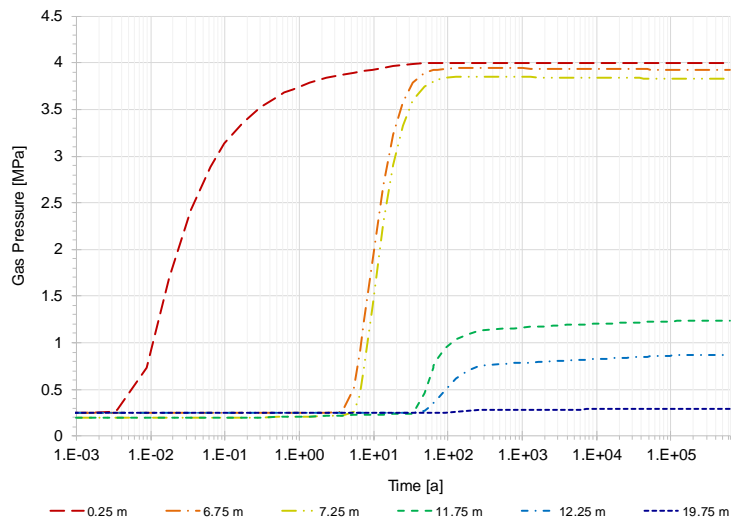
Fig. E. 8 Gas pressure evolution for model 3f
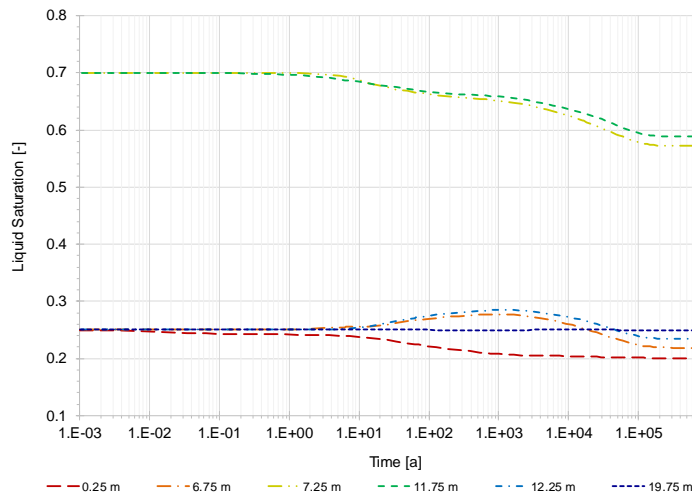
Fig. E. 9 Liquid saturation evolution for model 3f
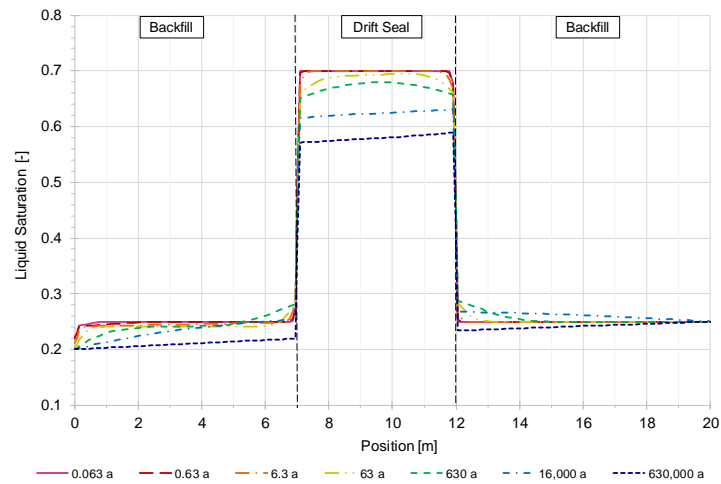
Fig. E. 10 Profiles of liquid saturation for model 3f

121
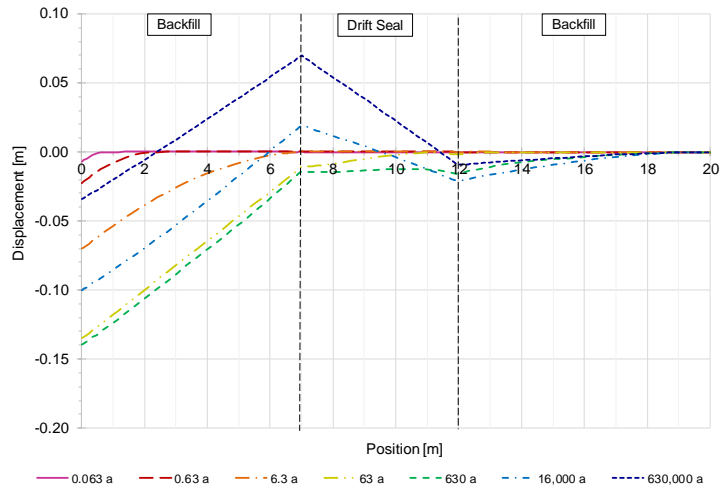
Fig. E. 11   Displacement profiles for model 3f

E.4 Scenario g – perfectly mobile fluids
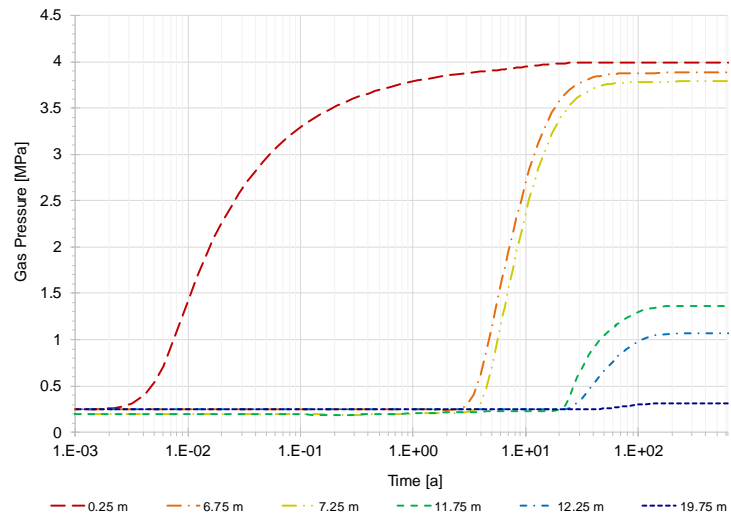
Fig. E. 12 Gas pressure evolution for model 3g
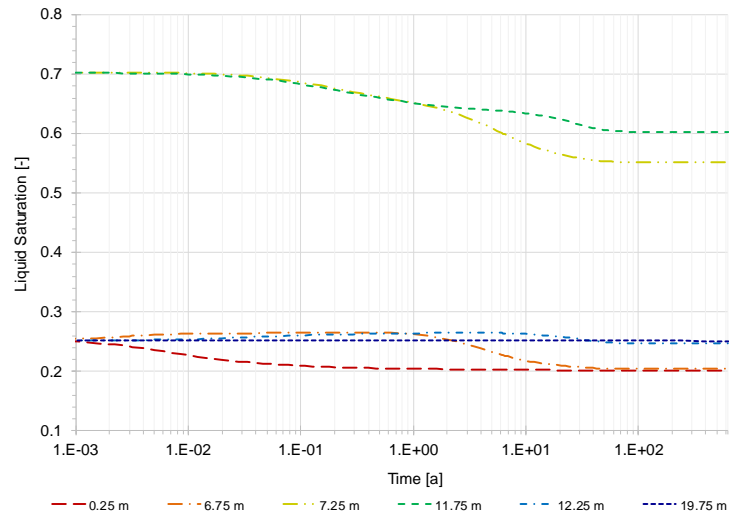
Fig. E. 13 Liquid saturation evolution for model 3g

E.5   Scenario h – homogenous retention curves
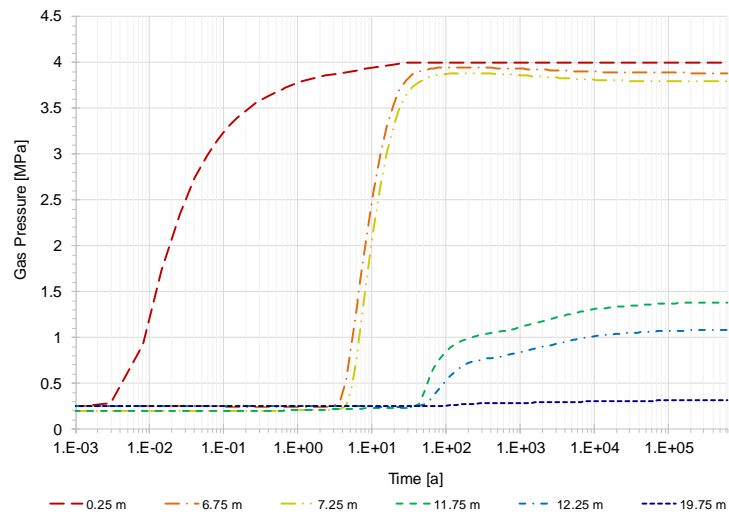
Fig. E. 14   Gas pressure evolution in model 3h
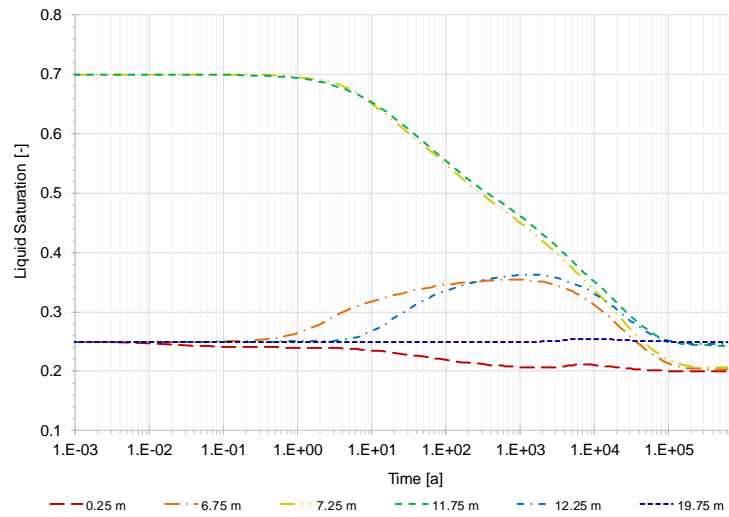
Fig. E. 15   Liquid saturation evolution in model 3h

F Supplements for the 4th modelling phase

F.1 TH-coupled model

In the following, additional plots of gas and liquid pressure evolution and temperature profiles are shown for the thermal-hydraulic coupled model of the fourth modelling phase which includes heat and gas production.
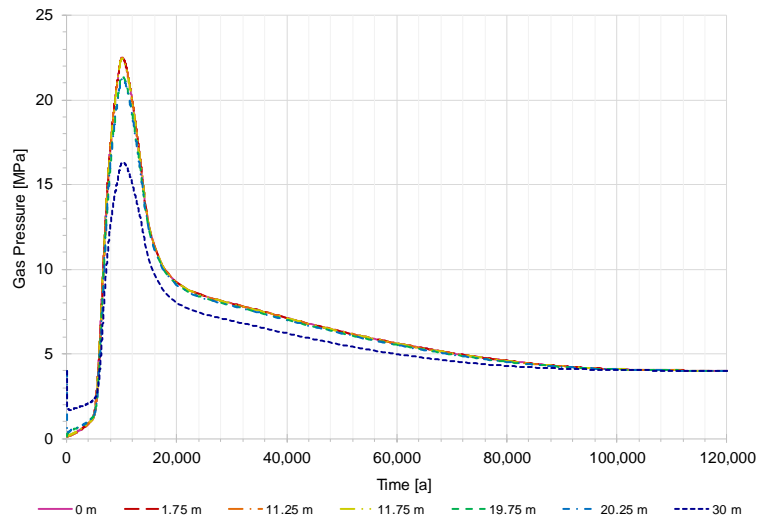
Fig. F. 1   Evolution of gas pressure for model 4b
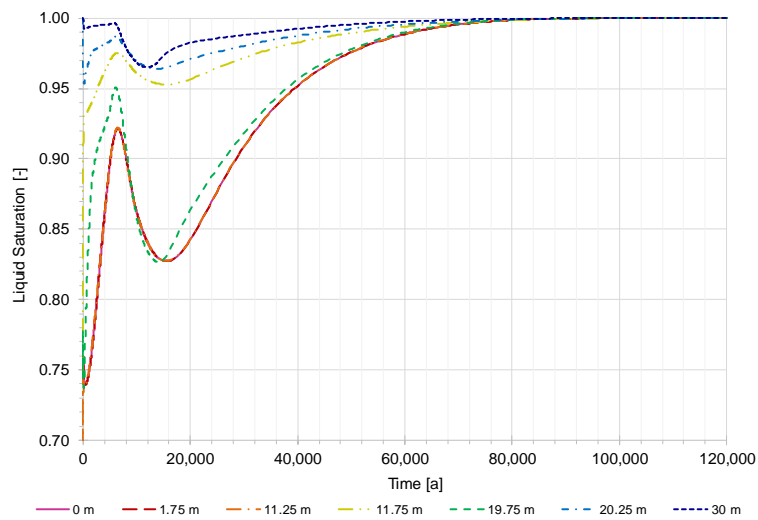
Fig. F. 2   Evolution of liquid saturation for model 4b
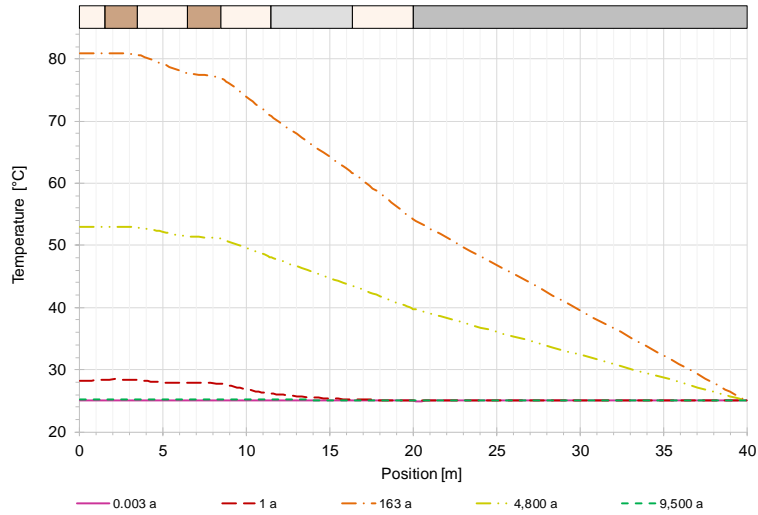
Fig. F. 3   Temperature profiles for model 4b

F.2   THM-coupled model with thermal source

In the following, additional diagrams for the gas and liquid pressure evolution and temperature profiles for the THM-coupled model of the fourth modelling stage are to be found. In this simulation only heat generation was considered.
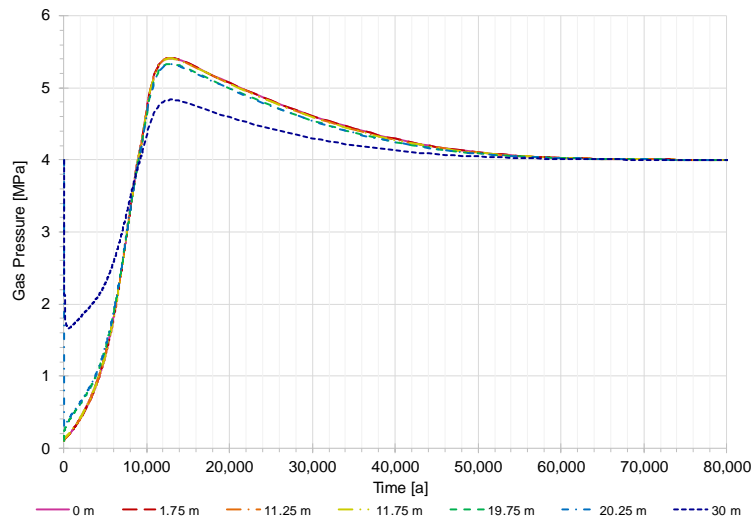
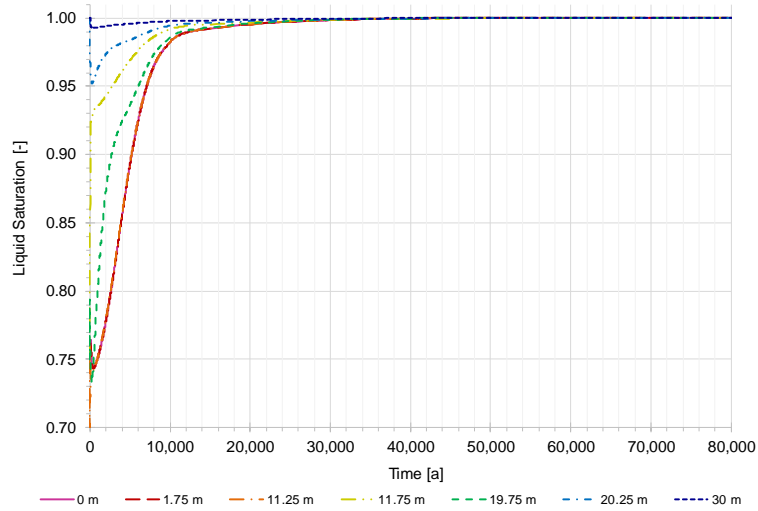**Fig. F. 4**   Gas pressure evolution for model 4c
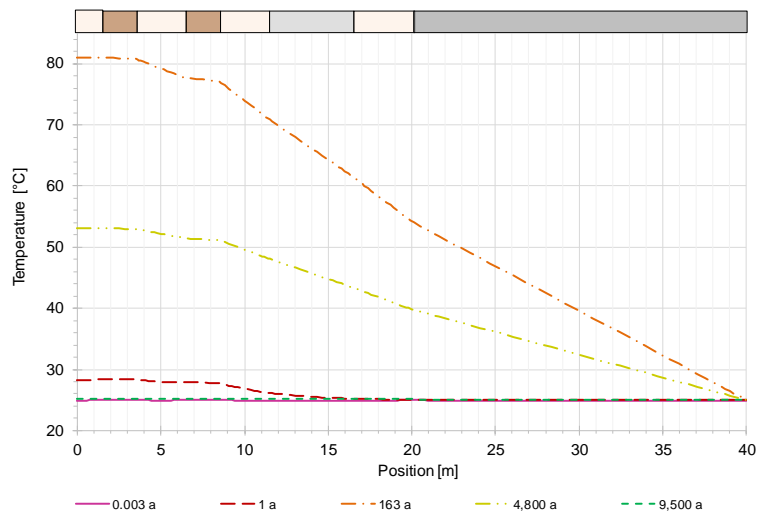
Fig. F. 5   Liquid pressure evolution for model 4c

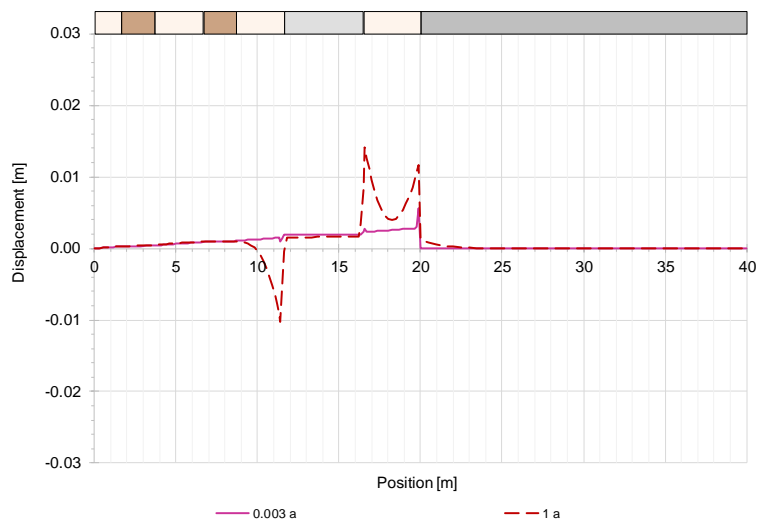**Fig. F. 6**   Temperature profiles for model 4c

Fig. F. 7   Displacement profiles at t = 0.003 a and t = 1 a for model 4c

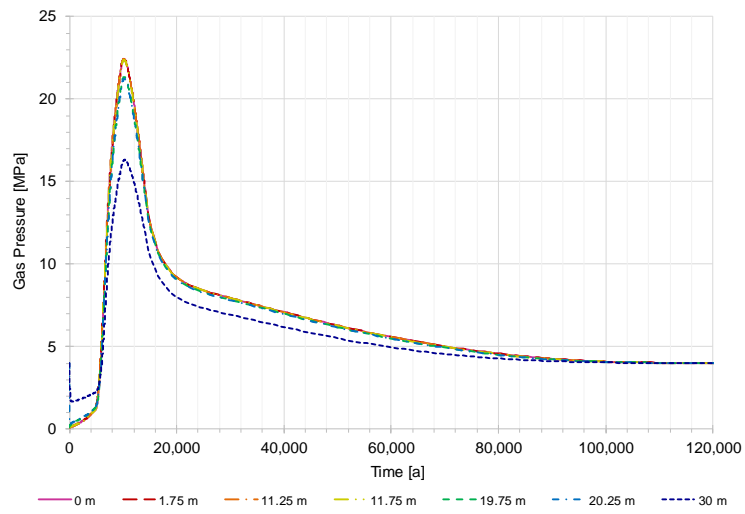## F.3 THM-coupled model with thermal and gas source

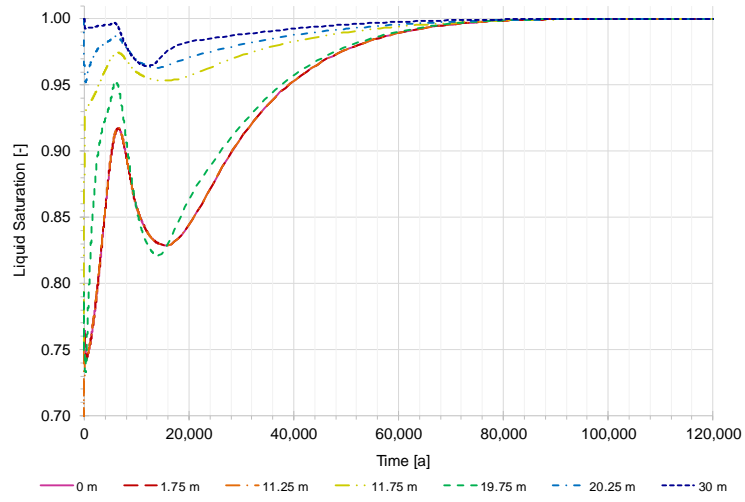**Fig. F. 8** Gas pressure evolution for model 4d
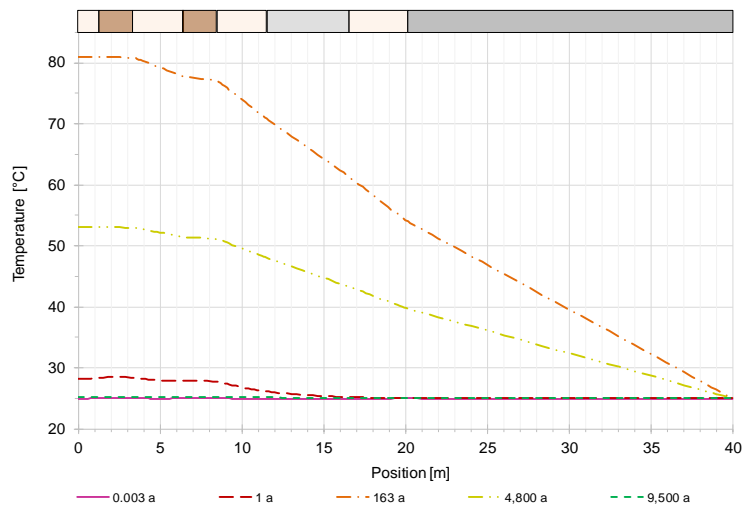

Fig. F. 9 Liquid saturation evolution for model 4d

Fig. F. 10 Profiles of temperature for model 4d